SEMI SOLID METAL CASTING OF ALUMINUM ALLOYS:

THE INFLUENCE OF SHEAR RATE ON VISCOSITY

A Thesis

Presented In Partial Fulfillment of the Requirements for

the Degree Master of Science in the

Graduate School of The Ohio-State University

By

Christian Charles Egli, B.S.

* * * * *

The Ohio-State University
1996

Master's Examination Committee:
Dr. Jerald Brevick
Dr. Taylan Altan

Approved by:

J. R. Brevick

Advisor
Mechanical Engineering

ABSTRACT

Semi solid casting is a new process which has its origins in the USA and has now been further developed by Bühler. Semi solid raw material with a special microstructure is being used allowing it to be injected with a solid fraction of 60%. The Bühler company has developed die casting machines that enable a "plastic-like" filling of the die cavities. This is done by tightly controlling casting parameters such as injection speed as well as injection pressure. This "plastic-like" behavior can be quantified by viscosity measurements -- the topic of this dissertation.

A semi solid metal, when properly heated, possesses a gradual resistance to change of form. This property acts very much like a sort of internal friction. Thus, when this gradual resistance is measured it is possible to obtain viscosity. Traditional viscometry has not been found to relate to a manufacturing environment. For this study rheological measurements are taken within shear rate ranges that reflect die casting conditions.

There exists a similitude between the operation of a die casting machine and that of a capillary viscometer. Thus, with the correct assumptions and correct mathematical treatment, it is possible to obtain viscosity measurements directly from die casting operations. For this experimental set-up a Bühler H-250 SC is used, furnishing data that pertains exactly to the field of semi solid metal casting.

It is seen also what effect temperature and machine settings have on the viscous behavior of semi solid aluminum. This effect is observed by several methods: (1) by tabulating the measured viscosity values in function of shear rate; (2) by performing partial fill tests; (3) by analyzing the microstructure on an optical microscope; (4) by analyzing samples on an electron scanning microscope; (5) by running filling simulations on Flow 3D.

To my mother, Theodora ,

who taught me by her example

to take pride in my work and

do my best no matter who

I worked for or what I did.

ACKNOWLEDGMENTS

It is a pleasure to acknowledge the assistance and support I have received from the Engineering Research Center at the Ohio State University. I am particularly indebted to Professor Taylan Altan for the financial support and for the opportunity to further my education.

In preparing for this research I have received great help from my advisor, Professor Jerald Brevick who kindly agreed to direct my efforts towards the successful completion of the thesis. Many other names could be mentioned, and to all these people I would like to express my most sincere appreciation.

It is customarily understood that family and friends provide the necessary moral support when achieving a task of this nature. I cannot emphasize enough how true this was for me. By being there, they added a meaning to my efforts.

Christian Egli

VITA

14th March 1970.................................... Born - Aigle, Switzerland

1995.. B. S. Mechanical Engineering

Cum Laude

With Distinction in Mechanical Engineering

1995 - present.. The Ohio State University

Graduate Fellow,

Engineering Research Center for

Net Shape Manufacturing,

The Ohio State University

FIELDS OF STUDY

Major Field: Mechanical Engineering

Manufacturing

TABLE OF CONTENTS

Page

LIST OF TABLES

LIST OF FIGURES

CHAPTER 1

INTRODUCTION

1.1 Preamble

The process of semi solid metal casting has been developed in an effort to improve the quality of traditionally die-cast parts. The main idea when casting semi solid aluminum is to reduce levels of porosity so that parts cast in such a fashion are weldable and heat-treatable, as well as leak-proof and generally stronger.

Semi solid casting is a new process which has its origins in the USA and has now been further developed by Bühler. Semi solid raw material with a special microstructure is being used allowing it to be injected with a solid fraction of 60%. In this state, semi solid materials exhibit a non-Newtonian behavior. Their viscosity drops as the shear rate they are subjected to increases. Due to the high shot capacity and the variability of the shot curve, the Bühler SC die cast machine enables a "plastic-like" filling of the die cavities and, with the pressure control, a controlled compensation for the solidification shrinkage [Bühler]. This "plastic-like" behavior can be quantified by viscosity measurements -- the topic of this research.

1.2 Objectives

In order to determine the flow characteristics of the semi solid aluminum as it is being cast, this project will develop a method for measuring the viscosity of the metal. The results obtained will depend on many factors, of which temperature and shear rate are the most important.

To date existing methods and techniques have not been capable of measuring the viscosity of this semi solid aluminum alloy 356 at the high shear rates that are seen in the semi solid die casting process.

1.3 Rationale

With a heavy emphasis in today's engineering world on computer simulations it is important to be able to simulate the semi solid casting processes accurately. Any such implementation necessarily requires that the viscosity of the medium be defined beforehand.

In simulation packages that have been developed for the simulation of regular liquid casting, the viscosity values are entered in function solely of temperature, such as in Magmasoft as to this date. Other software packages such as Flow 3D have the capability of simulating the flow of semi solid media, however these packages have not been developed uniquely for the die casting industry. A thorough knowledge of the properties of semi solid aluminum is therefore necessary, at the shear rates and under the particular conditions that are applicable to semi solid metal die casting.

CHAPTER 2

LITERATURE REVIEW

2.1 Introduction

The literature review presented in this section serves several purposes. First to restate the theoretical aspects of viscous behavior. Then, to describe the research done by other individuals in the field of semi solid metal rheology. And lastly to detail the method by which the Bühler SC can be used for viscometric measurements.

2.2 Viscosity

A fluid is a substance that deforms continuously under the action of a shear stress. Without shear-stress, there will be no deformation. Thus, fluids have broadly been classified according to the relation between the applied shear stress and the rate of deformation. [Fox, 1992]. In the simple Newtonian fluid model this relationship is linear, defined simply by a constant of proportionality, the *absolute viscosity:* η. In recent years however, there has been an increasing recognition of the importance of non-Newtonian flow characteristics displayed by most materials encountered in everyday life (such as in gums, proteins, biological fluids, polymers, plastics, emulsions, slurries and in semi solid metals) [Chabraa, 1993]. It would seem that indeed the Newtonian fluid behavior has become an exception rather than the rule.

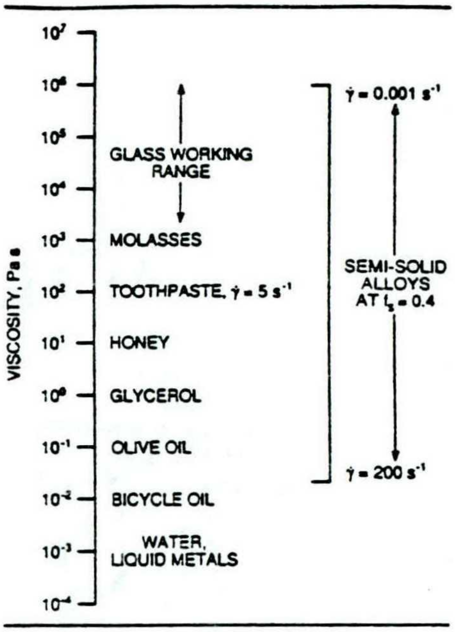

Figure 2.1 Typical viscosities of common fluids and of typical semi solid metals at a solid fraction of 40%; the viscosity of the same semi solid metal varies in function of shear rate; at high shear rate (200 /s) the semi solid metal has the viscosity of a liquid

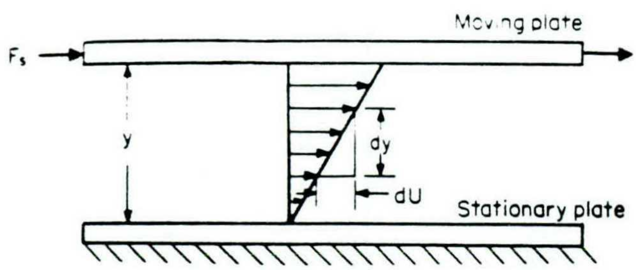

Figure 2.2 Flow between parallel plates; the shear rate is determined by the velocity gradient; the shear stress by the ratio of shearing force F to the area of the plate that is in contact with the fluid

2.2.1 Newtonian viscosity models

Most common fluids such as water, air, and gasoline are Newtonian under normal conditions. Considering the flow of such a liquid between two parallel plates, each of area dA_y [m^2] and dy [m] apart, as shown in figure 2.2. When a force dF_x [N] is applied to the upper plate, this force will cause it to move with a velocity du [m/s] relative to the lower plane.

The shearing stress τ_{yx} acting throughout the liquid is defined as the shearing force F divided by the area A over which it acts. Thus,

$$\tau_{yx} = \frac{dF_x}{dA_y} \quad \text{in} \quad N/m^2$$

The shear rate D equals the velocity difference du divided by the distance between the planes, dy. The shear rate is thus given in reciprocal seconds [s^{-1}]. In the simple case of the flat plates the velocity gradient is uniform throughout the sample. More generally the distance dy has to be measured perpendicular to the direction of shear.

$$D = \frac{du}{dy} \quad \text{in} \quad s^{-1}$$

The flow property, or viscosity η in [Ns/m^2] or [Pa s], can now be defined by the relation between shear stress and shear rate:

$$\tau_{yx} = \eta\ D \quad \text{or} \quad \eta = \tau_{yx} / D$$

2.2.2 Non-Newtonian viscosity

When the shear stress is no longer directly proportional to the shear rate, the fluid is non-Newtonian. Toothpaste is a familiar example. It behaves as a fluid when squeezed from the tube, however it does not run out by itself. Non-Newtonian behavior becomes apparent when the fluid in question is no longer uniform and composed of one ingredient. Clear water exhibits Newtonian properties. However, mud has non-Newtonian properties. Slurries and suspensions where there is a combination of solid particles and a liquid do not exhibit the linear relationship that was particular to the Newtonian fluids [Dabak, 1986].

Suspensions with low solid concentrations normally display Newtonian behavior, indicating that the viscosity is independent of the shear rate. Whereas non-Newtonian behavior is typical of highly concentrated suspensions.

2.2.2.1 Non-Newtonian viscosity models

Numerous empirical models have been proposed to model the non-linear relation between the shear stress and the shear rate for time-independent fluids. In many engineering applications they are represented by the power law model [Fox, 1992]. For one-dimensional flow it is given as:

$$\tau_{yx} = kD^{n}$$

where n is called the flow behavior index and k is the consistency index. When n = 1 this equation reduces to Newton's law of viscosity where $k = \eta$.

The *apparent viscosity* can be then obtained by the following transformation:

$$\tau_{yx} = \eta D = kDD^{n-1}$$

$$\eta = kD^{n-1}$$

Fluids in which the apparent viscosity decreases with increasing shear rate ($n < 1$) are called *pseudo plastic* or *shear thinning* fluids [Fox, 1992]. Most non-Newtonian fluids fall into this category; examples include polymer solutions and colloidal suspensions. Semi solid aluminum falls into this group.

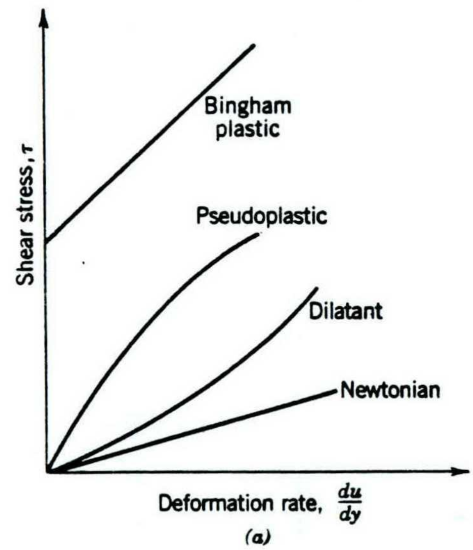

Figure 2.3 Qualitative viscous behavior curves for different fluids in a shear rate - shear stress plot

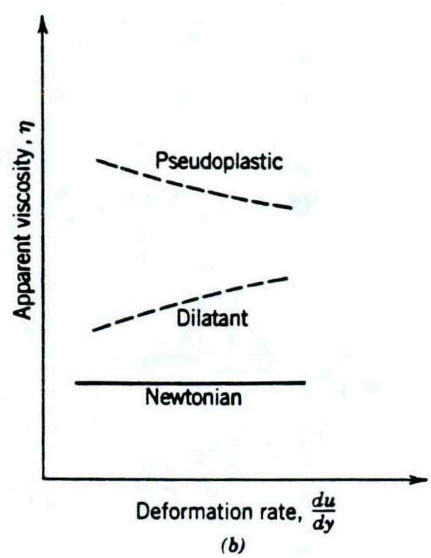

Figure 2.4 Qualitative viscous behavior curves for different fluids in a shear rate - viscosity plot

When the apparent viscosity increases with increasing shear rate ($n > 1$) then the fluid is termed *dilatant* or *shear thickening*.

In some instances the non-Newtonian media behaves as a solid until a minimum yield stress is exceeded and subsequently exhibits a linear relation between shear stress and shear rate. These are the *Bingham plastic* substances.

A further sophistication is introduced by the fact that sometimes the apparent viscosity may be time-dependent. *Thixotropic* fluids show a decrease in viscosity with time under a constant applied shear stress [Fox, 1992]. *Rheopectic* fluids, inversely, show an increase in viscosity with time.

2.2.2.2 Shear rate - shear stress relation

Three different regions are generally observed on the shear stress versus shear rate curve of a non-Newtonian substance such as a suspension of solid particles in a liquid matrix. The semi solid metal when heated to its "mushy" state is indeed such a suspension: solid non-molten grains in suspension in the already molten eutectic phase of the aluminum alloy. Those regions can be described as such:

(1) a low shear region, in which inter-particle forces are dominant

(2) an intermediate shear-rate region, in which the rheological behavior is a complex function of both solid and liquid properties; and,

(3) a high shear region, in which the rheological behavior tends to be largely Newtonian, exhibiting well-aligned particle movement, with very small effect of particulate forces as compared to hydrodynamic forces [Dabak, 1986].

At high shear-rates the viscosity is denoted by η_{∞}. This corresponds to the viscosity of the liquid component of the suspension, as if it were completely molten. The other limiting value is denoted by η_0. This value is measured at the lowest possible shear rate. Between these limits the viscosity varies in a manner that is entirely specific to the suspension.

2.3 Viscometers and viscosity measurements

Instruments of many designs are used to measure viscosity. They generally fall into three categories: the capillary, the rotational and the falling body type of viscometer. The falling body instruments are not suitable for use with non-Newtonian liquids, since the rate of shear can only be measured over a limited length of time, whereas with the rotational cylinder viscometer measurements can be taken for as long as may be required.

For measurements at very low shear rates (in the order of 10e-5 reciprocal seconds), the viscosity can be measured with an extensometer or by vibrational methods. Such shear rate ranges do not fall within the scope of this project. The practical application of each of these instruments is described in figure 2.5.

2.3.1 Capillary viscometers

Capillary viscometers, see figures 2.6, 7, 8, are the most common. They are comparatively simple and inexpensive and full mathematical treatment is possible. In general the liquid is made to flow through a capillary tube under a known pressure difference and the rate of flow is measured, usually by noting the time it takes for a given volume of liquid to pass through. In certain types of instruments, the liquid is forced through the tube at a predetermined rate while the pressure that it takes to do it is measured.

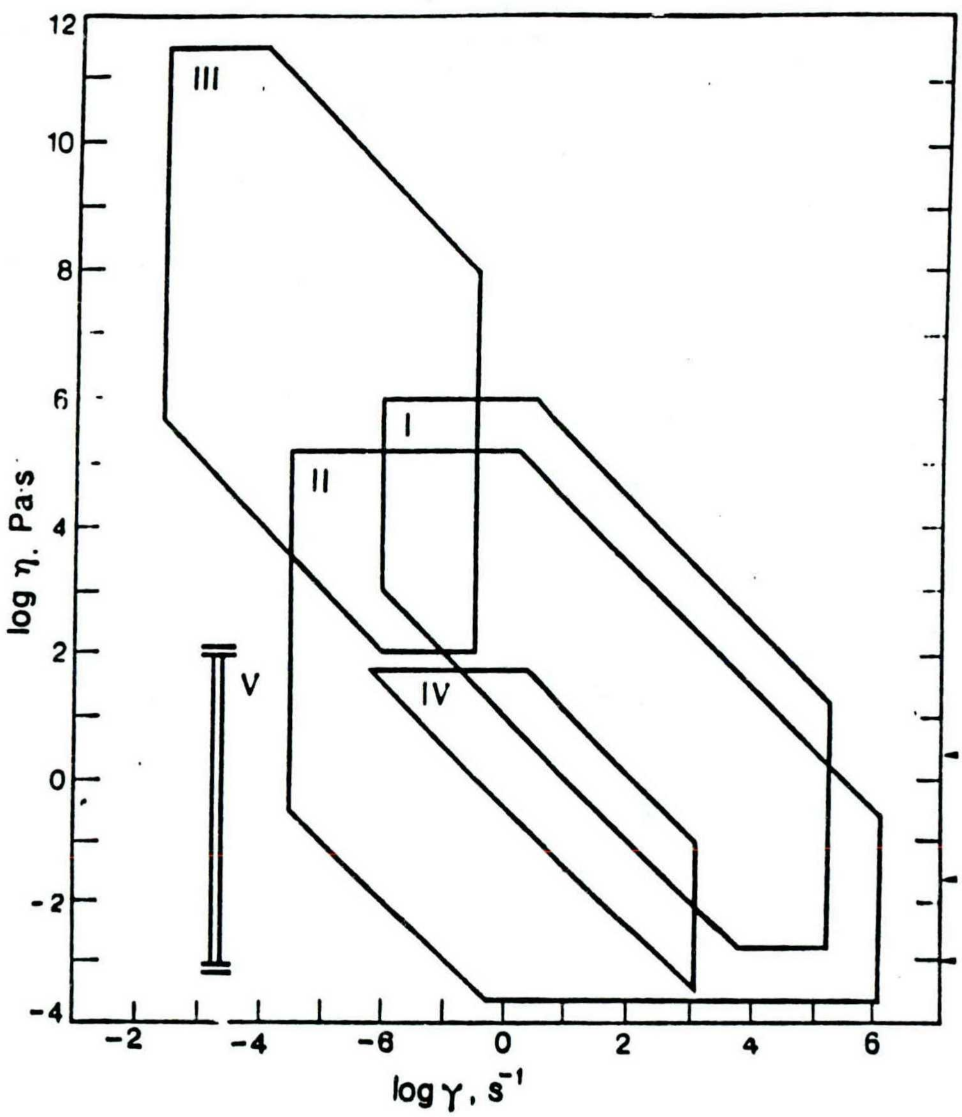

Figure 2.5 Approximate limits of application of basic viscometric methods from Malkin, in function of the shear rates and the viscosity applicable to the fluid sample;

The instruments are: (I) capillary; (II) rotational; (III) extensometers

(IV) falling ball method; (V) vibrational methods

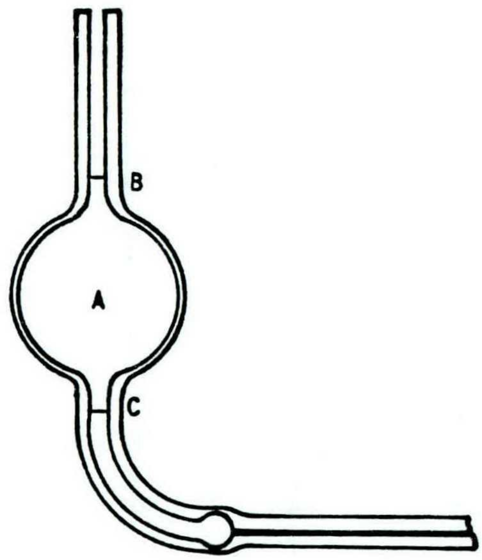

Figure 2.6 Poiseuille's viscometer; the flow restriction caused by the capillary is clearly visible; the large bulb in A momentarily provides a constant pressure head for the little flow rate induced by the capillary; the flow rate is measured by timing the flow out of the capillary

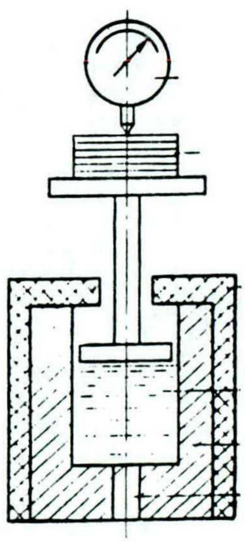

Figure 2.7 Backwards extrusion capillary viscometer; the restriction in the flow is caused by the controlled leakage around the piston

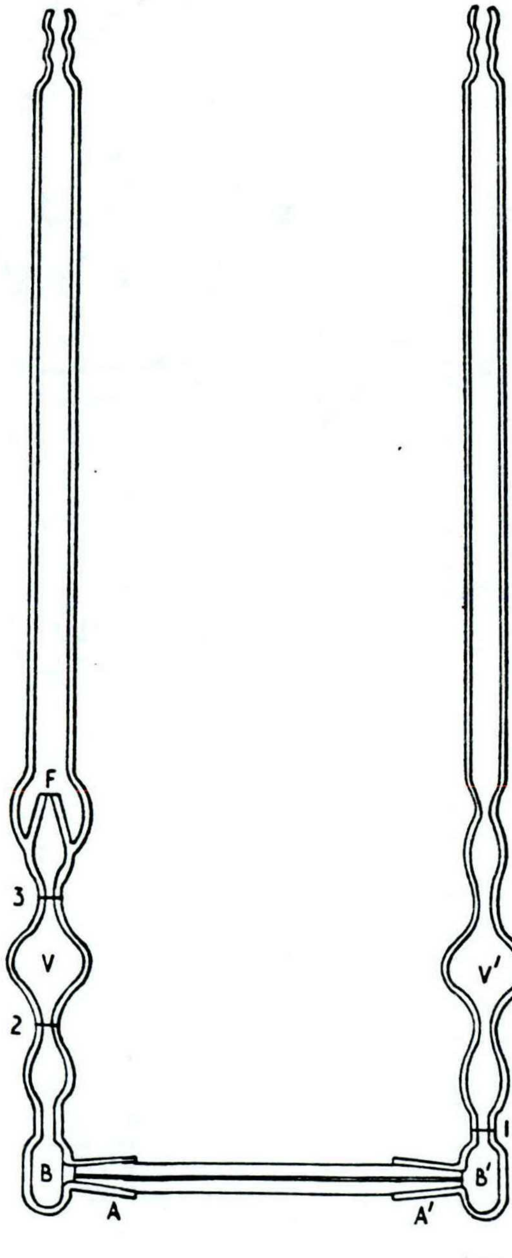

Figure 2.8 Bingham's viscometer which provides absolute pressure measurements

2.3.1.1 Assumptions made by Poiseuille

In 1846, Poiseuille was the first to develop the capillary viscometer as well as to derive the equations for viscosity. Of course specific assumptions need to be made when dealing with a capillary viscometer. It was assumed at the time:

(1) that there is a streamline flow within the tube;

(2) that the flow is steady and not subjected to accelerations at any point;

(3) that there is no slippage at the boundary layer with the walls of the tube, the liquid in contact with the wall is stationary;

(4) that the liquid obeys the Newtonian model.

This last assumption was made so that the relation between shear rate and shear stress would be linear, which would allow the derivation of an exact expression for viscosity.

2.3.1.2 Derivation of mathematical expression

Considering a capillary of radius a and length l with a pressure difference P between the ends.

Let the velocity of the liquid at a distance r from the axis of the capillary be v, the expression for velocity gradient D can be written as

$$D = -\frac{dv}{dr}$$

The force F acting on the cylindrical element of length l and radius r, coaxial with the capillary, is caused by the applied pressure P, see figure 2.9,

$$F = P \cdot \text{cross sectional area} = P \cdot \pi r^2$$

Due to the viscous resistance of the surrounding liquid, this force is counter-effected by the shearing force on the wall of the capillary cylinder, τ is the shear stress

$$F = \tau \cdot \text{cylindrical area} = \tau \cdot 2\pi rl$$

Thus, for these forces to balance

$$F = P \cdot \pi r^2 = \tau \cdot 2\pi r$$

$$\tau = \frac{Pr}{2l}$$

Newtonian behavior requires that $\tau = \eta D$, thus

$$\frac{Pr}{2l} = -\eta \frac{dv}{dr}$$

$$\frac{dv}{dr} = -\frac{Pr}{2\eta l}$$

Integrating this last expression, using the conditions that at the wall of the capillary $r = a$ and $v = 0$ gives the velocity distribution. The velocity distribution is parabolic, as shown in the following equation as well as in figure 2.10:

$$v = \frac{P(a^2 - r^2)}{4\eta l}$$

The volume of liquid flowing in unit time between radii r and r + dr is $2\pi rv$. The overall flow rate Q through the capillary is given by

$$Q = \int_0^a 2\pi r v \ dr$$

$$= \frac{2\pi P}{4\eta l}\int_0^a r\left(a^2 - r^2\right) \ dr$$

$$= \frac{\pi P a^4}{8\eta l}$$

Thus, the viscosity may be obtained from

$$\eta = \frac{\pi P a^4}{8Ql}$$

This last expression is known as Poiseuille's equation. It was first deduced by Poiseuille [Dinsdale, 1962].

2.3.1.3 Non-Newtonian fluids in a capillary

For the flow of non-Newtonian liquids in a capillary, Poiseuille's law is not obeyed because the flow rate is not proportional to the pressure gradient. In this case the calculations need to be done on the basis of the instantaneous pressure head (developed to force the liquid through the capillary) and the instantaneous flow rate.

It is thus possible to measure the viscosity of a non-Newtonian fluid with a capillary viscometer. The main difference here lies in the way the experimental data has to be acquired: not just measuring the total time and total force it takes for the liquid to flow but monitoring its progress throughout the capillary.

For non-Newtonian liquids an analytical expression is not obtained through calculus, like in the works of Poiseuille, but by fitting a curve through the shear rate versus shear stress plot obtained experimentally. These solutions are not exact and there are many ways of getting a satisfactory curve fit. This is the reason why there are many models in existence that describe the non-Newtonian viscous behavior of a liquid.

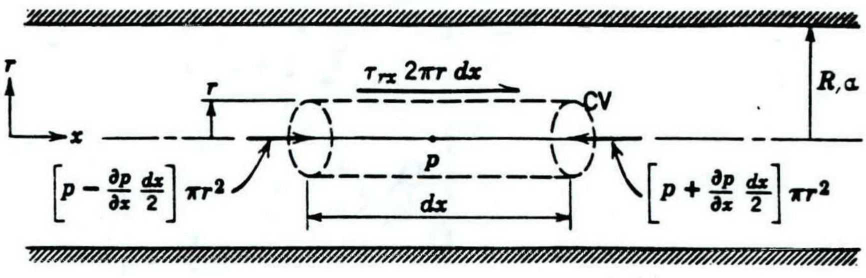

Figure 2.9 Flow in a circular pipe; the control volume assumed for the mathematical analysis of flow is represented by the dashed line

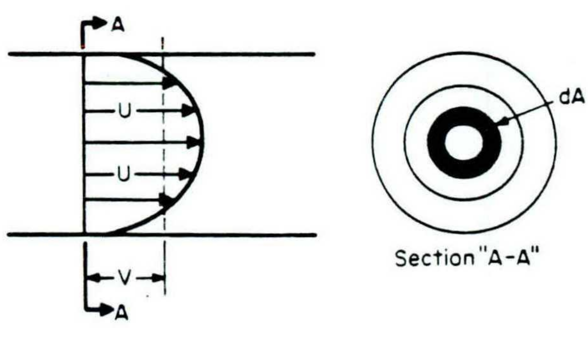

Figure 2.10 Parabolic velocity profile of a fluid in a pipe

2.3.1.4 Mathematical expression for non-Newtonian Bingham fluids

Analytical methods for deriving equations for viscosity with non-Newtonian fluids are only possible for the Bingham plastic materials. These fluids do have a linear relation between shear rate and shear stress, except that they differ form Newtonian liquids by an offset (see figure 2.3). This offset corresponds to the yield stress required to put the fluid in motion. The Buckingham-Reiner equation defines viscosity for Bingham materials:

$$Q = \frac{\pi a^4}{8lU}\left\{P - \frac{4p}{3} + \frac{p^4}{3P^3}\right\}$$

Where p is the pressure corresponding to the yield value [Dinsdale, 1962].

2.3.2 Rotational viscometers

The use of a rotational viscometer makes it possible to measure a variety of parameters characterizing the liquid. The use of this method for studying the mechanical properties is based on two features of the rotational viscometer:

(1) measurements are made under steady-state conditions and are homogenous over the volume of the specimen;

(2) prescribed conditions can be maintained over a an unlimited amount of time.

Under these conditions it is possible to observe the viscoelastic properties of a material. The same sample being used in different tests at different levels of shear rates readily indicates the non-Newtonian behavior of a specimen. Rotational viscometers are consequently widely used for the study of the flow properties of non-Newtonian materials.

Essentially a rotational viscometer comprises two members separated by the material under test, which are able to rotate relative to one another about a common axis. As one

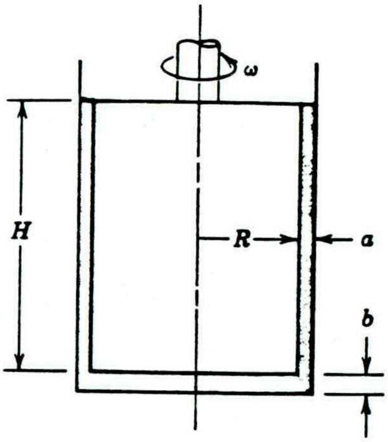

Figure 2.11 Cylindrical drum rotational viscometer

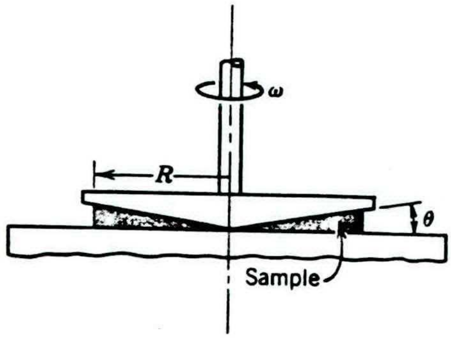

Figure 2.12 Conical rotational viscometer

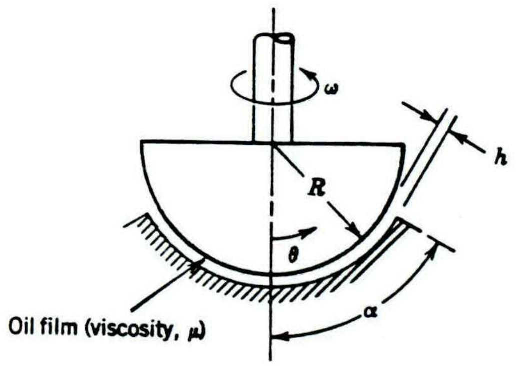

Figure 2.13 Spherical rotational viscometer

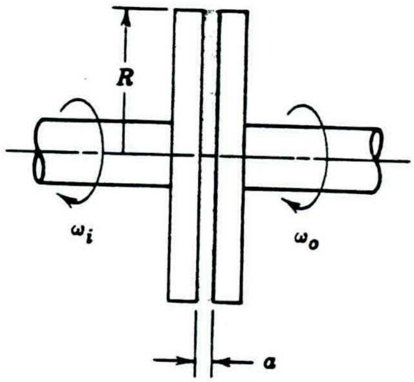

Figure 2.14 Flat plate rotational viscometer

member rotates, the other tends to be dragged. The test material transmits a torque to the second member. This torque may then be measured [Dinsdale, 1962].

The members of the rotational viscometers may take one of several shapes including coaxial cylinders or also conical or spherical forms. Flat plates, disks and paddles have also been used. Several devices are presented in figures 2.11, 12, 13, 14.

For non-Newtonian materials the shear stress is not directly proportional to the shear rate. Consequently the measured torque is not directly proportional to the angular velocity. Again the non-linear behavior it characteristic of the non-Newtonian fluids. Once obtained, this non-linear relationship is indicative of the specific behavior of the fluid, whether it is shear thickening or shear thinning or otherwise affected.

2.4 Experimental procedures described in literature

Control of semi solid processing requires the indispensable knowledge of the viscous behavior of the semi solid metal. Manufacturing of the raw semi solid metal billets has already lead to research on semi solid metal of different class with either high and low melting points.

This research has for the most part been conducted on laboratory equipment and specially built viscometers. The results obtained are thus limited by the ranges that are achievable on those specific machines. The maximum shear rate is often limited to a relatively low value.

Whereas these results are very helpful when analyzing the raw semi solid material, or when analyzing the raw material manufacturing processes, they do not remain indicative of the metal behavior that is observed within the die cavity and runner system of the semi solid die casting process. In the following paragraphs several of these studies will be presented.

2.4.1 Rheological research by Shinobu Okano

Okano has done some research and experimentations to determine some properties of semi solid metals such as: (1) viscosity; (2) growth rate of solidified shell; and their effect on production methods for raw material. The research on viscosity is of importance as it verifies the results of an analytical model.

Mori, Otake, et al. [1956] have derived an equation for the apparent viscosity of semi solid alloys (including Al-Cu and Al-Si). This formula has since been tested and satisfactorily compared with experimental results in the work of Okano. It takes into consideration the temperature, the shear rate and the solid mass fraction to determine the viscosity. As is, the formula is readily applicable, the coefficients having been approximated for shear rates up to 200/s.

$$\eta = \eta_{\infty}\left\{1+\frac{\alpha\rho C^{1/3}D^{-4/3}}{2\left(\frac{1}{fs}-\frac{1}{0.72-\beta C^{1/3}D^{-1/3}}\right)}\right\}$$

$$\alpha = 2.03\cdot 10^{2}\left(X/100\right)^{1/3}$$

$$\beta = 19.0\left(X/100\right)^{1/3}$$

η apparent viscosity in Pa s

η_{∞} apparent viscosity of liquid alloy in Pa s

ρ density of alloy at liquidus temperature in kg/m3

C average solidification rate in /s

D shear rate in /s

X main solute concentration in mass %

Figure 2.15 shows the relationship between the viscosity values calculated from these expressions and the viscosity obtained from measurements.

2.4.2 The Carreau viscosity equation

The Carreau viscosity equation has its origin in molecular network theories and accounts for all the features displayed by a pseudoplastic fluid in simple shear. This model has been developed primarily for polymeric solutions. This model is strongly non-linear with respect to the parameters and is of the form:

$$\frac{\eta - \eta_{\infty}}{\eta_{0} - \eta_{\infty}} = \left\{1 + (\lambda D)^2\right\}^{\frac{n-1}{2}}$$

η apparent viscosity in Pa s

η_{∞} viscosity at infinite shear rate in Pa s

η_{0} viscosity at zero shear rate in Pa s

D shear rate in /s

n parameter ($n < 1$)

λ parameter

n and λ are two disposable curve fitting parameters. Some typical values are indicated in the following table.

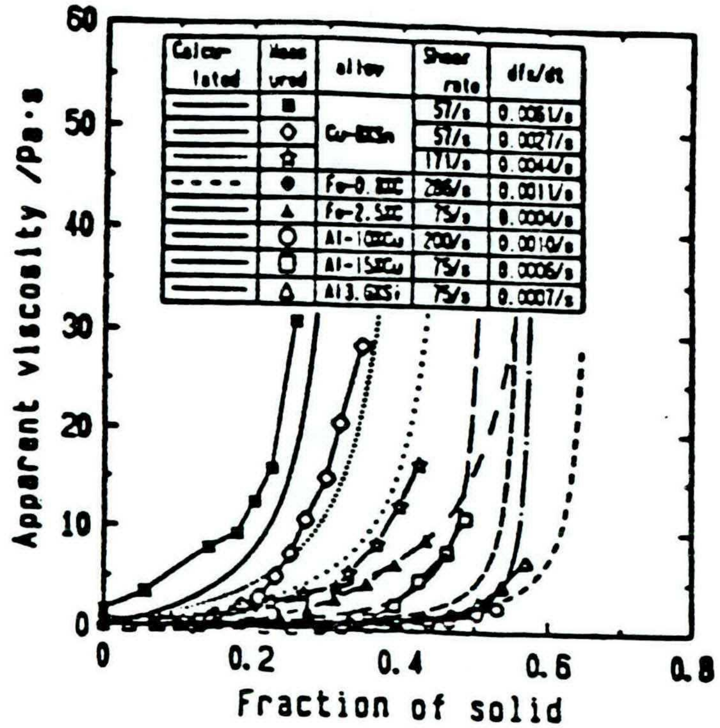

Figure 2.15 Results for Okano for several semi solid metals

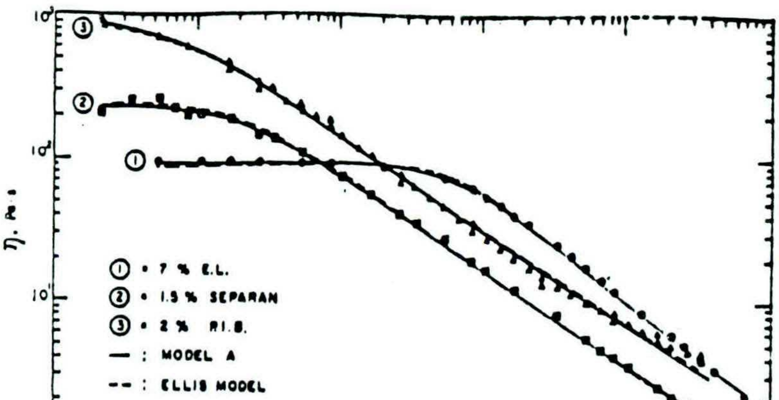

Figure 2.16 Viscous behavior from Carreau model for non-Newtonian fluids, from Bird

Material	η_0	η_∞	λ	n
2% PIB in primol 355	923	0.15	191	0.36
7% Aluminum soap in decalin	89.6	0.01 - a	1.41	0.2
High density polyethylene	8920	0 - b	1.58	0.5

a - Assumed to be equal to solvent density

b - Assumed

Table 2.1 Typical values of Carreau model parameters [Bird, 1987]

The method for using the Carreau equation is as follows:

1. With a viscometer, take measurements of shear rate in function of shear stress
2. Then plot these values on a graph
3. Curve fitting (regressions, etc.) will provide the parameters n and λ that describe the viscosity according to the Carreau model.

2.4.3 Rheological research by W. R. Loué

Up until recently it was found that most rheological behavior had been established mostly on the basis of parallel plate compression tests. In these tests the maximum shear rates that were reached did not exceed 0.1 /s[Laxmanan 1980, Suéry 1982, Pinsky 1984, Seconde 1984] These values of shear rate are evidently not representative of those achieved during industrial forming processes of semi solid metals. Loué thus investigated the rheological behavior of semi solid metal for shear rates up to at least 1000 /s. To that end a special backwards extrusion machine was built. A schematic of this apparatus is given in figure 2.17.

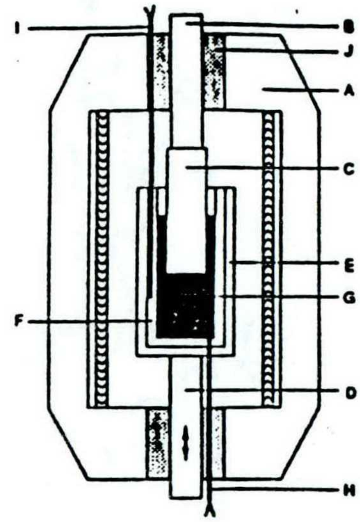

Figure 2.17 Backwards extrusion apparatus used as a viscometer by Loué

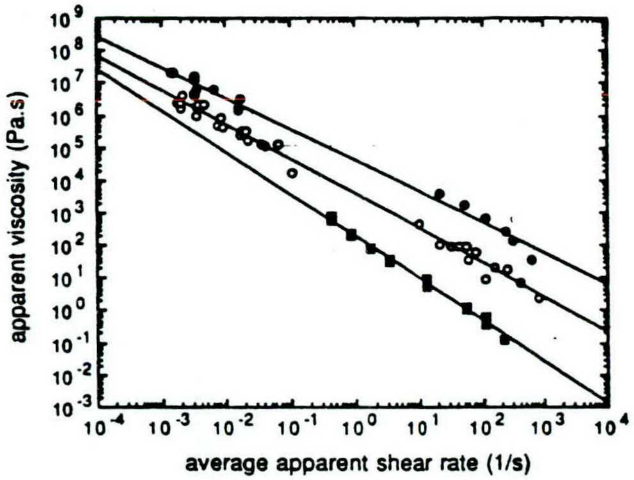

Figure 2.18 Results from Loué for semi solid aluminum at different fraction solid levels for Al-Si alloys with (●) 55% (○) 45% and (■) 30% fraction solid; the results at low shear rate are obtained from a compression test and the results at high shear rate, from the backwards extrusion test; the results for ■ are obtained by Searle viscometry

The machine consisted of a ram and a crucible in which the semi solid metal was placed . During the experiment the ram is pushed into the soft metal at a constant speed. The metal is thereby pushed out of the pot at a constant flow rate. The container was itself attached to a force transducer in order to measure the pressure gradient that was present at the time that the metal was being extruded.

The extrusion is done in the opposite direction of the ram displacement. This allows for an easy and accurate installation of the force transducer.

A set of equation was derived to compute first, the mean value of shear rate, then the viscosity value. This equation is based on mathematical theory governing extrusion processes.

$$\eta = \frac{1}{2\pi\lambda C_1 V_r}\frac{dF}{dt}$$

$$\lambda = \frac{R_c^2}{R_c^2 - R_p^2}$$

$$C_1 = \frac{1}{\ln\left(\frac{R_p}{R_c}\right)}\left(C_2\left(R_c^2 - R_p^2\right) - V_r\right)$$

$$C_2 = \frac{V_r}{\left(R_c^2 - R_p^2\right) - \left(R_c^2 + R_p^2\right)\cdot\ln\left(\frac{R_c}{R_p}\right)}$$

η apparent viscosity

V_r velocity of ram

R_C radius of container

R_P radius of piston

C_1 constant

C_2 constant

λ constant

2.4.4 Other rheological studies

Rheological behavior of metals were also studied by the following individuals, among others: H. K. Moon et al., 1991; S. P. Wang et al.; Flemings, 1991; M. R. Barkhudarov et al.; P. Kumar et al., 1992; Joly; and D. Gosh et al., 1991.

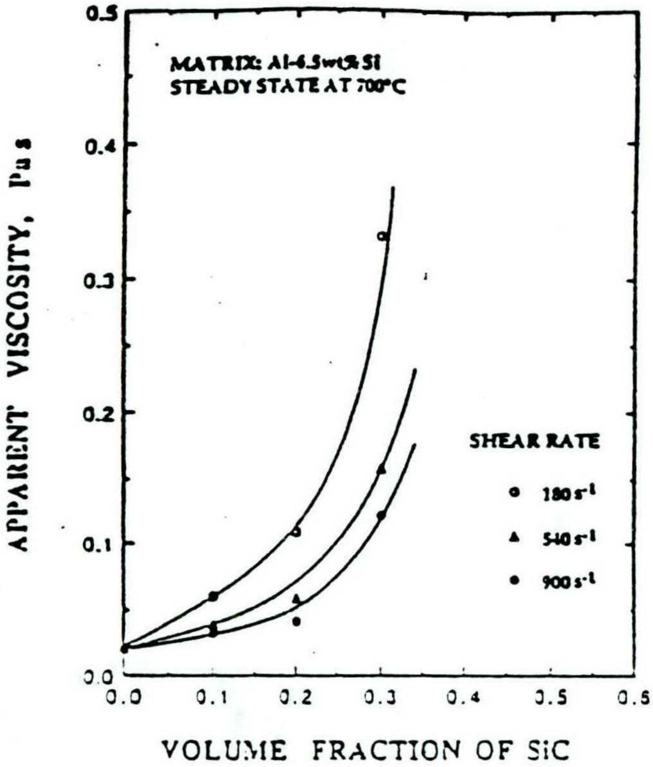

Figure 2.19 Results for Moon for Al-6.5wt% Si at steady-state temperature

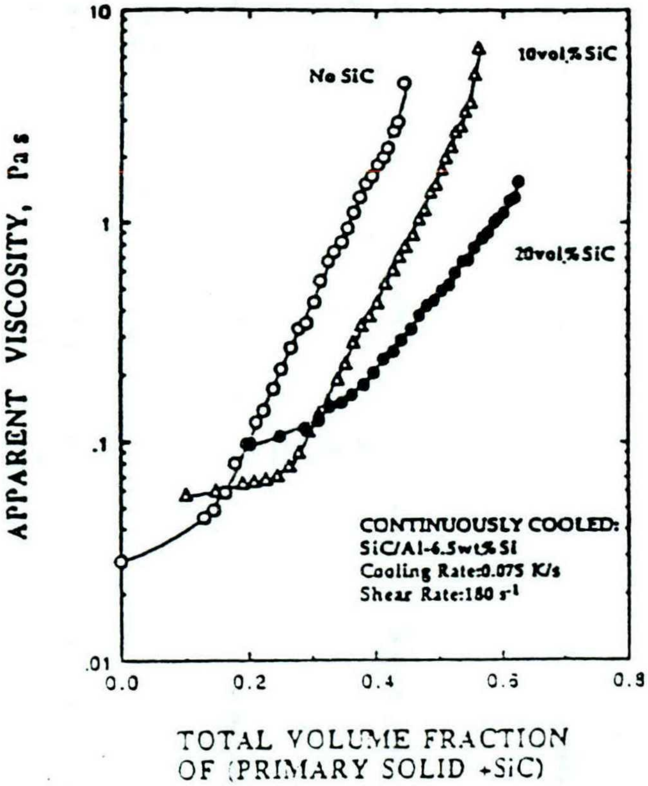

Figure 2.20 Results for Moon for Al-6.5wt% Si continuously cooled

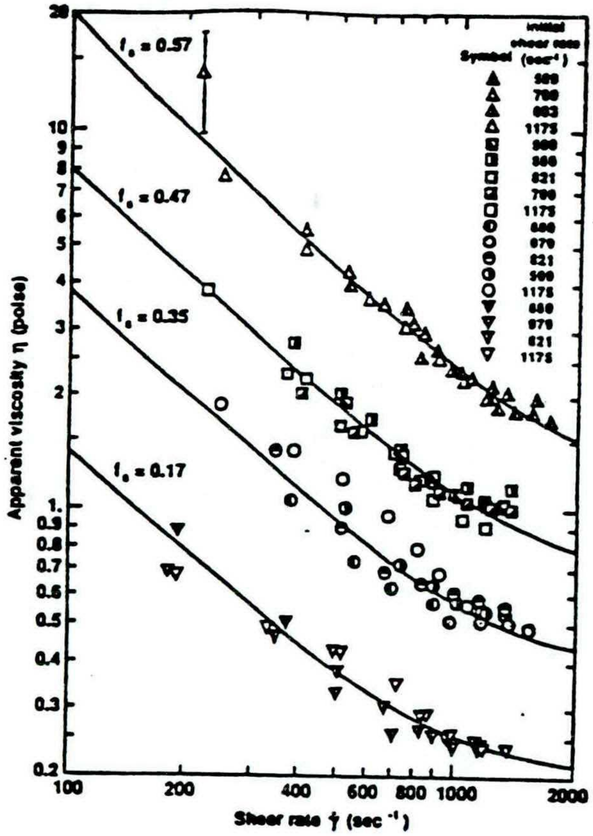

Figure 2.21 Results from Wang for Sn-15wt% Pb

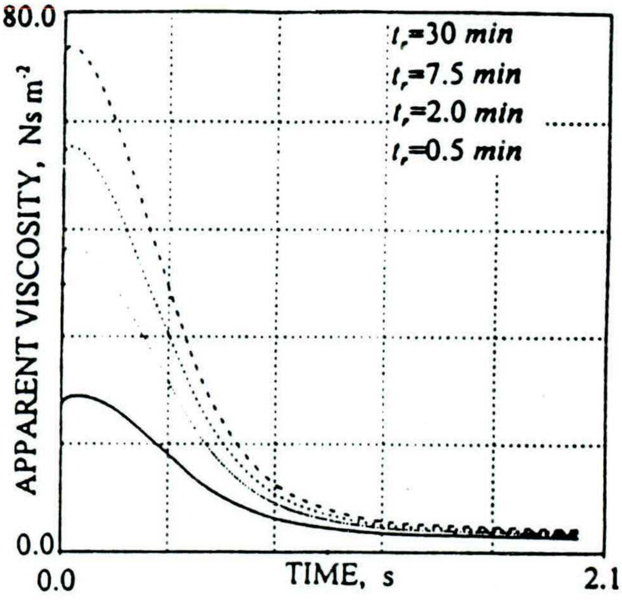

Figure 2.23 Results from Barkhudarov for Sn-15wt% Pb

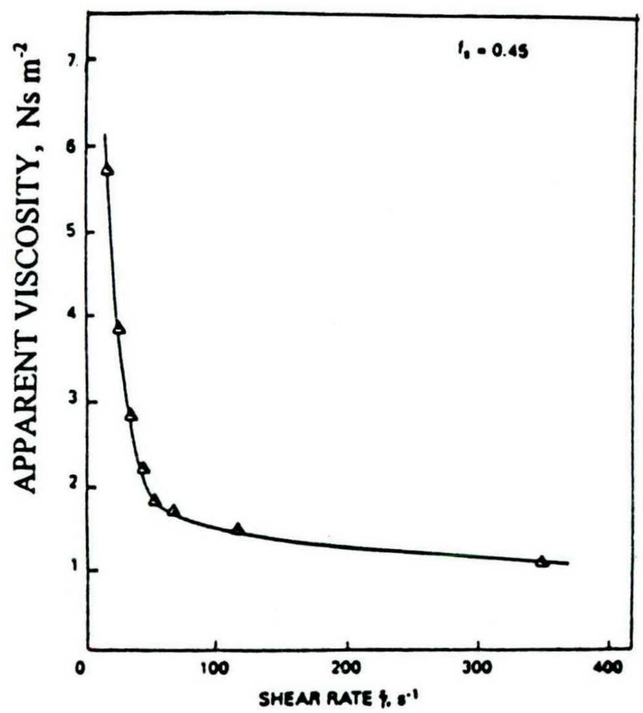

Figure 2.24 Results from Joly, Kumar for Sn-15wt% Pb

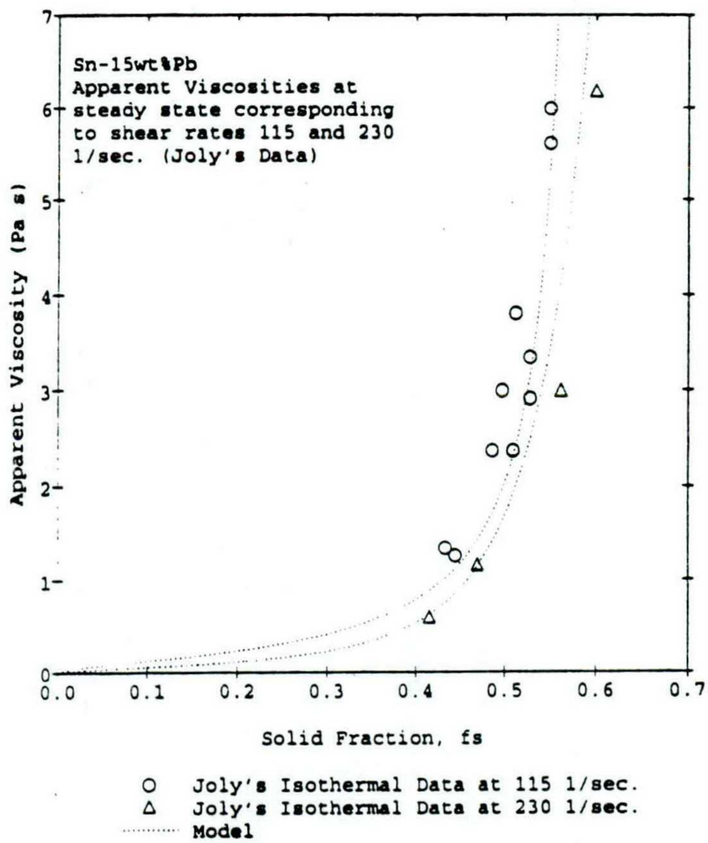

Figure 2.22 Results from Flemings for Sn-15wt% Pb

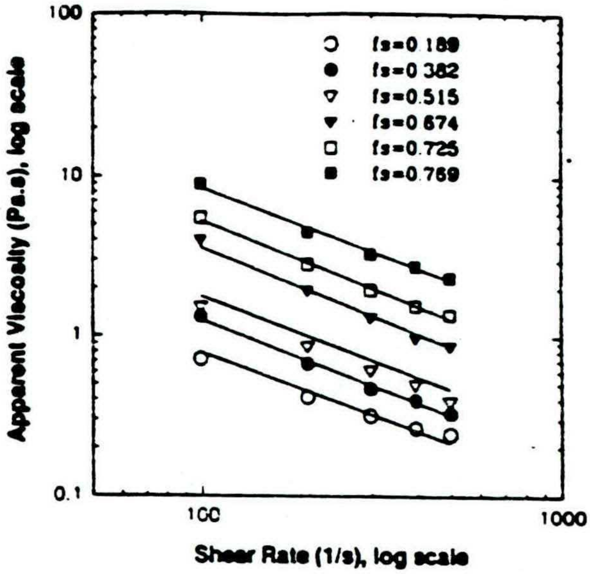

Figure 2.25 Results from Gosh for semi solid magnesium alloy AZ91D

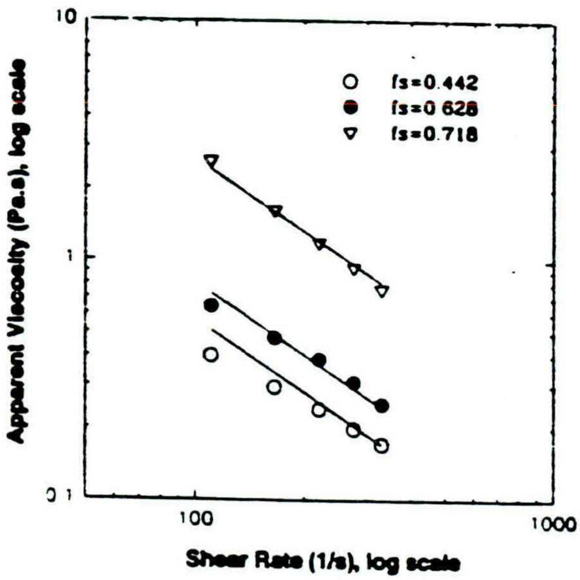

Figure 2.26 Results from Gosh for semi solid magnesium alloy AM50

Plots of the most significant results are shown in figures 2.19 sqq. while the relative value of each of these studies towards the focus of this paper are presented in the following table.

	Material		Viscosity obtained in function of:				
Research	Aluminum	Other	Shear rate	Time	Geometry	Solid fraction	% Composition
Mori, Okano	X	Cu; Fe	X			X	X
Carreau		Polymer	X				
Loué	X		X		X	X	
Moon	X		X			X	
Wang		Sn-Pb	X			X	
Flemings		Sn-Pb	X			X	
Barkhudarov		Sn-Pb		X		X	
Joly, Kumar		Sn-Pb	X			X	
Gosh		Mg	X			X	

Table 2.2 Compared studies

2.5 Semi solid casting process characteristics

Semi solid metal die casting is a method of producing finished castings by forcing mushy metal into a hard metal die. The die is arranged to open once the metal has solidified so that the casting may be removed.

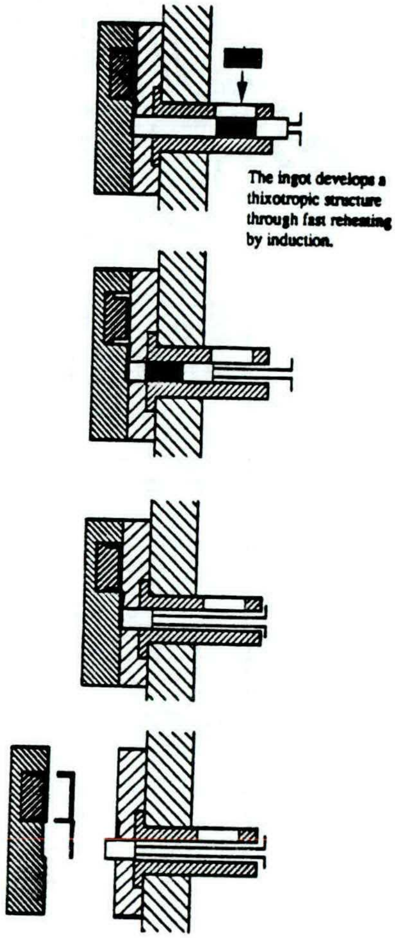

Figure 2.27 Semi solid die casting process

Once the die halves are closed and locked by the clamping force of the machine the injection phase may begin. The billet, previously heated until it became mushy, is placed in the shot sleeve. Then the plunger advances and pushes the metal into the die cavity. To prevent a premature solidification, rapid filling is desirable. The typical filling occurs within milliseconds.

Filling patterns show that the metal is initially squeezed until it fills the entire section of the shot sleeve. It then proceeds up the runner, then through the gate and finally fans out into the part cavity. Once the cavity is full, the remaining space in the various vents are filled. These vents are located in the extremities of the casting which the injected metal reaches last. During a final consolidation phase, more pressure may be applied to the shot so as to fill-in any voids.

2.6 Manifestations of viscous behavior

Several features are indicative of the viscous properties of the metal that is used for semi solid aluminum die casting.

2.6.1 Partial cavity filling

The metal along its path fills these cavities in a successive order: (1) the piston sleeve; (2) the runner; (3) the gate; (4) the part cavity and (5) the vents. Experimental step-casting have shown this progression. Step-castings are obtained when the injection cycle is cut short at a specified level of filling. For instance, partial fillings of 30, 60 and 90% of the total volume will produce castings that represent the frozen evolution of the metal in the die assembly at various stages.

2.6.2 Viscometric measurements

A semi solid metal, when properly heated, possesses a gradual resistance to change of form. This property acts very much like a sort of internal friction. Thus, when this gradual resistance is measured it is possible to obtain viscosity.

There are two principal methods for quantifying viscosity: (1) the dynamic viscosity, which is the ordinary viscosity derived form Poiseuille's work and is measured in units of pressure times seconds; whereas (2) the kinematic viscosity is the ratio of ordinary viscosity to density, and it is measured in units of area per time.

2.6.2.1 Kinematic viscosity

The kinematic viscosity is used chiefly when dealing with gravity type viscometers where no external pressure is required to force the liquid through a capillary. Gravity viscometers rely on the pressure arising from the head of the liquid being tested. Since this pressure is proportional to the density of the liquid, these instruments readily measure the kinematic viscosity. The principal unit used for kinematic viscosity is the Stokes (cm2/s) and the centistokes.

2.6.2.2 Dynamic viscosity

The dynamic viscosity was developed by Poiseuille as early as 1846 [Dinsdale, 1962]. The first units used were therefore the Poise (gm / cm s) and the Centipoise. A unit that is similar but more modern is the Pa s (Pascal second).

$$1 \ \text{Poise} = 1\frac{\text{gm}}{\text{cm} \cdot \text{s}}$$

(1 Centipoise = 0.01 Poise)

$$1 \ \mathrm{Pa \cdot s} = 1\frac{\mathrm{N}}{\mathrm{m^2}} \cdot \mathrm{s} = 1\frac{\mathrm{kg \cdot m}}{\mathrm{s^2}} \cdot \frac{\mathrm{s}}{\mathrm{m^2}} = 1\frac{\mathrm{kg}}{\mathrm{m \cdot s}}$$

Tables that list the viscosity of various liquids and gases, such as those that can be found in the *Handbook of Chemistry and Physics,* use chiefly the unit of Poise and Centipoise. American units for viscosity exist, such as the lb / ft sec, though seldom uses.

For practical reasons that are explained further the dynamic viscosity was used for this research. The unit of Pa s was retained, as it is consistent with the new MKS and SI systems rather than the old CGS system of units, while the Poise is in units of the CGS system.

2.7 Modeling of flow in semi solid metal casting experiments

Just as in the research conducted by Loué, traditional viscometry has not been found to relate to a manufacturing environment. Rheological measurements need to be taken at much higher shear rate ranges.

There exists a similitude between the operation of a die casting machine and that of a capillary viscometer. This similitude is even more obvious between the die casting machine and the experimental backwards extrusion viscometer built by the team of Loué. With the correct assumptions and correct mathematical treatment, the SC control system of the Bühler functions on the same principles than a capillary viscometer, working precisely in the ranges of particular interest to die casting of semi solid aluminum.

2.7.1 Physical analogies

The main feature of a capillary viscometer is the capillary tube which acts as a flow restriction along the path of the liquid. The size and nature of the restriction is well known and recorded for use in mathematical formulae. In a die casting machine, providing the die cavity is suitably designed, it too can act as a flow restriction.

Whereas in a capillary viscometer the pressure to move the liquid may be applied externally, in the Bühler H-250 the force is applied by the piston plunger.

2.7.2 Measurement analogies

The data available on the data acquisition system of the Bühler SC suits just the purpose of the viscosity equations. Just as for the capillary viscometer, values for the flow rate and for the pressure gradient can be obtained.

Using the sophisticated data acquisition of the Bühler SC allows for accurate and reliable measurements.

2.7.3 Operating analogies

The mathematical analysis of the capillary viscometer requires that a few assumptions be made. Consequently these assumptions have to hold as well in the die casting environment.

In summary, the Bühler H-250 SC with its digital control and its digital and graphical displays can provide all the necessary information for viscosity measurements.

Other knowledge that is pertinent to the viscous behavior of semi solid metal is obtained by devices external to the die casting machine itself. This includes the temperature measurements of the re-heated billet and the temperature measurements of the die.

Some after the fact knowledge can even be obtained by observing the microstructure of the cast part in various locations of the casting. These observations on the microstructure coupled with knowledge of the composition of the samples (such as can be obtained by a scanning electron microscope) can further yield information about the fraction solid content in the metal as it was being cast. This all serves to refine the rheological analysis of the semi solid metal aluminum.

2.8 Computer simulation

2.8.1 Using Flow 3D

Flow 3D is a software package that is used to simulate fluid flow. It has the intrinsic capability to simulate the flow of non-Newtonian fluids. For that reason it is a powerful tool when it comes to simulating the casting of semi solid materials.

These simulation packages are important and useful in the developmental stages of a die design. Accurate simulations may very well eliminate some of the expensive iterative processes used in finalizing the design of a die.

2.8.2 Viscosity database in Flow 3D

Flow 3D does not infer the viscosity of a fluid from a numerical database, but rather uses an analytical model to compute the viscosity in function of shear and temperature. Thus correctly defining the parameters that make up this analytical model is the key to developing successful simulations.

2.9 Nature of this research

The usefulness of the rheology having been described, the next chapter gives the specific steps that were taken in order to use the Bühler SC die casting machine. The Bühler SC was used following the methodology specific to viscometric measurements.

Complemented by a thorough microstructure analysis, the nature of this research is essentially experimental with results in the specific fields of application.

CHAPTER 3

EXPERIMENTAL WORK & RESULTS

3.1 Rheological experiment with the Bühler H-250 SC

3.1.1 Equipment

The equipment that was available for this research is remarkable for the fact that it consists of truly industrial and manufacturing machines. The results obtained are thus representative of true die casting operating conditions, and are not the result of an attempt to recreate these conditions in an experimental setup.

The following equipment was used:

1. Bühler H-250 SC die casting machine [Bühler]

    - The SC technology offered by Bühler provides a high dynamic shot capacity that ensures universal application of the machine in the field of high pressure die casting as well as for the processing of semi solid metal [Bühler]. The entire spectrum of extremely thin-walled die castings up to thick-walled components is covered.
    - SC machines come with a real time control ensuring that the pre-selected shot curve is actually followed, regardless of disturbances such as dynamic head pressure, temperature fluctuations, etc.
    - Variability of shot profile curve programming for optimum cavity filling

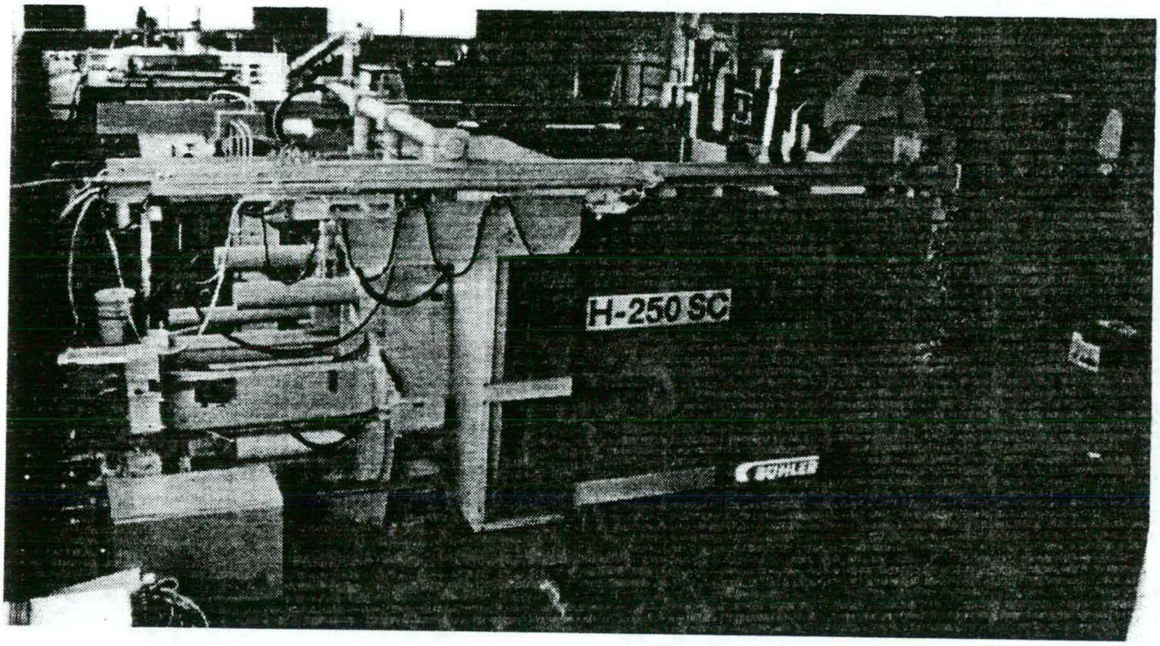

Figure 3.1 250t Bühler H-250 SC die casting machine

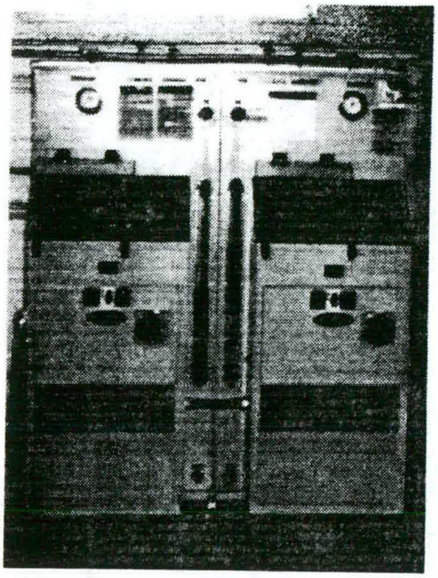

Figure 3.2 Sterling temperature control unit

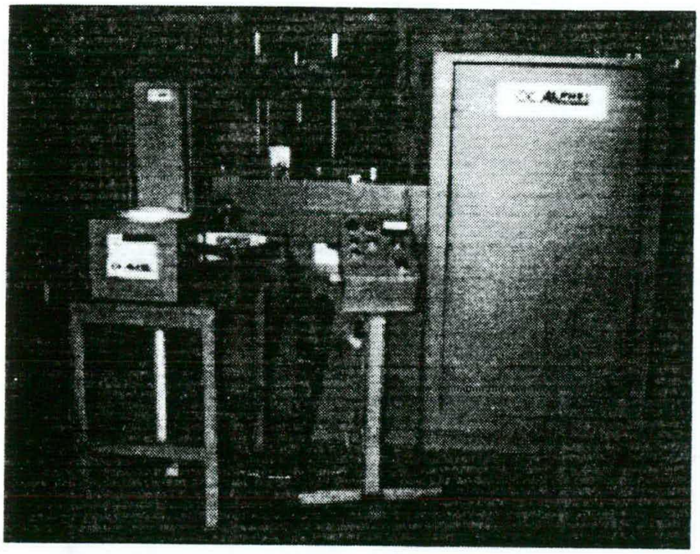

Figure 3.3 Alpha 1 Induction heating unit

- Programmable pressure intensification phase for selective final metal feed
- Excellent reproducibility of the shot parameters form shot to shot
- The control system is composed of a PLC control with standard components and subordinated microprocessor system for computing functions
- Nominal / actual display of the shot curves for a high process transparency
- All operating parameters displayed by color graphics with a good overview
- Data carriers in the form of hard disk and floppy disk

The main research was performed on the Bühler SC, however additional equipment was required for the heating of the die unit and for the heating of the metal billets. This equipment consisted of the following:

2. Sterling temperature control unit with dual zone for die and shot sleeve independent heating and cooling
3. Alpha 1 single coil induction heating unit, 100 kW, 600 - 1000 Hz

3.1.2 Data acquisition

The data acquisition system of the is a part of the programmable controller.

All the data necessary for the calculation of the viscosity are related to the piston plunger speed, position and force. For the experiment the data was gathered on the *Datacess* (TM) control system of the Bühler H-250 SC.

The *Datacess* is very flexible in the way it may be configured for data output. Options include the selection of data values, the various sampling rates, specific triggering points, duration of data recording and many more features that enhance the transfer of data and plotting capabilities of the machine.

Through either of two data monitoring systems, *Lancast* (TM) and *Provis* (TM), hard data may be recorded. Figure 3.4 presents a typical plot that fits the purpose of this project.

There are three pairs of curves that represent pressure p, position s and velocity v. For this particular graph the scale on the abscissa is in time increments while the ordinate represents (1) the pressure measured in bar, (2) the position measured in mm, and (3) the velocity measured in m/s.

Parameter	Symbol	Preset	Actual	Unit
position	s	sI	sI*	mm
velocity	v	vI	vI*	m/s
pressure	p	pI	pIK	bar

Table 3.1 List of parameters used by Bühler

Each pair consists of two curves: one to represent the set value and an other one for the actual value. A selection of these data plots is presented in the appendix.

Note:

On the graph, the two curves in a pair are offset by a specific value so as to create a visual difference between the two when they read the same value.

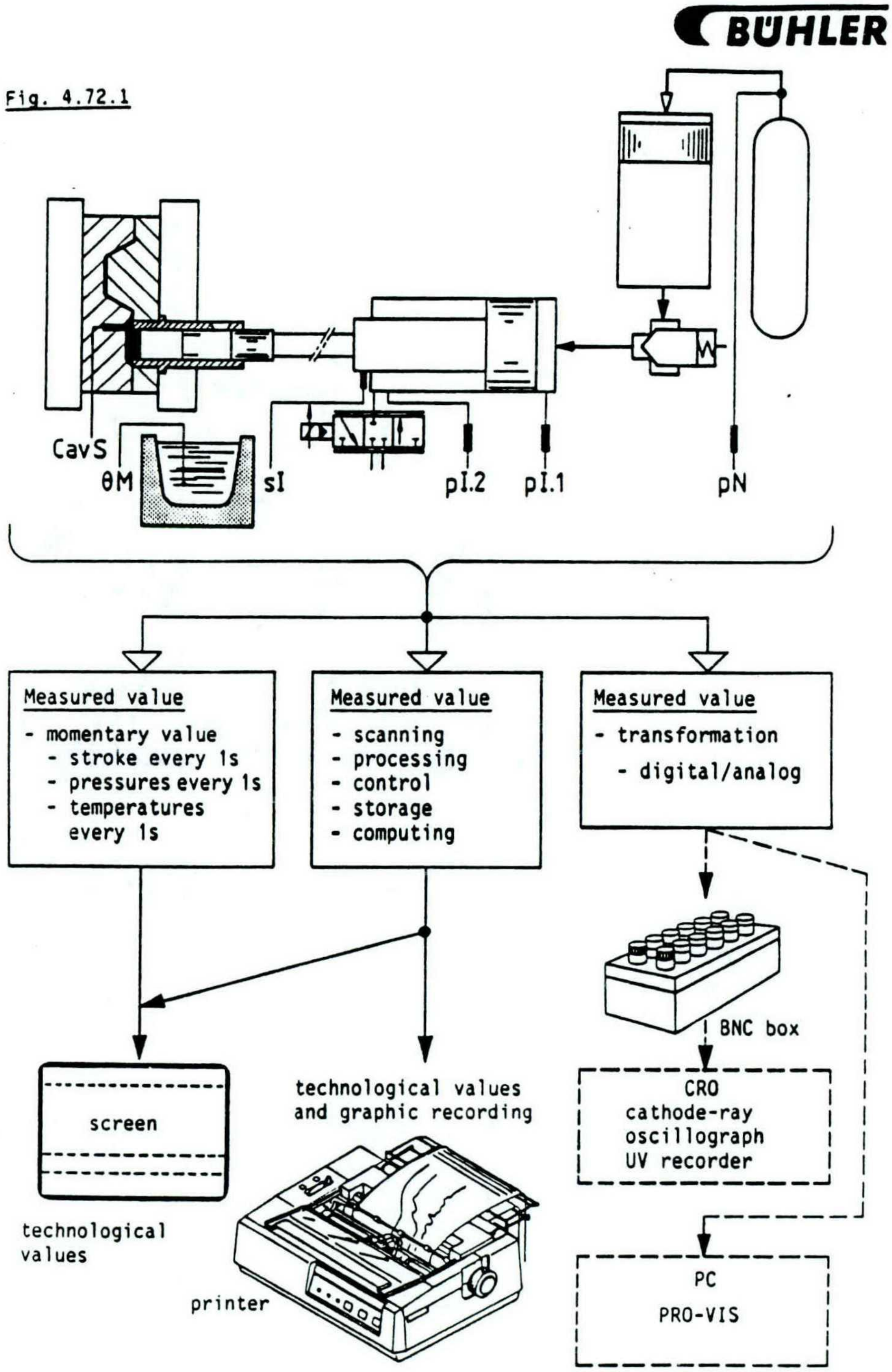

Figure 3.4 Lay-out of Bühler data acquisition devices

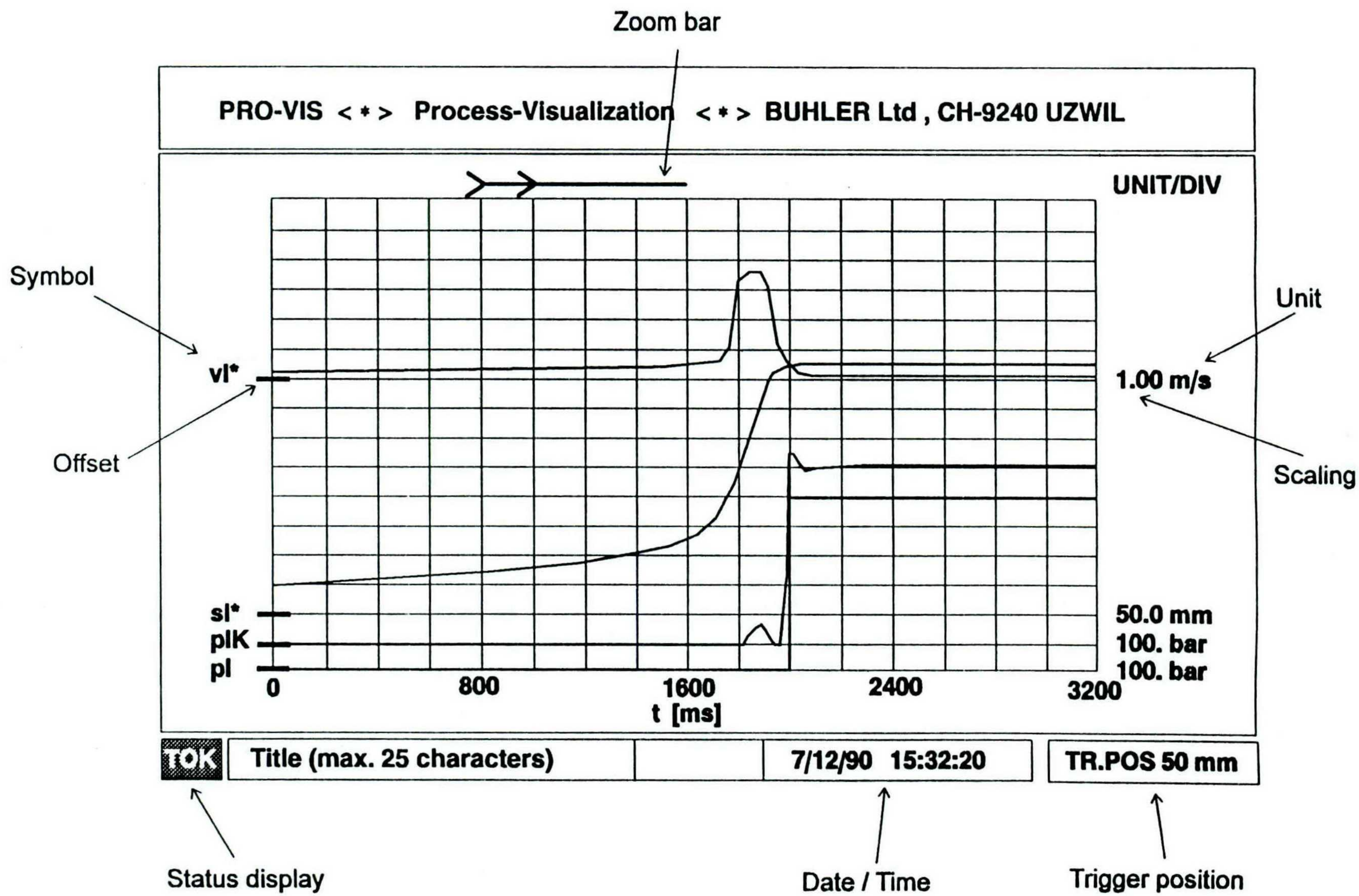

Figure 3.5 Single shot plot output of Pro-Vis data recorder displaying actual values for velocity, position and pressure

3.1.3 Control system

3.1.3.1 Feedback

The goal of the PLC controller of the Bühler is to match the operation of the machine with the set values entered by the operator. The actual position, pressure and velocity values are continually measured and constitute the feedback for the control system, see figure 3.6. When the difference between the set value and the measured value indicate a deviation a correction is immediately made. The use of a control system with feedback results in reproducible casting movements [Bühler].

3.1.3.2 Break-point

The control of the casting phase is divided into two portions: (1) the filling phase and (2) the consolidation phase. The switch between filling and consolidation phase occurs at the break-point *Br*. The break-point is set in relation with the type of cavity filling that is desired. Such schemes may include a slow approach, or sensing the metal at the gate (with an optional metal front sensor), or determining when the cavity is full.

The break-point, whether it is set manually or occurs automatically, separates two distinct modes of operation of the control system.

When a casting cycle is initialized the machine is in speed control. The plunger will push the metal into the cavity at the specified velocity values. In this mode the feedback for the controller comes from the actual velocity of the plunger. This situation remains active up until the piston has significantly lost its speed. This is the break-point. So far the pressure seen on the plunger (p curve) has been measured as a free variable but has not been a part of the control system; no pressure control is exerted yet.

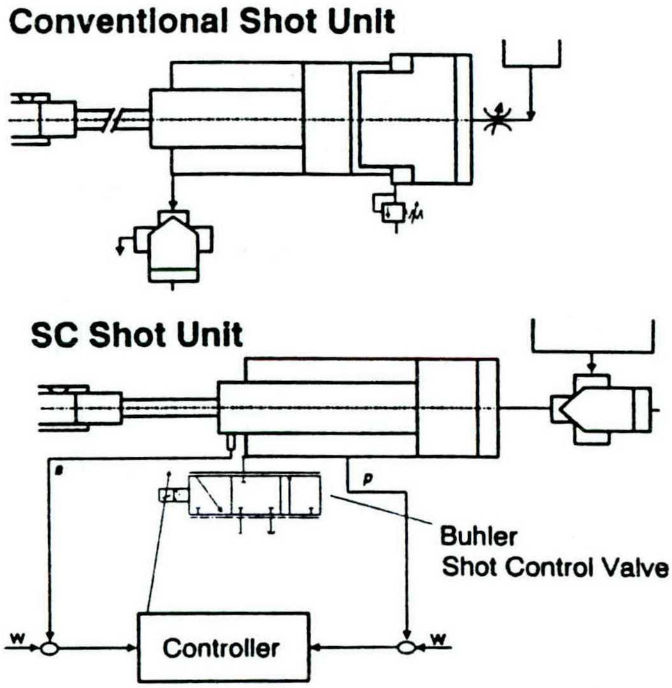

Figure 3.6 Description of Bühler SC shot control for plunger piston actuator; unlike the conventional shot unit, the SC control system is equipped with feedback (s) for velocity / position control mode and (p) for intensification pressure control

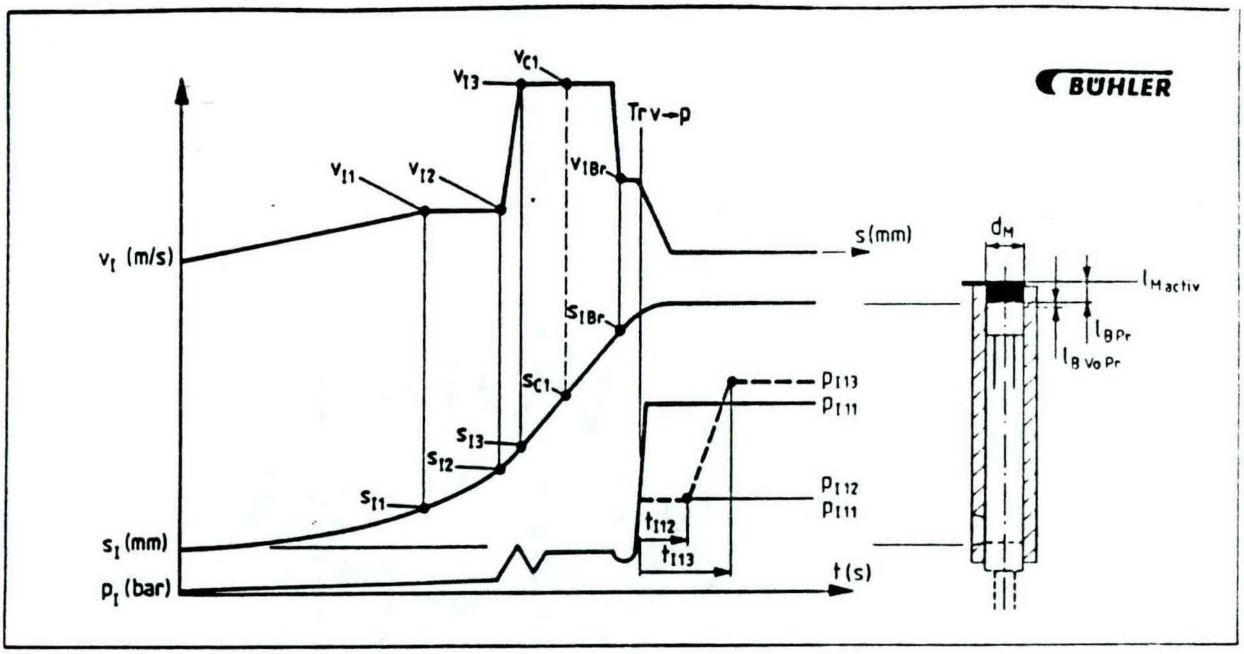

Fig. 4.70.2

INJECTION UNIT: TABLE P. 1/2

STROKES		SPEEDS		TIMES		PRESSURES	
s I1	2ØØ.	v I1	Ø.5Ø			p I11	15Ø.
s I2	34Ø.	v I2	Ø.5Ø	t I12	Ø.Ø5Ø	p I12	15Ø.
s I3	37Ø.	v I3	4.5Ø	t I13	Ø.Ø75	p I13	3ØØ.
s I4				t I14	Ø.1ØØ	p I14	3ØØ.
s I5				t I15	Ø.125	p I15	45Ø.
s I6				t I16			
s I7				t I17			
s I8							
s I9							
s IBr		v IBr	2.ØØ				
s IBr K	48Ø.					profile-Go	

Figure 3.7 Settings of shot parameters with break-point Br defined in the velocity and position listings

When the motion of the piston is nearly stalled because the cavity is nearly full, the operation mode will switch to the consolidation phase. At this point the deviation indicated by the velocity feedback are not indicative of the casting operation. As the velocity feedback becomes obsolete, the pressure feedback gains in significance.

Past the break-point, the aim of the controller is to match the actual pressure curve with the set pressure curve in order to obtain the desired intensification phase. Now it is the turn of the velocity measurement to become the free variable.

3.1.4 When the machine acts as a viscometer

The capillary viscometer analogy holds until the occurrence of the break-point. The machine operates with a set flow rate while the incurred pressure is measured. The viscosity analogy functions only in speed control when the machine operation follows the set velocity values and when the pressure observed on the plunger is measured and recorded while no external pressure control is enacted. In fact, velocity control and pressure control cannot physically be used at the same time.

3.1.5 Recorded data

For each shot, numerical data can be obtained from the graphs and transposed into tables. The raw data consists of position, velocity and pressure in function of time. But before the viscosity values may be obtained, values for shear stress and shear rate have to be calculated. Sample calculations are presented in the appendix.

3.1.6 Mathematical treatment

The characteristic of the capillary tube viscometer is that it offers a flow restriction to the passing liquid. It is this flow restriction that allows the subsequent viscosity measurements.

In the case of the die used in this experiment, the necessary flow restriction is also provided.

Unlike the capillary viscometer, the die geometry does not provide cylindrical channels. In Poiseuille's law the geometry is described by only one radius. Due to that fact several simplifications on Poiseuille's formula are possible. For the purpose described here a less general form of Poiseuille's law is necessary, were the values of the radii are all individually kept.

$$\eta = \frac{\tau}{D} = \frac{\pi P a^4}{8Ql}$$

This was the form of the equation of Poiseuille that was obtained earlier.

Viscosity is given by the ratio of shear stress τ to shear rate D, this ratio may thus be de-coupled in Poiseuille's formula in order to yield the following:

$$\eta = \frac{Pa}{2l} \cdot \frac{\pi a^3}{4Q}$$

Now taking into account several simplifications that were made earlier, it is possible to rewrite:

$$\tau = \frac{Pa^2\pi}{\pi 2al} \qquad \text{and} \qquad D = \frac{4Q}{\pi a^2 \cdot a}$$

Without assimilating all radii values of a to a same constant, but identifying them separately we get:

$$\tau = \frac{\text{pressure} \cdot \text{section}}{\text{cylindrical area}} \qquad \text{and} \qquad D = \frac{\text{flow-rate}}{\text{section} \cdot \text{width}}$$

This formulation now takes into account the specific variations in geometry of the experimental die.

As a recall, the shear stress is the ratio of force applied to move a specific section of liquid, to the area of the "sleeve" in which the liquid flows. The shear rate is the ratio of flow velocity through a channel, to the distance from the wall of the channel at which this flow velocity is occurring.

3.1.6.1 Effect of changes in die geometry

The die that was used for this experiment consisted of a simple flat plate. The die cavity can be roughly divided into two major zones: (1) the runner, and (2) the plate. These two areas a very different compared to each other thus requiring different mathematical treatment.

However, both these sections are linearly uniform. That is to say that from the time the metal enters the flat plate itself, it will not encounter any geometry variation until the plate is full. The metal then enters the next cavity: the vents. The same holds true for the runner while the gate provides a transition section between the runner and the plate.

Further more, the transition zone offered by the gate acts as a buffer before the filling of the plate occurs. Shear stress calculations show that the plate offers more of a resistance to the filling than the runner, and that the gate offers less resistance than either of the plate or runner. For that reason this die geometry offers the possibility of computing the viscosity for two sections in one run.

During the filling of the die cavity, the runner will act as the first capillary restriction. Then the gate will buffer the flow without disturbing the flow in the runner. Finally, while the plate is filling, the second set of calculations can be performed on this second restriction.

The specifics of the die geometry can be obtained from figure 3.9. The values of shear rate expressed in function of the velocity of the plunger (which sets the flow rate) are given in the next table. Values have been computed for the various significant portions of the die cavity.

	Piston chamber	Runner	Plate
Metal velocity	U (plunger speed)	7.86·U	4.23·U
Shear rate D	0.037·U	1.25·U	1.7·U
For the following piston speeds we see:			
at U = 2 m/s	D = 74 /s	D = 2500 /s	D = 3400 /s
at U = 3 m/s	D = 111 /s	D = 3750 /s	D = 5100 /s

Table 3.2 Values for shear in the flat plate

3.1.6.2 Influence of shot profile parameters

The programming capabilities of the Bühler H-250 SC are such that the shot profile parameters may all be set individually thus allowing a precise control of the casting operations. With regards to viscous behavior, these parameters may have an important effect.

3.1.6.2.1 Influence of the velocity of the shot plunger

The plunger velocity setting is the most influential inasmuch as the viscous behavior is concerned. Modifying this velocity consequently modifies the metal flow rate. This is true whether the velocity is changed between different set-up or during the casting cycle.

Increasing the flow rate also increases the individual flow velocities at different sections of the cavity being filled. These modifications, in turn cause modifications of the shear rate.

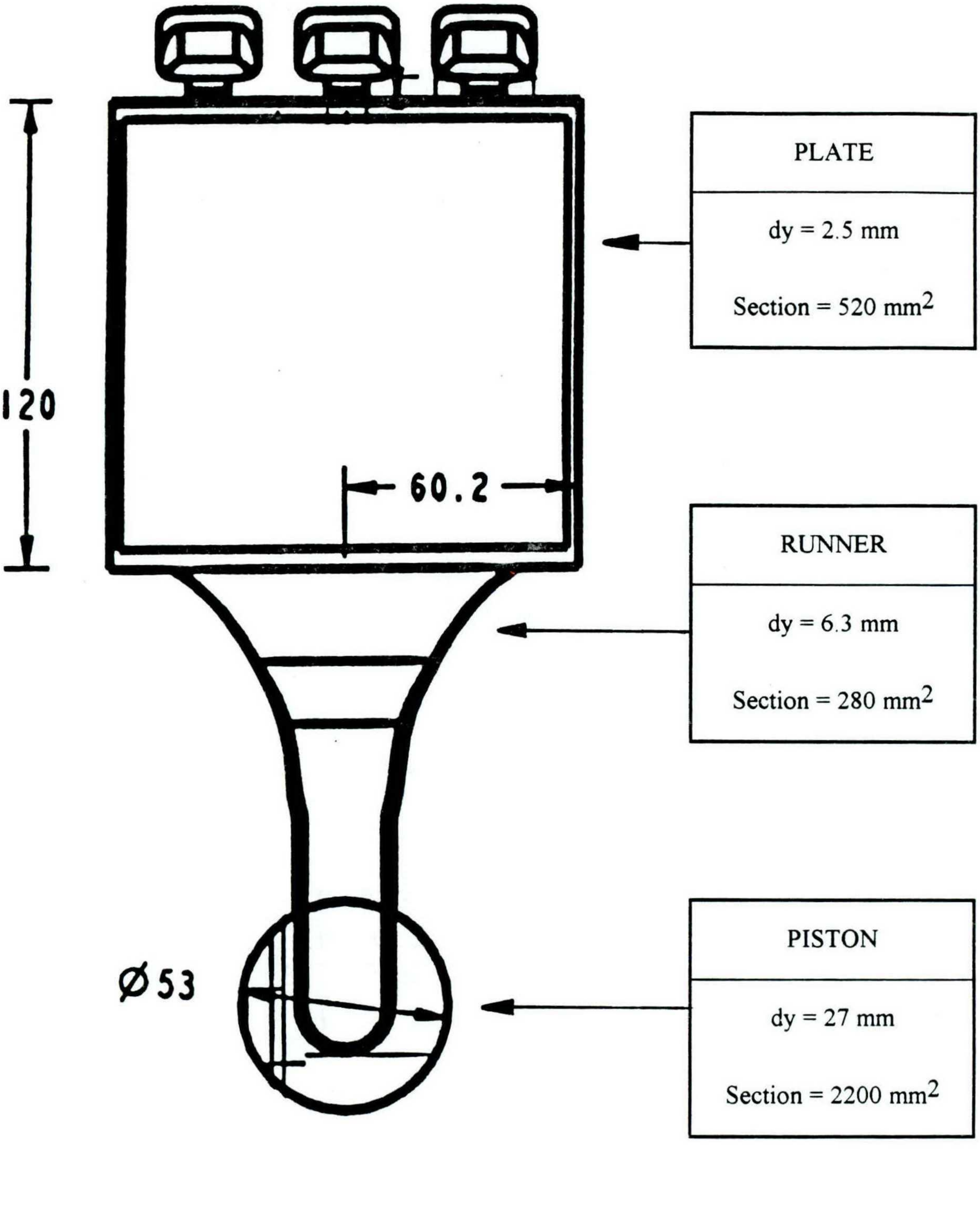

Figure 3.9 Die geometry for flat plate

The shear rate may however change in function of the die geometry given a constant velocity.

The changes in velocity settings between the different set-up (see the appendix) are automatically taken into considerations in the calculations for viscosity. Thus running the experiments for several different velocity profiles will yield a cumulative viscosity plot that covers a wider range of shear rate values.

3.1.6.2.2 Shear rate considerations

The shear rate ranges that are observed in a die casting process are very high for several reasons. The first one being a question of time. Shot velocities are typically high because molten metal freezes rapidly when injected into the die. The die itself is a large heat sink. Of course the die could be heated to a temperature very close to the melting point of the aluminum to allow for a slow cooling and a slow injection speed, but this solution would not be economically viable as it would considerably increase the cycle time of the whole operation.

The second reason for the shear rate to be very high is encountered when the cross-sectional area of the cavity is restricted and thus causes the local velocity to be high. This situation typically arises in the runner and gating system. Of course again this situation could be remedied if the die were designed to provide for a constant shear rate. This can be done by keeping the ratio of area to perimeter constant at any cross section through the die. This way, the shear rate would only be affected by changes in the preset flow rate. However insuring a constant shear rate throughout the length of the flow of the metal is not necessarily practical.

From section 2.1.1 the shear rate is obtained by the following computation:

$$D = \frac{du}{dy} \quad \text{in} \quad s^{-1}$$

It is evident that when only du increases, D will increase as well. Inversely, when increasing only dy the value of D will decrease.

These parameters, du and dy, depend on the geometry of the part itself. For instance, for two channels of same cross area but of different shape, let one of them be round and the other one rectangular, then for a given metal flow rate the shear rate will be greater in the rectangular section than in the round one. It is thus evident that the shear rate will be affected by the shape of the die, especially when casting thin wall section for example.

Nevertheless it is still possible to create a situation where constant shear rates are observed. This can be done by cleverly combining the opposite effects of: (1) changes in cross sectional area which modify the velocity of the flow; and (2) changes in the cross sectional shape which change the restricting size of the metal path.

These efforts, though, can hardly be expected in a real production environment were the bottom line is to produce parts and not to observe rheological characteristics. Such requirements would also seriously constrain the diversity in geometry of the parts cast by semi solid methods.

3.1.7 Discussion of results

The plot shown in figure 3.10 is the type of plot that is obtained for one single set of data. It can be seen that this data fits well the model for non-Newtonian, pseudo-plastic fluids. However, not all the single plots are similar. There is some variation, not in the general shape but in magnitude, between each various shot. The cause of these differences lies principally in slight temperature differences and different soaking times that set each particular billet apart.

The cumulative plot presented in figure 3.11 shows all the data points for all of the successful castings. This plot has the advantage of showing the viscous behavior range in which the experimental castings were obtained. This plot is truly characteristic of the viscous properties of the aluminum 356 semi solid alloy that was used. The upper viscosity limit is determined by the fact that the parts did not cast successfully. The lower limit, by the fact that the billets could not have been completely liquefied upon reheating and then subsequently cast.

There appears to be a large scatter of viscous measurements, especially at the lower shear rates. In fact this is not a discrepancy introduced by the viscometric analysis but rather by the lack of repeatability of the experimental die casting operation.

At the time of this research, no actual temperature measurements were available for each individual billet. The machine was run on the basis of general reheating guidelines that ensured that the billet was indeed reheated into its semi solid range. Meaning that the temperature was somewhere in between 577 and 622 degrees centigrade, with the intent to remain around the target temperature range of 580 - 590 degrees centigrade.

According to the temperature at which a billet is reheated and according to the time given to the billet to reach that temperature, the amount of solid fraction will vary according to the chart presented in figure 3.17 as well as in table 3.5.

It is thus understood that the specimen cast in the scope of this research do not all come with the same solid fraction. Since viscosity is highly dependent on fraction solid, the scatter will appear on the cumulative result plot in function of fraction solid.

This occurrence is beneficial as it allows a correlation between viscosity and fraction solid. The actual measurements for fraction solid can be made from the microstructure analysis. For the casting of semi solid aluminum alloy 356, average fraction solid levels fluctuated between 52 and 69% +/- 3% (as discussed later). The viscous behavior curves may now be bounded by fraction solid limits.

The next graph, in figure 3.12, shows the same cumulative plot but on logarithmic axes and with labels for fraction solid. The linearity of the data points here shows the pseudo-plastic property of the alloy. Note that this linear relationship was first obtained with plots for individual shots.

On figure 3.13 the results of this experiment are compared to those of Loué. The correspondence is striking. Loué obtained data for levels of solid fraction at 30, 45 and 55%. For the alloy presented in this report, the solid fraction fluctuates between 52 and 69%. This explains the offset from Loué. The solid fraction percentage is obtained from the microstructure analysis, which is described here below.

Because of the method used in this research for measuring viscosity, no values were obtained at low shear rates. Furthermore, the aim of this experiment was to measure viscosity at the high levels of shear rate present in die casting operations.

The general sloping of the curves on the log-log plot indicate in any case that the measurements made by Loué and others at low shear rate are valid as well.

These plots are the ones that will be used in determining the correct viscosity parameters for Flow 3D. They are representative of the experimental knowledge gained in this study.

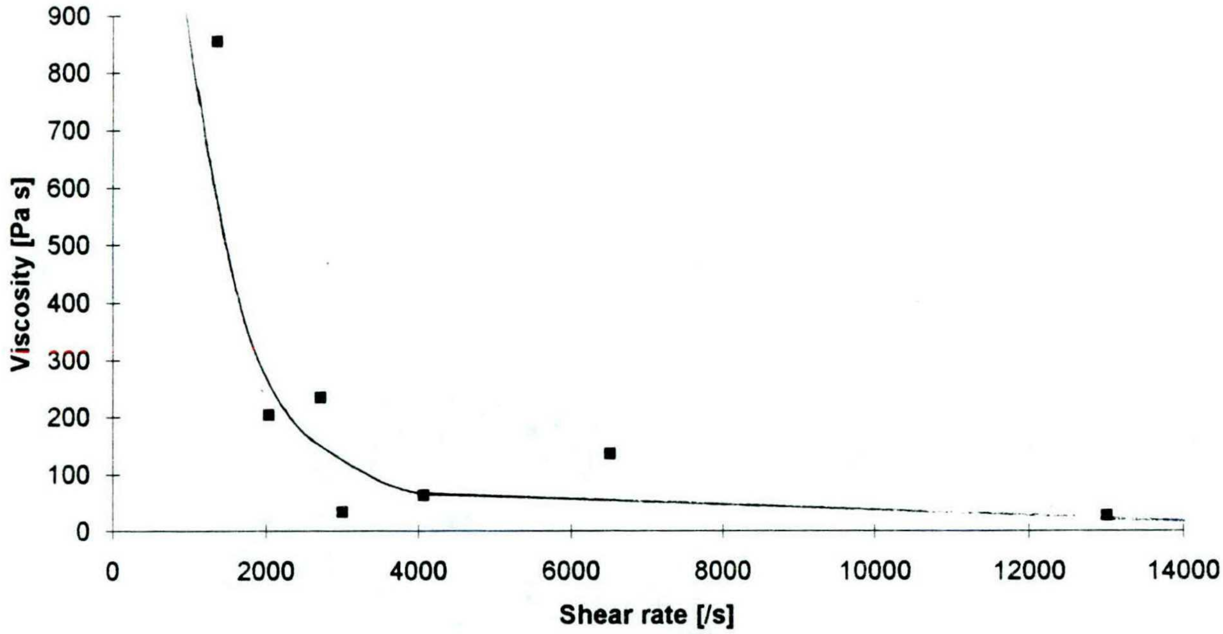

Figure 3.10 Experimental results from shot 951 which is representative of the general viscosity of semi solid aluminum alloy 356; this plot shows the relation between viscosity and shear rate with asymptotic behavior at very high shear rate; shot 951 is indicative of one fraction solid value only; for a given shear rate when the fraction solid is increased, the viscosity increases; with decreasing fraction solid, the viscosity decreases

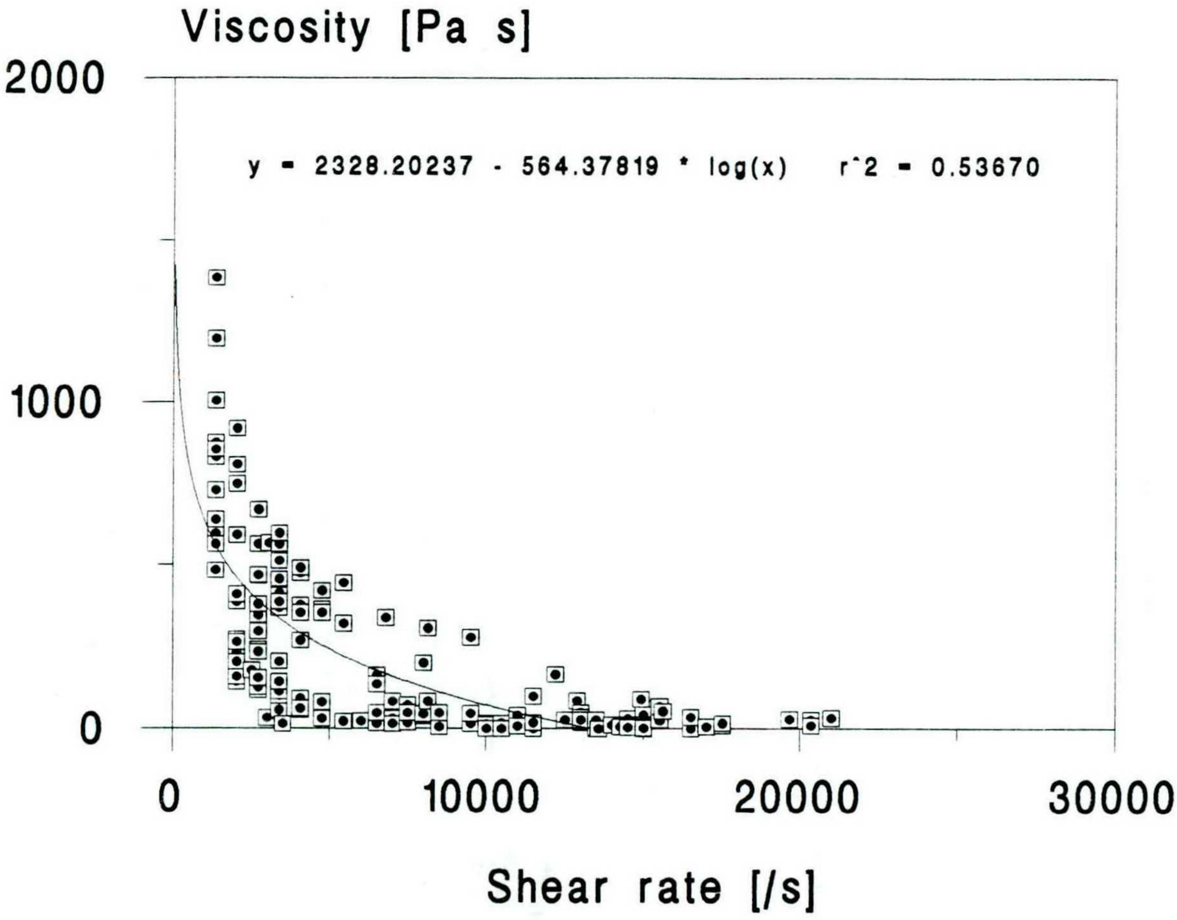

Figure 3.11 Cumulative experimental results for semi solid aluminum alloy 356 showing the extent of scatter due to the dependence on fraction solid

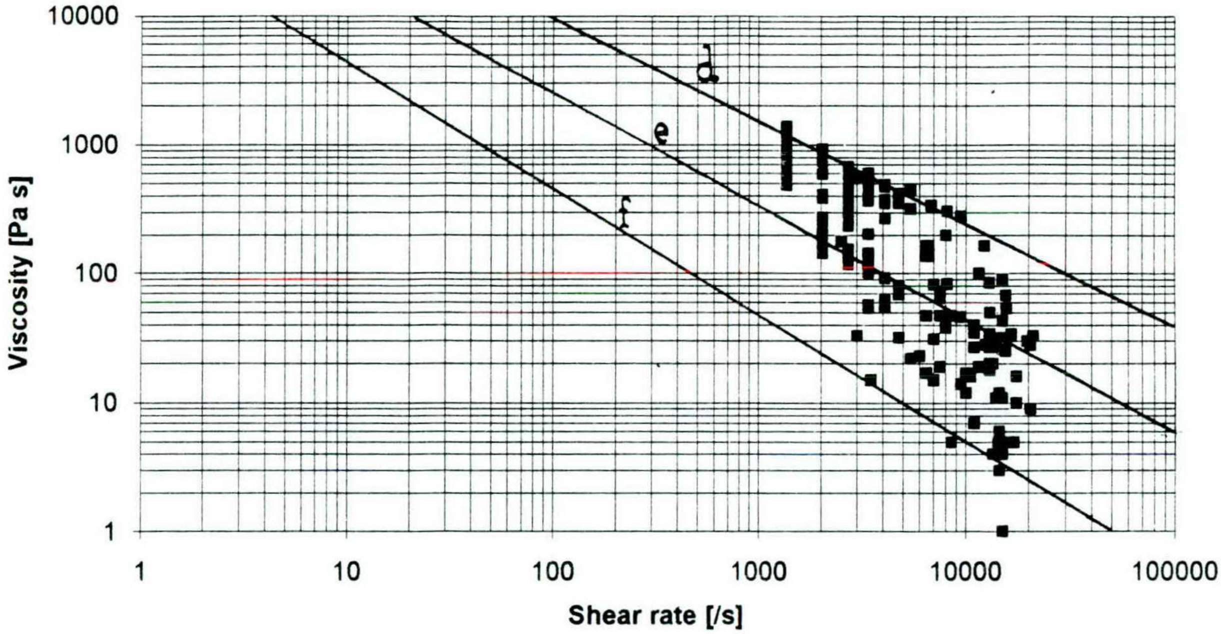

Figure 3.12 Cumulative experimental results for semi solid aluminum alloy 356 on log-log plot in function of both shear rate and fraction solid;
curves represent: (d) 70%, (e) 60%, (f) 50% fraction solid

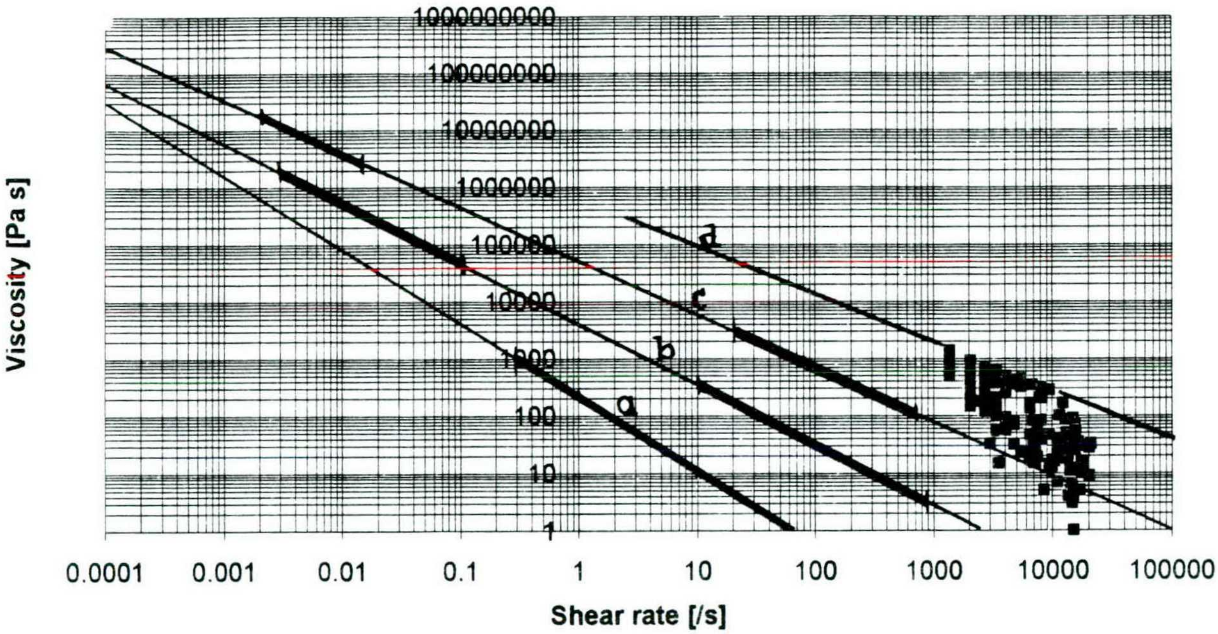

Figure 3.13 Experimental results compared to those of Loué

(a) from Loué and Searle for 30% fraction solid, (b) from Loué for 45%

(c) from Loué for 55%, and (d) from experimental results for 70 %

3.2 Characterization of the flow, Reynolds number

3.2.1 Internal incompressible flow

Flows that are completely bounded by solid surfaces are called internal flows by opposition to external flow, which occurs in open channels. For the case of the die casting cavity filling, the flow is of course internal. However both internal and external flows may be laminar or turbulent, compressible or incompressible [Fox, 1992]. Though compressibility may significantly change the properties of the flow, in engineering applications this situation arises only in the flow of gases [Fox, 1992]. The Mach number is used in gas flow theory whereas the Reynolds number is used for the flow of liquids.

This die casting application may thus be treated as in the case of the incompressible flow trough a pipe.

Now the nature of the flow is determined by the value of a dimension-less parameter, the Reynolds number.

$$Re = \frac{\rho V T}{\eta}$$

where:

where:	ρ	density
	V	average flow velocity
	T	pipe diameter
	η	viscosity

	Piston chamber	Runner	Plate
Metal velocity	U (plunger speed)	7.86·U	4.23·U
Average diameter T	0.054 m	0.014 m	0.005 m
With ρ = 2700 kg/m3, and $\eta \approx$ 20 Pa s For the following piston speeds we see:			
at U = 2 m/s	Re = 15	Re = 21	Re = 30
at U = 7 m/s	Re = 51	Re = 75	Re = 105

Table 3.3 Reynolds number attained in the flat plate

According to the Reynolds number obtained, the flow may be classified based on the following table [Fox, 1992].

Reynolds number	Type of flow
Re < 1000	Streamline
Re < 2300	Laminar
Re > 2300	Turbulent

Table 3.4 Type of flow in function of Reynolds number

It is customary in viscometry to operate at small values of Reynolds number as this avoids undue disturbances. It has been observed in experimental viscometry that turbulence in the flow occurs at similar Reynolds values for non-Newtonian liquids [Dinsdale, 1962].

The values in table 3.3 are only indicative. They show however, that only low Reynolds numbers characterize the flow of semi solid aluminum in the die cavity. Inspection shows that when the viscosity increases, the Reynolds numbers become smaller. As velocity increases, the Reynolds numbers increase as well. Since the plunger velocity of 7 m/s was not exceeded for this project's experiments, these Reynolds values are conservative and indicate that the flow of metal is laminar and streamlined.

Note however, that the flow may encompass turbulences that are caused by abrupt changes in shape or in section of the cavity.

3.2.2 Partial filling test results

On a macroscopic level the flow behavior may be observed by looking at the partial filling test. The metal flow front is clearly distinguishable and does not show the turbulent filling patterns that are customary to ordinary die casting.

Semi solid casting shows no sign of jetting, splashing or formation of metal droplets or atomized spray. This in turn allows the tracking of a relatively simple flow front in free surface modeling.

This highly viscous flow also ascertains the fact that less air is being entrapped in the solidified casting. It must also be noted that the specific gate design of this particular part promotes a smoother flow. As is customary with semi solid metal casting, the gate is designed in the shape of a channel that opens up into the cavity in a wide-mouthed opening.

3.2.3 General considerations

Though the widening of the gate towards the part cavity is beneficial to metal flow characteristics, it is also an economic detrimental factor.

Large gating systems can constitute a substantial volume of metal. Though the cost of casting this extra metal is not necessarily prohibitive it is the cost of the raw material that makes this practice less desirable. Semi solid raw material is a specially processed material and any waste material cannot simply be recycled into the production line. For each die cast part a new raw semi solid billet is necessary. Minimizing the size of the gate minimizes the amount of waste material and thus minimizes costs.

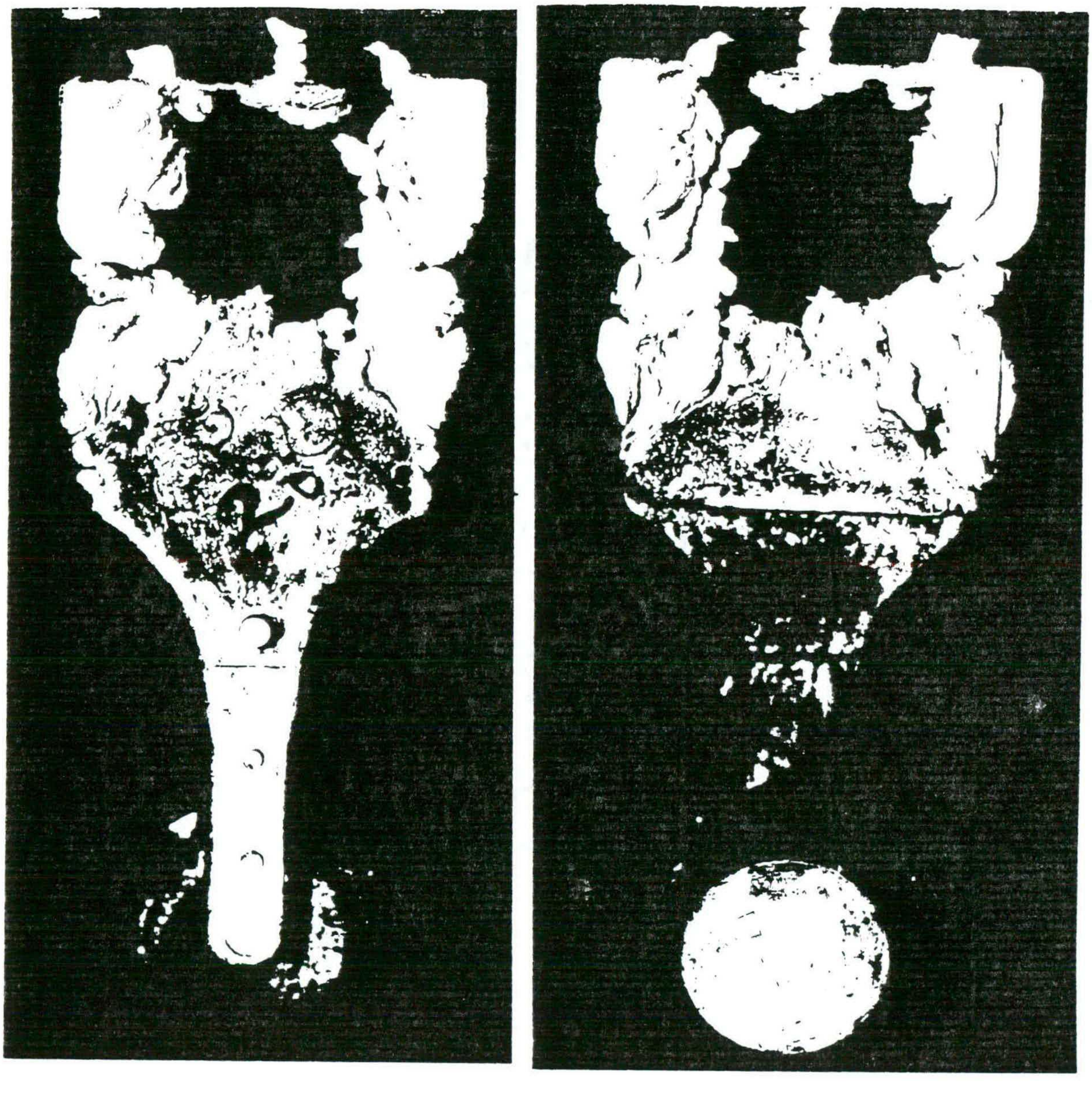

Figure 3.14 Two views of a typical partial fill test

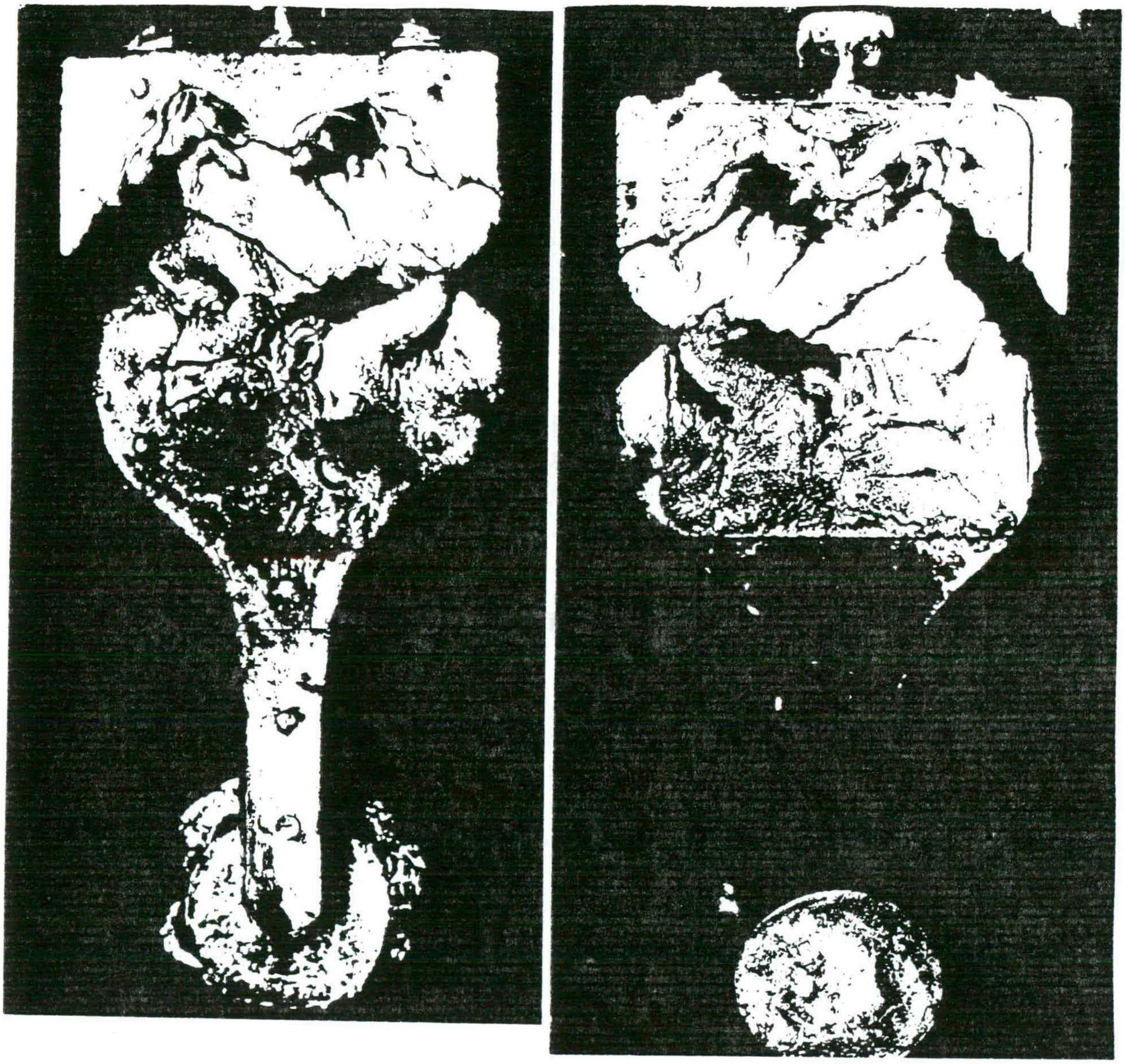

Figure 3.15 Two views of a typical partial fill test

3.3 Microscopic analysis

Semi solid metal when heated into their semi solid range are composed of a mixture of liquid eutectic phase and a solid alpha phase. The grains constitute the solid phase.

Since non-Newtonian viscous behavior is largely dependent upon the presence of solid grains, it is important to study the microscopic structure of the metal. The data of particular interest is the concentration factor of the solid mass. Further more the size and shape of the solid grains may be indicative of some specific behavior.

3.3.1 Sample analysis

Multiple sections were sampled throughout the castings as well as throughout the raw billets. The samples were prepared for viewing according to the specified methods. These procedures included some or all of the following: polishing with silicon carbide, polishing with diamond paste, polishing with powdered alumina, cleaning, etching with a solution of HF acid. Images were then obtained on an optical microscope.

The microscope images were processed on an image analyzer. The numeric values that describe each picture are only valid inasmuch as the grain / matrix boundaries were accurately defined. This task relies heavily on visual appreciation of the image and is therefore not necessarily accurate. This is especially true for the small sized grains. However it may be stated that the measurements were made consistently from one picture to another, thus comparisons between different pictures are valid.

3.3.2 Relationship to phase diagram

Solid mass fraction were found in accordance with what is described in literature. The accordance was also found when performing an analysis on a scanning electron microscope.

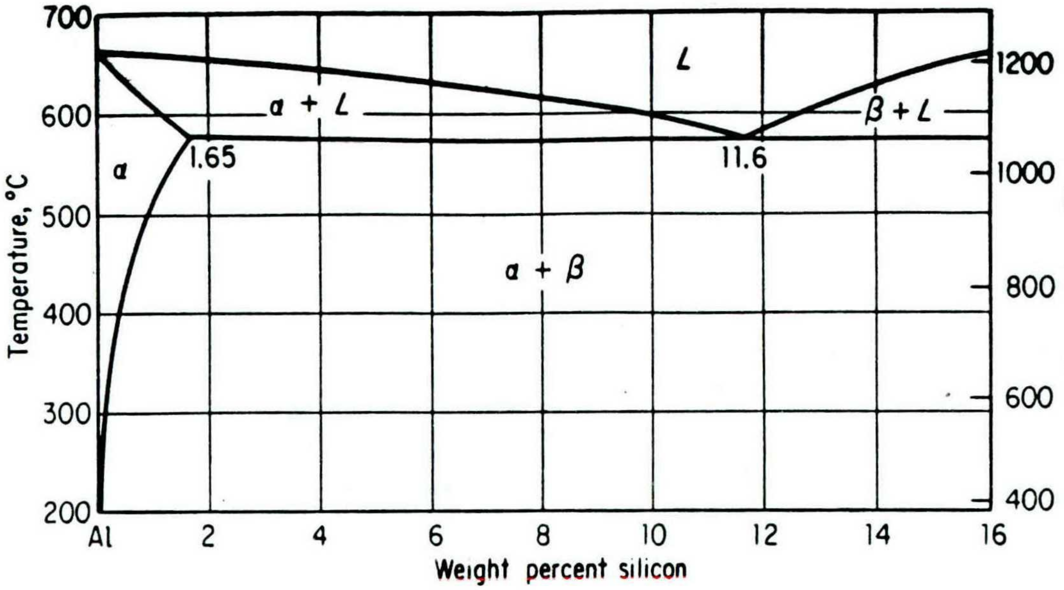

Figure 3.16 Phase diagram for aluminum-silicon alloy from Metals Handbook

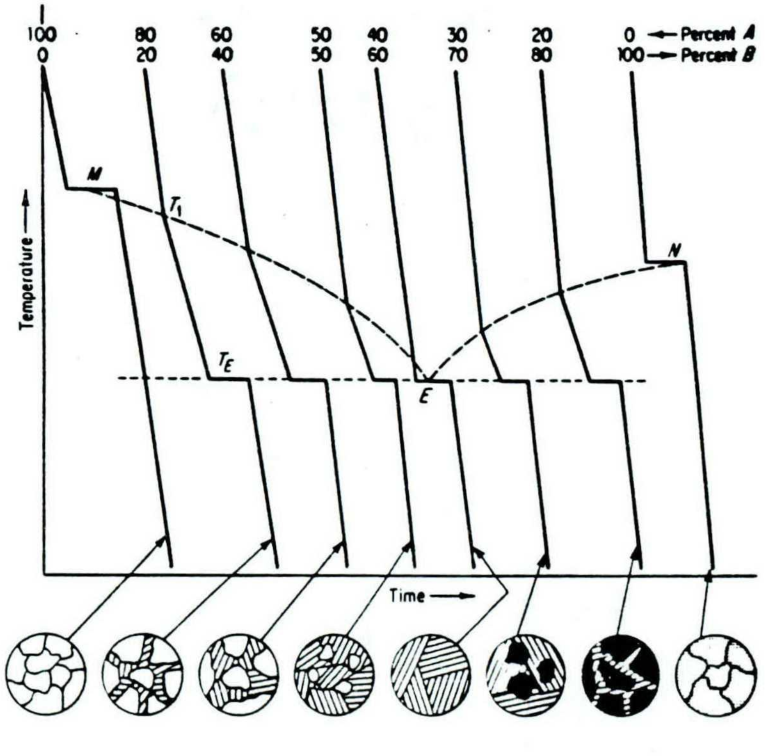

Figure 3.17 Cooling curves for metal alloys showing that the fraction solid of an alloy depends on temperature as well as soaking time; direct cross relation from fraction solid measurements to determine temperature is not possible

Element	Atomic Mass	Density	Weight Percent	Volume Fraction	Mole Fraction
Al Si Mg	26.982 28.086 24.305	2.7 2.33 1.74	92.7 7 0.3	91.54 8 0.46	93 6.7 0.3

Table 3.6 Relative composition of aluminum alloy 356

Temperature	Phase	% Composition
below 577 C - 1070 F	Liquid Solid	0 100
577 C - 1070 F	Liquid Solid	54 46
589 C - 1092 F	Liquid Solid	60 40
600 C - 1112 F	Liquid Solid	67 33
612 C - 1134 F	Liquid Solid	79 21
622 C - 1152 F	Liquid Solid	100 0
above 622 C - 1152 F	Liquid Solid	100 0

Table 3.5 Steady state fraction solid of aluminum alloy 356 in function of temperature

Preparation of the samples for the scanning electron microscope was similar to the previous procedure. In this case no alumina powder was used as a polishing media as it would have otherwise corrupted the composition of the aluminum sample. Also, extensive degreasing measures had to be taken to thoroughly clean the samples.

Besides analyzing the composition of the grains and matrix of the aluminum sample, the scanning electron microscope also yielded good images of the very small grains. The scanning electron microscope, thanks to the principles on which it operates, can achieve much greater magnification ranges. Here magnifications of up to 10'000 times were achieved while an optical microscope usually stops at 4000 times.

3.3.3 Results

Rapid processing of the billets is essential in maintaining the optimal shape of the grains. As can be seen in the pictures of metal that was held at temperature for a several minutes, the shape of the grains evolves form being spherical to becoming more complex. The solid mass fraction does not increase significantly, however the number of grains per unit area decreases. This means that with time smaller grains are combining together to form larger grains.

Table 3.7 lists the analysis results for many of the samples that were taken from several cast parts as well as from several billets, raw and reheated. General fluctuation for the percentage of solid grains to liquid matrix go from 52 to 69%.

Segregation can also be seen in some cases. Typically the smaller grains accumulate near the exterior surface of the plate. During the casting process it appears that the smaller grains can squeeze themselves past larger grains. This could be explained by a different drag coefficient between a large and a small grain allowing one to travel with less hindrance. The analysis on the scanning electron microscope shows that the small grains have the same composition than the large ones thus indicating that they all are created form the same metal phase.

There is no evidence that this accumulation is in any way detrimental to the quality of the parts. It can be said that these small grains have little or no incidence on the viscosity of the metal: (1) there is a much smaller proportion of small grains than large ones; and (2) this accumulation occurs well within the boundary layer of the flow. This boundary layer was never found to exceed 0.5 mm in thickness.

Some grain growth was observed as well. It is very different in shape and can easily be identified by the intricate dendritic growth. It only occurred in marginal instances and only in the upper extremity of the plate, near the vents.

This indicates in the instances where it occurred that the metal billet was probably overheated in the induction furnace. This overheating caused some of the silicon rich grains to dissolve into the eutectic phase only to recreate new dendritic growth upon cooling. This dendritic growth occurred in areas of the die where a large temperature gradient was present.

This occurrence is readily observable and indicates roughly what temperature may have been reached by the billet. It is however not possible to directly correlate temperature to fraction solid, as the solid fraction is also a function of soaking time.

Though the exact relationship between temperature, time and fraction solid is not known, upper and lower boundaries may be set, between which the viscous behavior of the semi solid aluminum is observed. This information is useful for describing viscosity in function of shear rate as well as fraction solid.

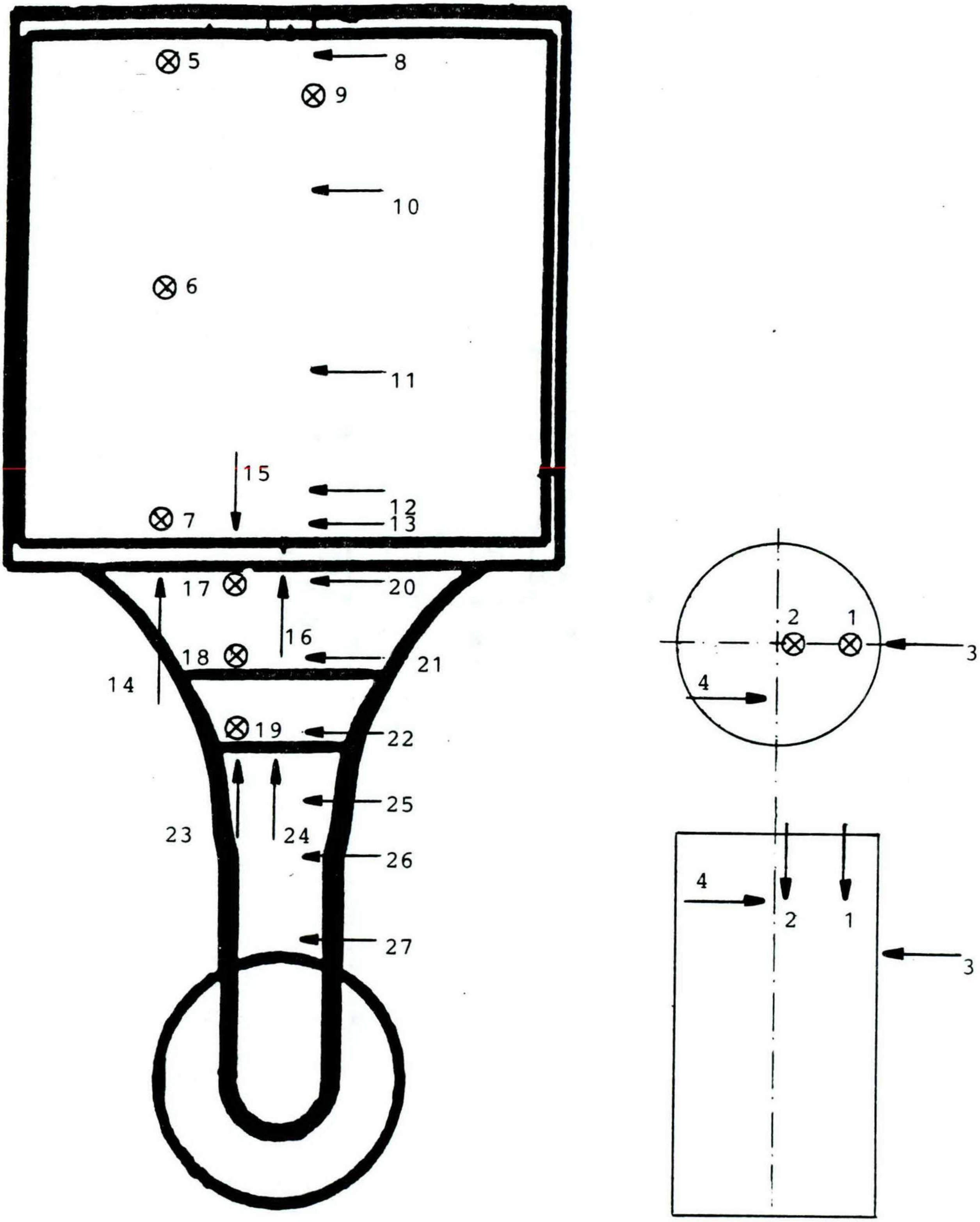

Figure 3.18 Locator chart of samples used in optical microstructure analysis; note that not all specimen were taken from the same sample casting

No	Description	View	Magni-fication	Area Percent Grain	Spheri-city	Size range of Grains	Average size of grains	Aspect ratio
1	Raw billet	longi.	100 x	68 %	0.64	43-62μm		1.72
2	"	"	100 x	65 %	0.68		28 μm	1.72
3	"	skin	100 x	75.6 %	0.4	11-94μm		1.75
4	Reheated billet	perp.	100 x	54.8 %		0-29μm	3.5μm	
5	Plate surface	skin	100 x	47 %	0.84	61-105μm		1.68
6	"	"	100 x	47.6 %	0.6		64μm	1.71
7	"	"	100 x	31.4 %	0.6		72μm	1.7
8	Plate section	perp.	100 x	72.7 %	0.62		62μm	1.51
9	"	skin	100 x	60 %			44μm	
10	"	perp.	100 x	69.8 %	0.57		54μm	
11	"	"	100 x	65 %			54μm	
12	"	"	100 x	56 %			80μm	
13	"	"	100 x	64.2 %		40-140μm		
14	Gate in section	longi.	200 x	67.4 %	0.81		80μm	1.81
15	"	"	200 x	52.9 %	0.4			2
16	"	"	200 x	77.6 %	0.89		72μm	1.6
17	Runner surface	skin	100 x	72 %	0.9		82μm	1.8
18	"	"	100 x	68 %	0.87	58-92μm		1.65
19	"	"	100 x	69 %	0.9	77-120μm		1.9
20	Runner in section	perp.	200 x	72.6 %	0.8	52-88μm		1.9
21	"	"	200 x	67.1 %	0.9	75-130μm		1.7
22	"	"	200 x	75.6 %	0.88		62μm	1.7
23	"	longi.	100 x	65.5 %	0.8		57μm	1.7
24	"	"	200 x	65 %	0.9		68μm	1.7
25	"	perp.	100 x	78 %	0.9	58-94μm		1.7
26	"	"	100 x	58.4 %	0.85	42-90μm		1.6
27	"	"	100 x	62 %	0.86	51-90μm		1.6
28	"	longi.	100 x	68.4 %	0.8	49-100μm		1.5

longi. : longitudinal view to the flow
perp. : perpendicular view the flow
skin : polished exterior skin surface

Table 3.7 Summary of results from optical microstructure analysis

Sample	Magnification	Size	Element	Weight %	Atomic %
Small grain 1	9895 x	1μm	Al Si	98.75 1.25	97.90 2.10
Small grain 2	2473 x	8μm	Al Si	97.72 2.28	96.19 3.81
Small grain 3	4947 x	4μm	Al Si Mg	98.79 0.90 0.31	97.71 1.52 0.77
Large grain 1	309 x	110μm	Al Si Mg	98.71 0.89 0.40	97.51 1.49 1.00
Large grain 2 Area scan	309 x	90μm	Al Si Mg	98.48 1.08 0.44	97.10 1.81 1.09
Matrix	619 x		Al Si Mg	85.38 14.55 0.07	77.44 22.40 0.16

Average values		Element	Weight %	Atomic %
	Grain	Al Si Mg	98.66 0.96 0.38	97.44 1.61 0.95
	Matrix	Al Si Mg	85.38 14.55 0.07	77.44 22.40 0.16

Table 3.8 Summary of results from scanning electron microscope analysis

3.4 Modeling of fluid flow in simulations

3.4.1 Operation of the Flow 3D viscosity subroutine

Flow 3D does not infer the viscosity of a fluid from a numerical data base, but rather uses an analytical model to compute the viscosity in function of shear and temperature.

Shear rate and temperature dependent viscosities are computed within Flow 3D by a set of subroutines. These subroutines are included in the non-Newtonian flow option. There are many models to express the fluid viscosity in function of shear rate and temperature. These models could not all be included in the code, therefore a generic expression was developed. This expression is based on the Carreau model but has been featured with many variable parameters so as to make it universal. Careful selection of these parameters allows for a correct modeling of viscosity.

The subroutine MUCAL calculates viscosity using the following formulae. The similarity with the Carreau model is obvious.

$$\eta = \eta_\infty + \frac{\eta_T - \eta_\infty}{\left(\lambda_0 + \lambda_T^2 E^2\right)^{\frac{1-n}{2}}}$$

E, an input to the subroutine, is the fluid shear rate. In Flow 3D it is defined in tensor notation.

$$E^2 = e_{ij} e_{ij}$$

$$e_{ij} = \frac{1}{2}\left(\frac{\partial u_j}{\partial x_i} + \frac{\partial u_i}{\partial x_j}\right)$$

The temperature dependence is expressed in following formulae.

$$\eta_T = E_T \eta_0$$

$$\lambda_T = E_T \lambda_1$$

$$E_T = \exp\left[a \frac{TSTAR}{T-b} - c \right]$$

T, another input to the subroutine, is the fluid temperature. Note that when a = 0 there is no temperature dependence.

All parameters that are necessary for the simulation to run, are entered in the data input file: the *prepin* file. The parameters that define the viscosity calculation are entered as:

MUI = η 0	MUTMP1 = a	TSTAR = TSTAR
MUC0 = λ 0	MUTMP2 = b	
MUC1 = λ 1	MUTMP3 = c	
MUC2 = n		
MUC3 = η ∞		

A sample of a *prepin* file is shown in the appendix.

3.4.2 Mathematical model

The use of Flow 3D is cumbersome, at least in the initial stages when trying to model viscosity correctly. After setting all the parameters in the *prepin* file the simulation may be run, but even if the simulation provides a plausible answer, there is no real guarantee that the viscosity is correctly modeled.

It is thus useful to set up a separate code that will run just like the viscosity subroutine of Flow 3D in order to preview the viscosity computations. This also allows a big time and cost saving because Flow 3D does not have to be used to merely set viscosity parameters.

3.4.2.1 Matlab code

The Matlab code that transcribes the operation of the Flow 3D viscosity subroutine uses the functions and parameters described earlier. Two variable inputs are used: the shear rate E and the metal temperature T. A sample copy of this Matlab code is exposed in the appendix.

The outcome of the Matlab code is the calculated viscosity. In turn, this viscosity can be plotted in function of shear rate for several temperatures. Parameters can then be modified in an iterative manner until the plotted results match the known experimental viscosity found earlier.

Once armed with the correct parameters for the viscosity subroutine, one can confidently proceed to Flow 3D and start the cavity filling simulations.

3.4.2.2 Characteristics of the Flow 3D subroutine

Clearly three general behaviors can be developed in the subroutine: (1) pseudo-plastic; (2) Newtonian; and (3) dilatant. These are observed at low shear rates. At an infinite shear rate the behavior of each of these curves becomes asymptotic. This follows from the fact that rheological behavior tends to be largely Newtonian at high shear due to uniform particle movement [Dabak, 1986]. Figure 3.19 and figure 3.17 show the distinctive properties that can be mimicked by the viscosity subroutine of Flow 3D.

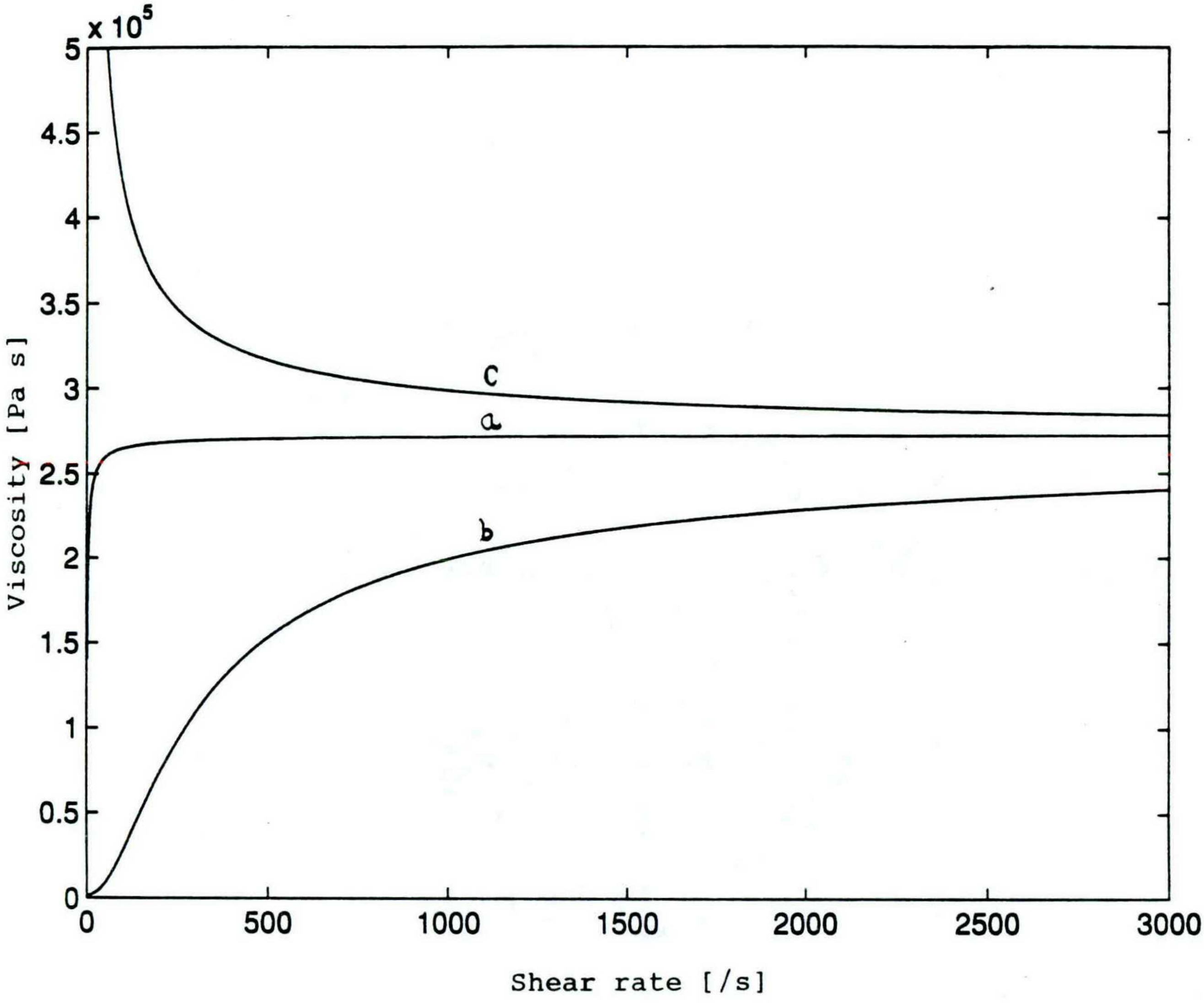

Figure 3.19 Sample of viscosity modeling possibilities of Flow 3D showing the (a) Newtonian and the non-Newtonian, (b) dilatant and (c) pseudo plastic representations of viscous behavior

3.4.3 Simulation results

Some simulation were run so as to test the methodology used in experimentally determining the viscous behavior of the semi solid aluminum.

From the results obtained it appears that Flow 3D correctly simulates the filling of the die cavity. The sequential images of the filling process match the results of the partial filling test. Flow patterns also exhibit the highly viscous property of the aluminum. The apparent metal front is in accordance with the flow assumptions made earlier, thus showing the laminar motion.

Furthermore, Flow 3D provides a graph of the simulated casting pressures as may be measured behind the shot plunger. These plots have the same appearance as the ones measured on the Bühler for the actual pressure values. This is a good sign indeed that the simulation was successfully tested.

Flow 3D Parameter	Value
MUI	3.66
MUC0	1.0
MUC1	1.34e-05
MUC2	0.15
MUC3	0.01
MUTMP1	2
MUTMP2	814
MUTMP3	16.85
TSTAR	886

Table 3.9 Mucal Flow 3D parameters for aluminum alloy 356

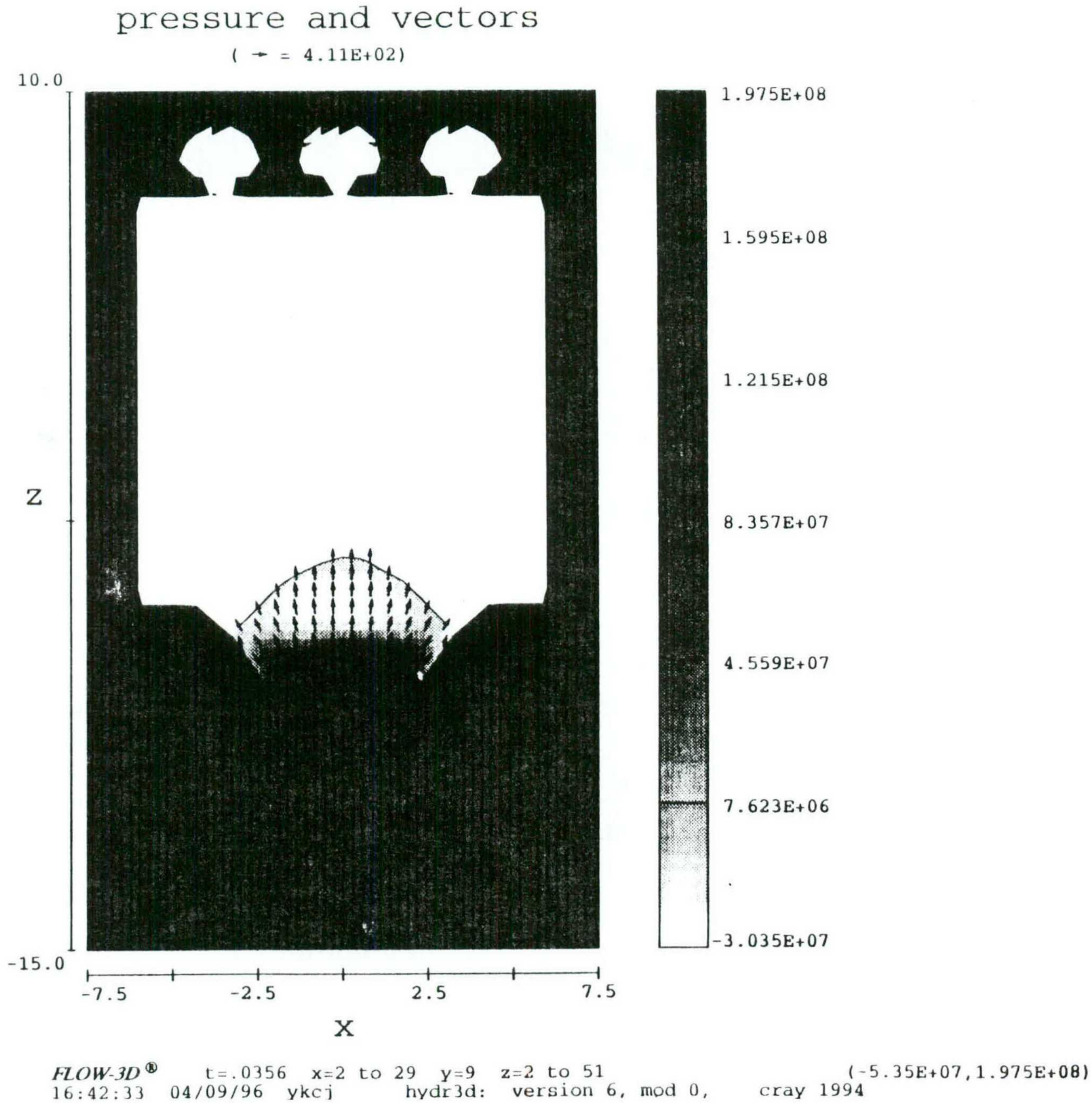

Figure 3.20 Flow 3D simulation outcome showing the possible simulation of semi solid metal cavity filling patterns

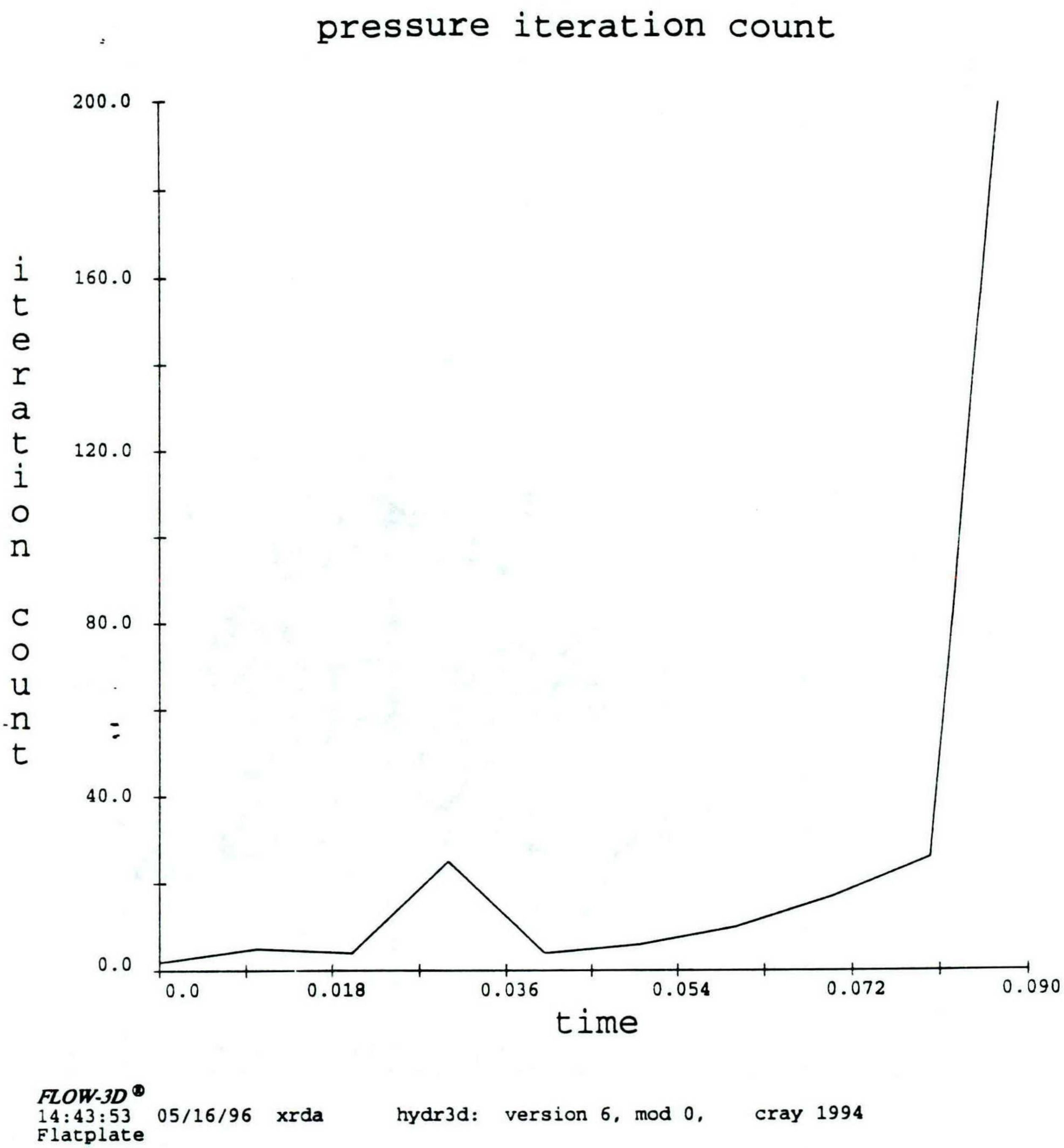

Figure 3.21 Flow 3D simulation outcome showing the simulated pressure required to fill the cavity; such results can be matched to the experimental data charts

CHAPTER 4

CONCLUSIONS

4.1 Future work

This research succeeded in presenting and developing a method for measuring the viscosity of the semi solid metal as it is being cast. This method was tested and verified in an experimental set-up that operated in a true manufacturing environment.

It was seen also what effect temperature and machine settings had on the viscous behavior of the semi solid aluminum. This effect was observed by several methods:

(1) by tabulating the measured viscosity values;

(2) by performing partial fill tests;

(3) by analyzing the microstructure on an optical microscope;

(4) by analyzing samples on an electron scanning microscope;

(5) by running filling simulations on Flow 3D.

This project was intended as a start up work, the viscosity behavior being a key element in semi solid flow analysis. Future projects and projects already on the run can constructively benefit from the work done here.

4.2 Viscometry

Further sophistication could be added to the method presented for viscous measurements. For instance the die cavity that was used in lieu of a capillary tube could be calibrated by measuring the viscosity of a reference substance. This substance would have a known viscosity that would have been measured in a true viscometer. For Newtonian liquids a substance such as a thick grease would be suitable. For non-Newtonian fluids, the procedure would be of more interest though it would be difficult to find adequate reference substances. Fluids such as slurries of known composition or polymers would probably be investigated.

4.3 Software package

Another useful aspect of this work could be its application into a software package to be added to the die casting machine. This software package would compute the observed viscosity during the cavity filling process thus providing a useful indicator of the casting operations. Relations to part quality may also be better understood.

Alternatively, the subroutine that is used in Flow 3D could be transformed from its generic format to one specifically designed for semi solid metals. This could, perhaps, alleviate many of the problems in accurately determining the viscous behavior of semi solid metals. It could also shorten the set-up time of a simulation by reducing the iterative process involved in modeling viscosity.

4.4 Die geometry analysis

The mathematical treatment of the die assembly presented in this paper could be further developed to categorize different die geometries in function of their effect on the viscous behavior of the metal flow. Systematic study of several dies could be of instructional value to the designer. The mathematical analysis could evolve into a moldability theory. Similar work has been done by Lenk for polymer injection.

4.5 Gate design

In this study the gate and runner geometry were found to have a significant impact on the flow patterns of the semi solid metal. Either software packages or analytical methodologies could be developed for optimization of the gate volume to gate shape ratio. Developments of hypothetical gateless and runnerless dies could be of economic worth. Guidelines for runner size could be developed based on the Reynolds number calculations.

LIST OF REFERENCES

Anderson, R., : "The Metallurgy of Aluminum and Aluminum Alloys", Bird, New York.

Avallone, E., : "Mark's Standard Handbook for Mechanical Engineers", McGraw-Hill, 9th Edition, New York, 1992.

Barkhudarov, M. R., Bronisz, C. L., Hirt, C. W., : "Three Dimensional Thixotropic Flow Model", Flow Science, Los Alamos.

Bird, R. B., : "Dynamics of Polymeric Liquids", Vol. 1, 2nd Edition, Wiley, New York, 1987.

Boucher, J., : "Initiation à la fonderie", Syndicat général des fondeurs de France, Dunod, Paris.

Brown, S. B., Flemings, M. C., : "Net Shape Forming via Semi Solid Processing", Advanced Material and Processes, pp. 36-37, Jan. 1993.

Bühler, "Instruction Manual", 1995.

Casas-Vazquez, J., "Rheological Modeling", Springer-Verlag, Berlin, pp. 187sqq, 1990.

Carreau, P. J., : "An Analysis of the Viscous Behavior of Polymeric Solutions", The Canadian Journal of Chemical Engineering, Vol. 57, pp. 135-140, Apr. 1979.

Chhabra, R. P., : "Bubbles, Drops and Particles in Non-Newtonian Fluids", CRC Press, Boca Raton, 1993.

Dabak, T., : "Shear Viscosity of Dense Phase Slurries at Varying Shear Rates", International Symposium on Slurry Flows, Vol. 38, pp. 31-38, 1986.

Denn, M., : "Extensional Flows: Experiment and Theory", The Mechanics of Viscoelastic Fluids, The American Society of Mechanical Engineers, Vol. 22, pp. 101sqq, 1977.

Dinsdale, A., Moore, F., : "Viscosity and its Measurement", The Institute of Physics and the Physical Society, London, 1962.

Flemings, M. C. Young, K. P., : "Thixocasting of Steel", SDCE Transactions, G-T77-092, 1977.

Flemings, M. C., Mehrabian, R., : "Casting Semi Solid Metals", AFS Transactions, Vol. 81, pp. 81-89, 1973.

Flemings, M. C., Rieck, R. G., Young, K. P., : "Rheocasting Process", AFS International Cast Metal Journal, pp. 11-22, 1976.

Flemings, M. C., : "Behavior of Metal Alloys in the Semi Solid State", Metallurgical Transactions, Vol. 22A, p. 967, May 1991.

Fox, R., McDonald, A., : "Introduction to Fluid Mechanics", John Wiley, New York, 4th Edition, 1992.

Gerald, C., Wheatley, P., : "Applied Numerical Analysis", Addison-Wesley, Reading, 1989.

Gosh, D., : "Thixotropic of Semi Solid Magnesium Alloys AZ91D and AM50", The Third International Conference on Semi Solid Processing of Alloys and Composites, pp. 37sqq, 1994.

Horsten, M. G., Qaak, C. J., Kool, W. H., : "Pseudo Plastic and Thixotropic Behavior of Al-SiC Composites in the Semi Solid State", Proceedings of the Second International Conference on the Processing of Semi Solid Alloys and Composition, p. 359-.363, 1992.

Jerichow, U., Brevick, J., Altan, T., : "A Review of the Development of Semi Solid Metal Casting Processes", Engineering Research Center for Net Shape Manufacturing Report No. ERC/NSM-C-95-45, The Ohio State University, 1995.

Joly, P. A., Mehrabian, R., : "The Rheology of a Partially Solid Alloys", Journal of Material Science, Vol. 11, pp. 1392-1420, 1976.

Kumar, P., Martin, C. L., Brown, S., : "Flow Behavior of Semi Solid Alloy Slurries", Proceedings of the Second International Conference on the Processing of Semi Solid Alloys and Composition, pp. 213-220, 1992.

Kumar, P., Martin, C. L., Brown, S., : "Predicting the Constitutive Flow Behavior of Semi Solid Metal Alloy Slurries", The Third International Conference on Semi Solid Processing of Alloys and Composites, pp. 37sqq, 1994.

Langlois, W. E., : "Slow Viscous Flow", MacMillan, New York, 1964.

Lenk, R. S., : "Polymer Rheology", Applied Science Publishers, London, p. 157, 1978.

Loué, W. R., Suéry, M., : "Microstructure and Rheology of Partially remelted Al-Si Alloys", Proceedings of the Second International Conference on the Processing of Semi Solid Alloys and Composition, p. 119, 1992.

Malkin, A. Y., Askadsky, A. A., Kovriga, V. V., Chalykh, A. E., : "Experimental Methods of Polymer Physics", Mir, Moscow, 1983.

Monard, J.-A., : "Mécanique des fluides", Ville de Bienne, Bienne, 1981.

Nguyen, T. G., Suéry, M., Favier, D., : "Mechanical Behavior of Semi Solid Alloys under Drained Compression with Lateral Pressure", Proceedings of the Second International Conference on the Processing of Semi Solid Alloys and Composition, p. 296-305, 1992.

Okano, S., : "Research Activities in Rheo-Technology", The Third International Conference on Semi Solid Processing of Alloys and Composites, pp. 7sqq, 1994.

Persoz, B., : "Introduction à l'étude de la rhéologie", Dunod, Paris, 1960.

Pichard, M.-A., : "Formulaire et tables", Tricorne, Genève, 1985.

Raichura, N. A., Jerichow, U., Altan, T., : "The Effects of Process Parameters on the Porosity and Mechanical Properties of Semi Ssolid Aluminum Alloy Castings", Engineering Research Center for Net Shape Manufacturing Report No. ERC/NSM-C-96, The Ohio State University, 1996.

Reiner, M., : "Lectures on Theoretical Rheology", North-Holland, Amsterdam, 1960.

Venkatesan, K., Shivpuri, R., Altan, T., : "A Flow 3D Investigation of the Effect of Gate Geometry, Gate Velocity and Gate Size on the Quality of Die Casting Parts", Engineering Research Center for Net Shape Manufacturing Report No. ERC/NSM-C-95-18, The Ohio State University, 1995.

Wang, N., : "Tensile and Compression Properties of Stircast Al-5% Cu and Al-80% Zn", The Third International Conference on Semi Solid Processing of Alloys and Composites, pp. 127sqq, 1994.

Westhoff, B., Ahmetoglu, M., Altan, T., : "Viscous Material testing and Simulation of Viscous Pressure Forming", Engineering Research Center for Net Shape Manufacturing Report No. ERC/NSM-S-95-43, The Ohio State University, 1995.

Young, K. P., Fitze, R., : "Semi Solid Metal Cast Aluminum Automotive Components", The Third International Conference on Semi Solid Processing of Alloys and Composites, pp. 155sqq, 1994.

APPENDIX A

SAMPLE DATA FROM THE BUEHLER SC

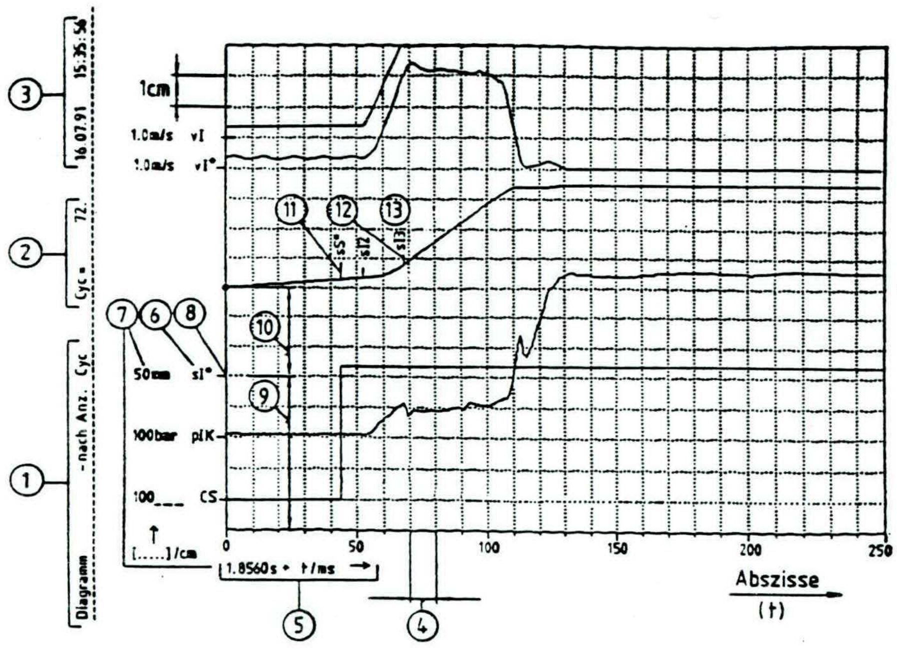

Selected curves

- vI   nominal speed of plunger
- vI*   actual speed of plunger
- sI*   plunger momentary
- pIK   metal pressure momentary
- CS   Cav S* metal front sensor momentary

Title line

(see also operating instructions for printer, Paragraph "Configuration output")

1) Text corresponds to output command: "Diagram after No. of cyc"
2) Cycle counter position (Σ Cyc tot*)
3) Date and time

Abscissa (time or displacement axis)

4) Time/grid (the example shows: 10 ms/grid)
   or
   displacement/grid
5) Time measuring: command "plunger forward" till "starting point for recording" (the example shows: 1.8560s)
   or
   Stroke measuring: starting point for recording

Ordinates (example: sI* curve)

6) Indication of curve
7) Recording scale (the example shows: 50 mm/cm)
8) Dash marking of the zero point
9) Starting height, distance of zero point from the abscissa (the example shows: 50 mm)
10) Starting point for recording (the example shows: 150 mm)

Curve markings on the sI* curve

11) Technological value sS* "metal at sensor"
12) Curve point "stroke sI3"
13) Indication of curve markings

Figure A-1 Sample output plot

agram to printer -after numb. cyc Cyc = 934 14.11.95 06:25:57

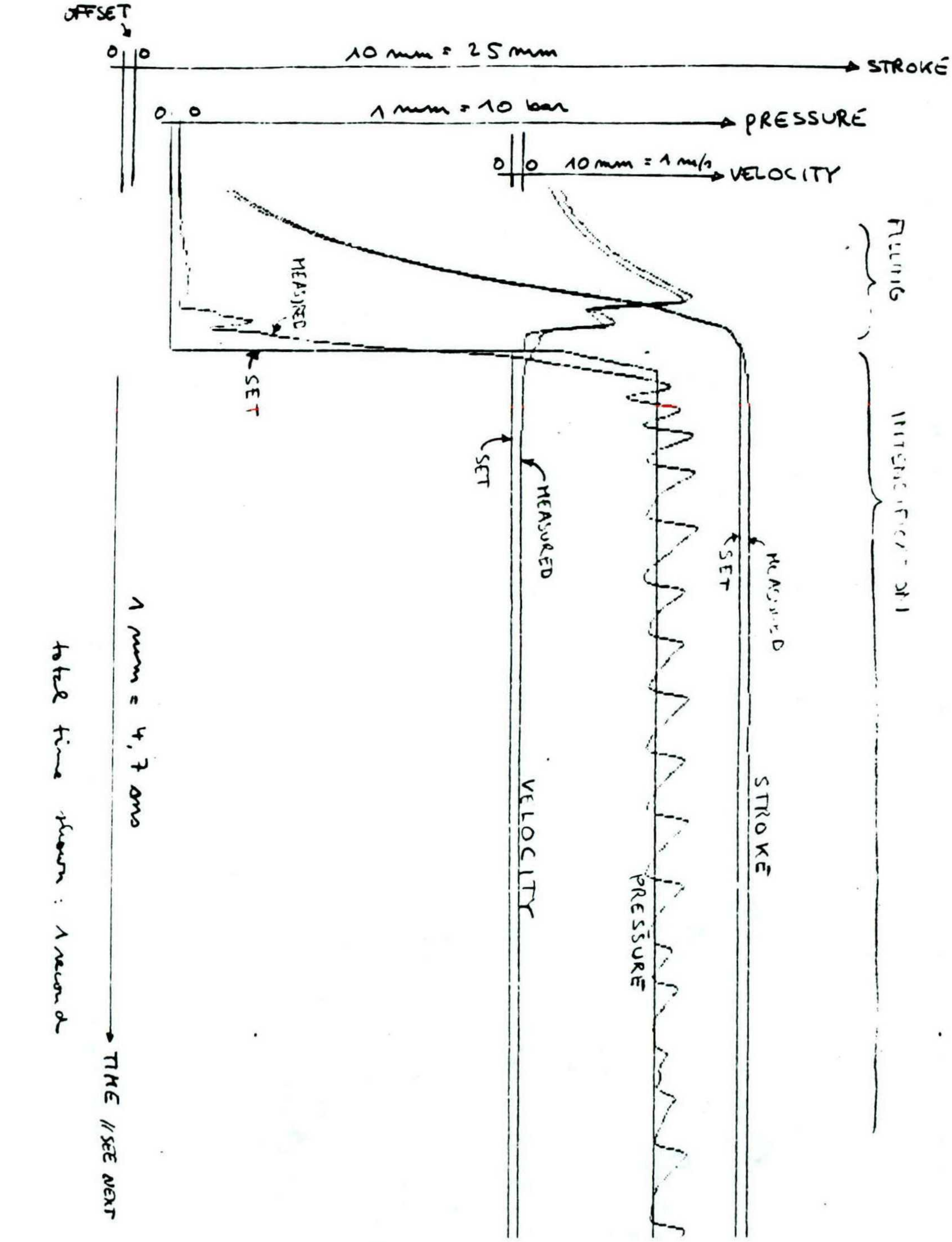

Figure A-2 Plot 934

Diagram to printer -after numb. cyc Cyc = 937 14.11.95 06:37:52

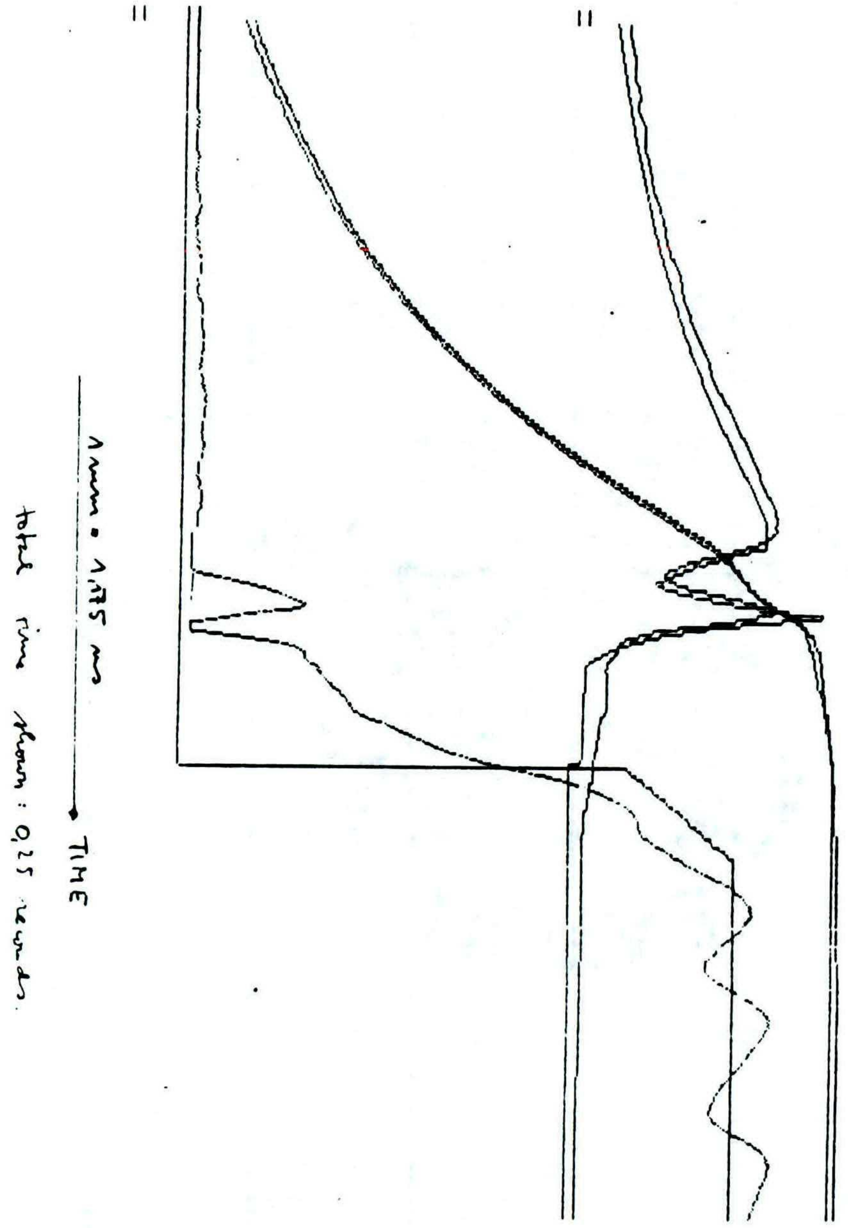

Figure A-3 Plot 937

Diagram to printer Filter numb. Cyc Cyc = 939 14.11.9[illegible] 06:4[illegible]

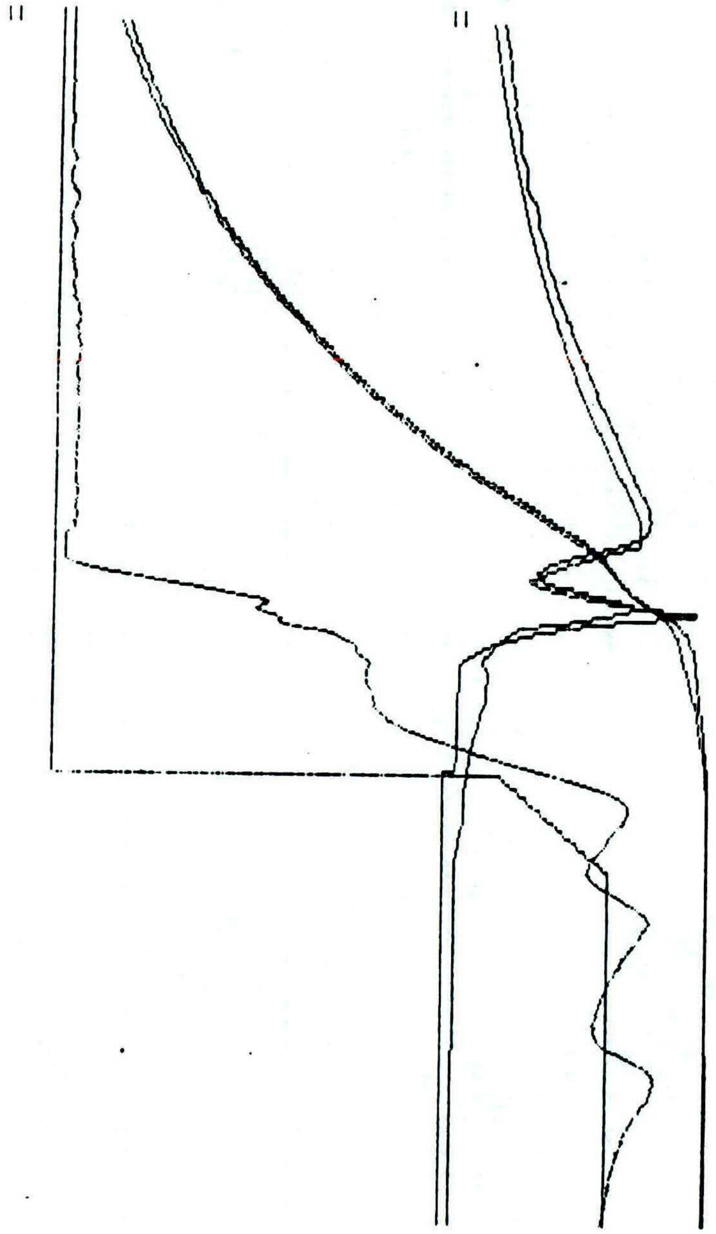

Figure A-4 Plot 939

Diagram to printer -after numb. cyc Cyc = 940 14.11.95 06:49:34

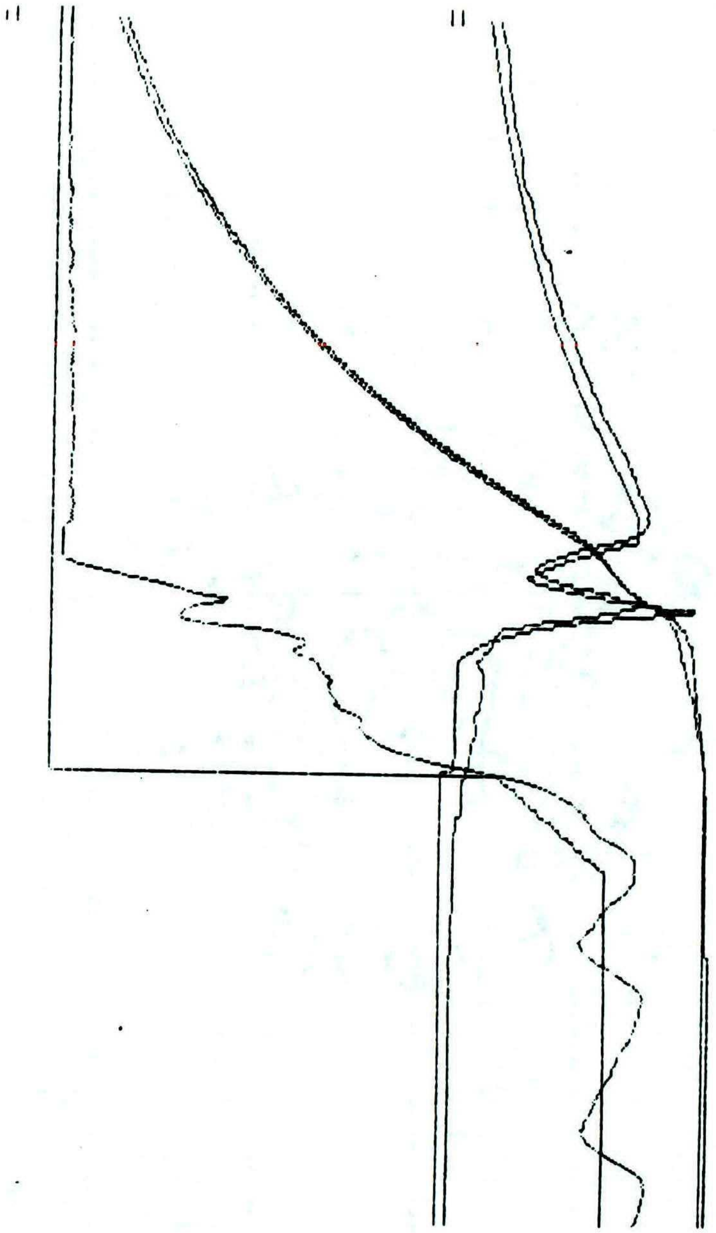

Figure A-5 Plot 940

Diagram to printer -after numb. cyc   Cyc =   944   14.11.95 07:09:28

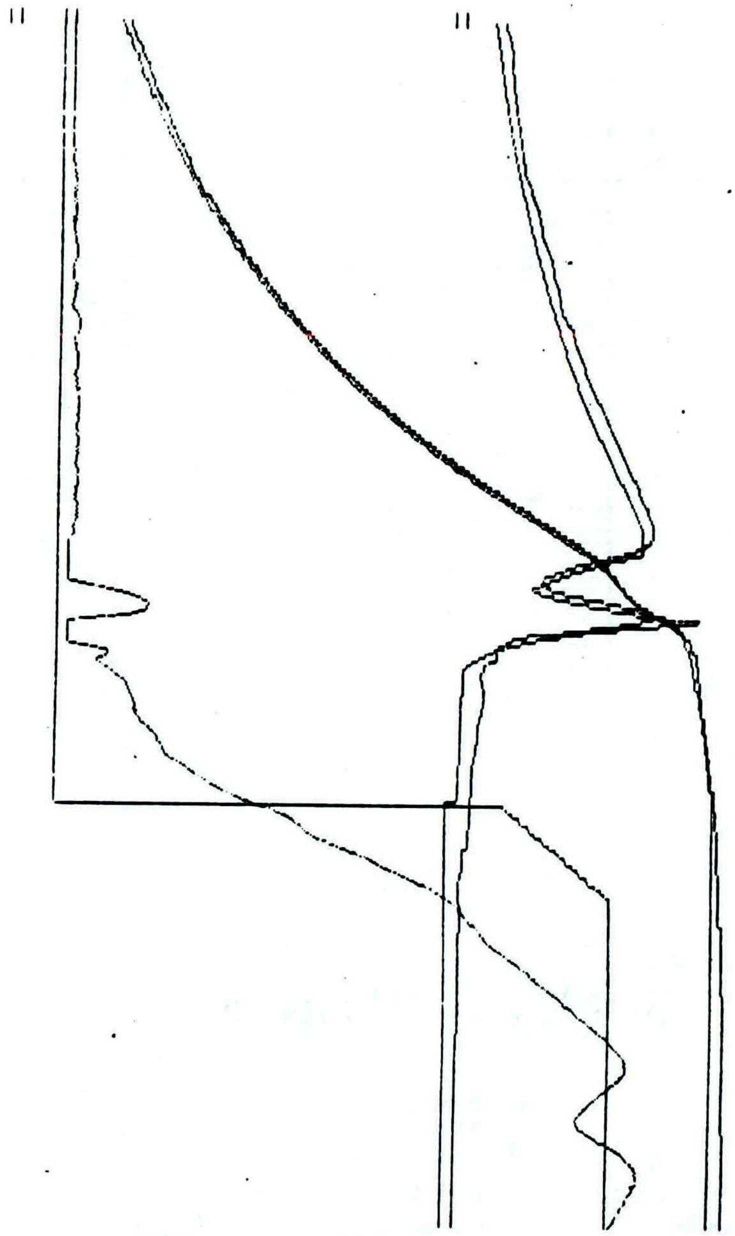

Figure A-6 Plot 944

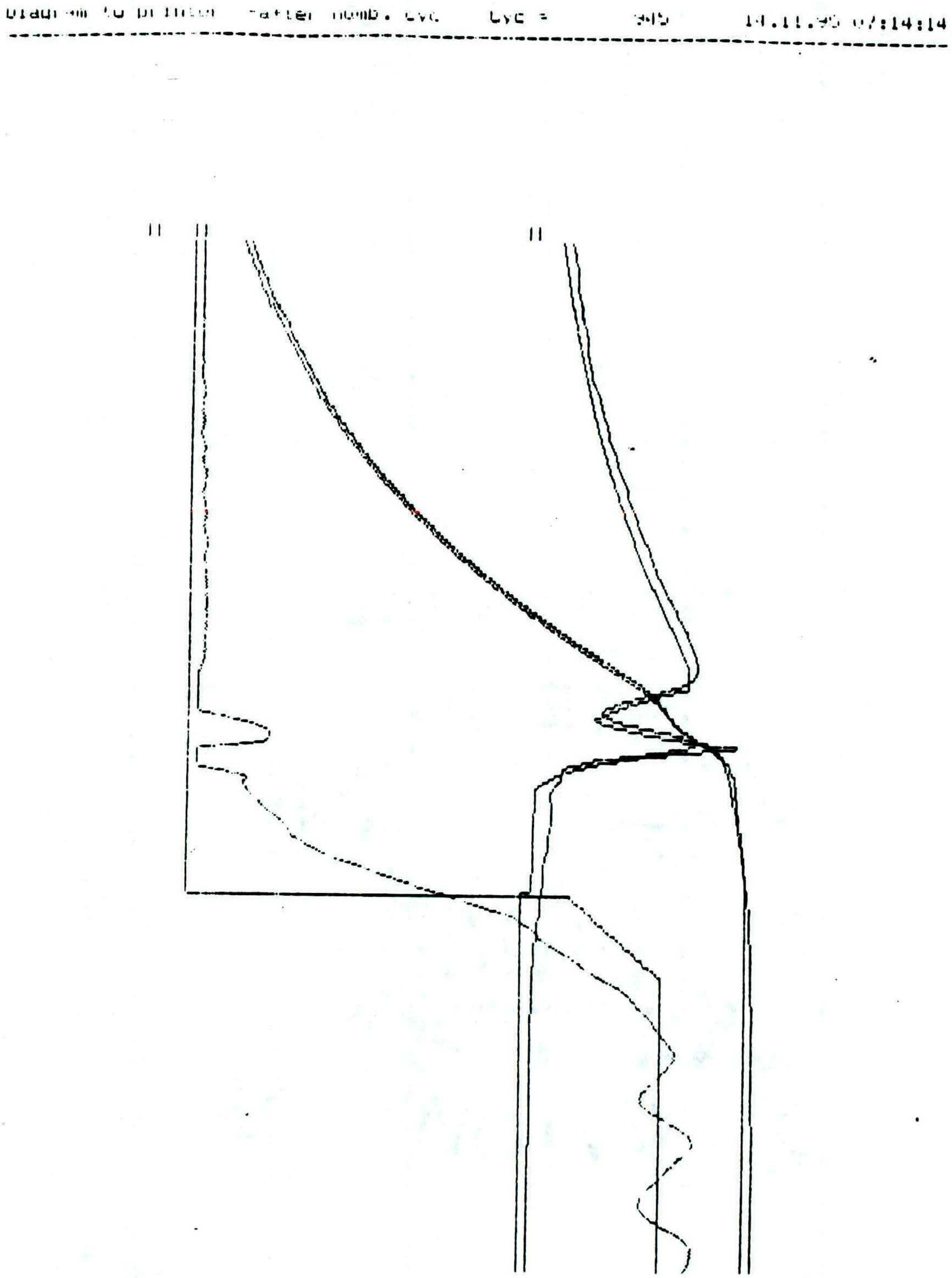

Figure A-7 Plot 945

Diagram to printer -after numb. cyc Cyc = 946 14.11.95 07:50:41

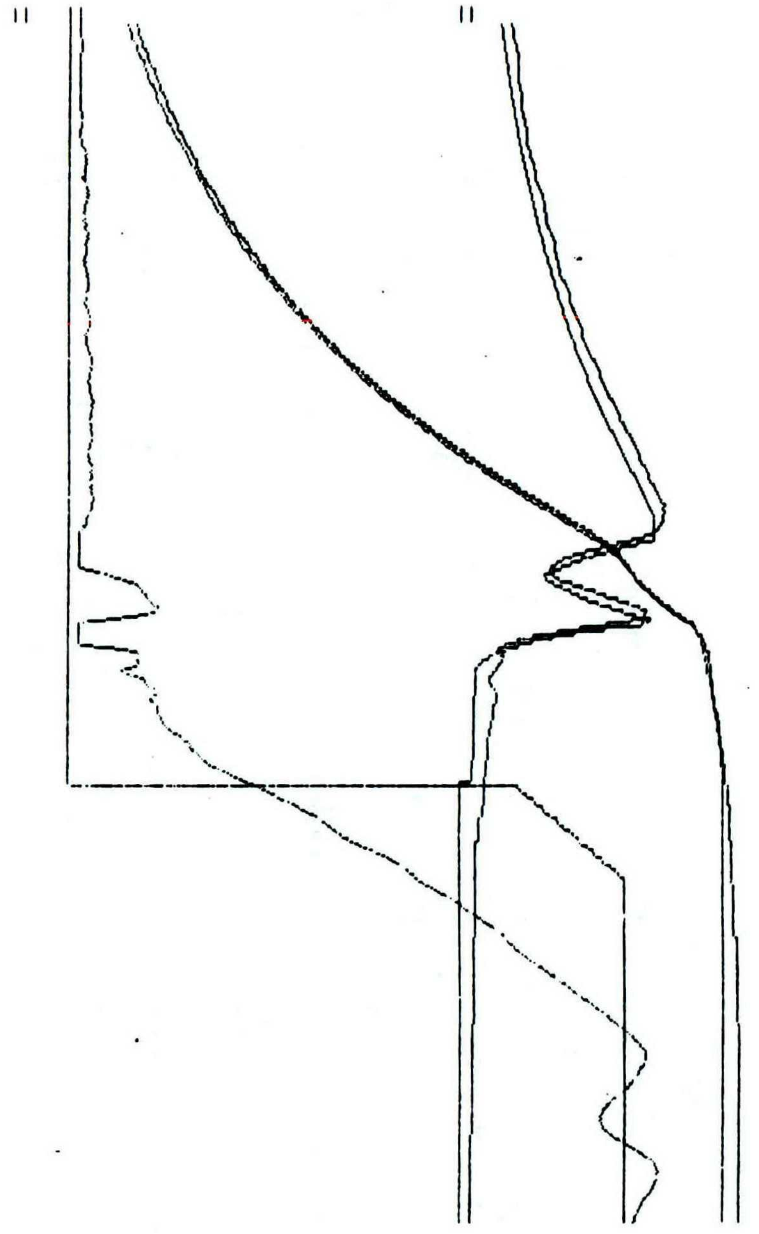

Figure A-8 Plot 946

Diagram to printer -after numb. cyc Cyc = 947 14.11.95 07:34:48

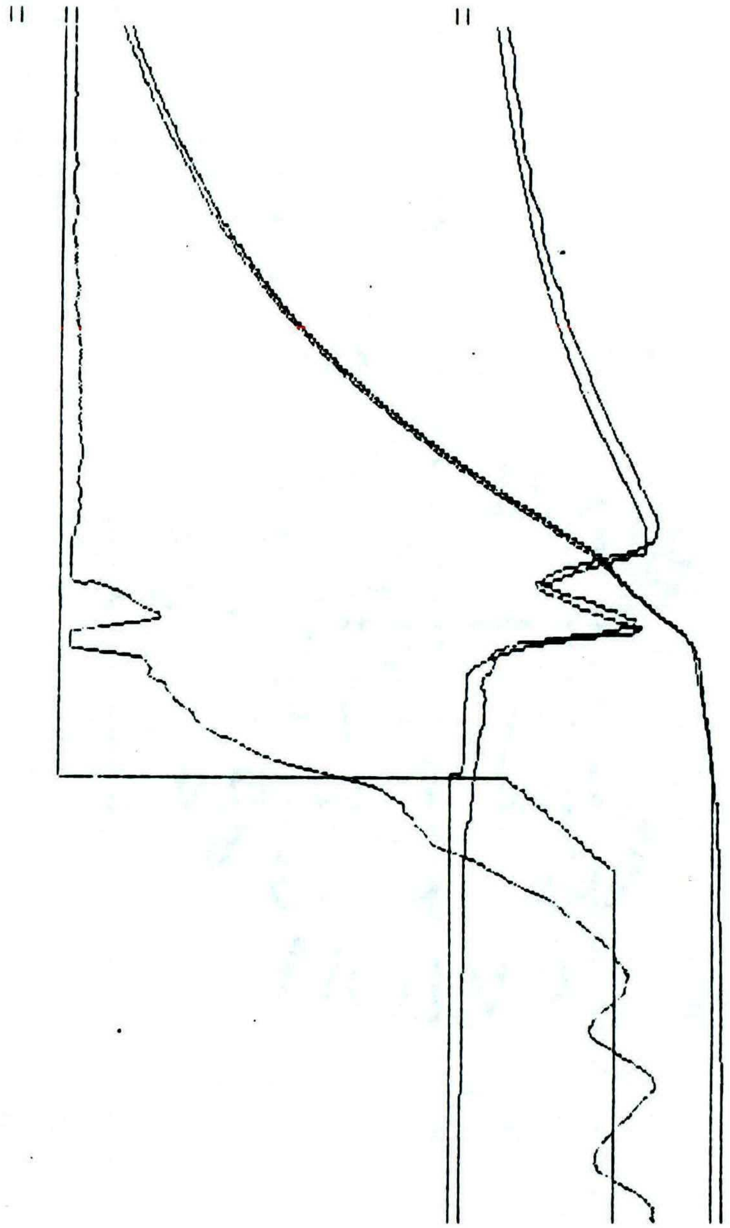

Figure A-9 Plot 947

Diagram to printer -after numb. cyc Cyc = 949 14.11.95 07:43:12

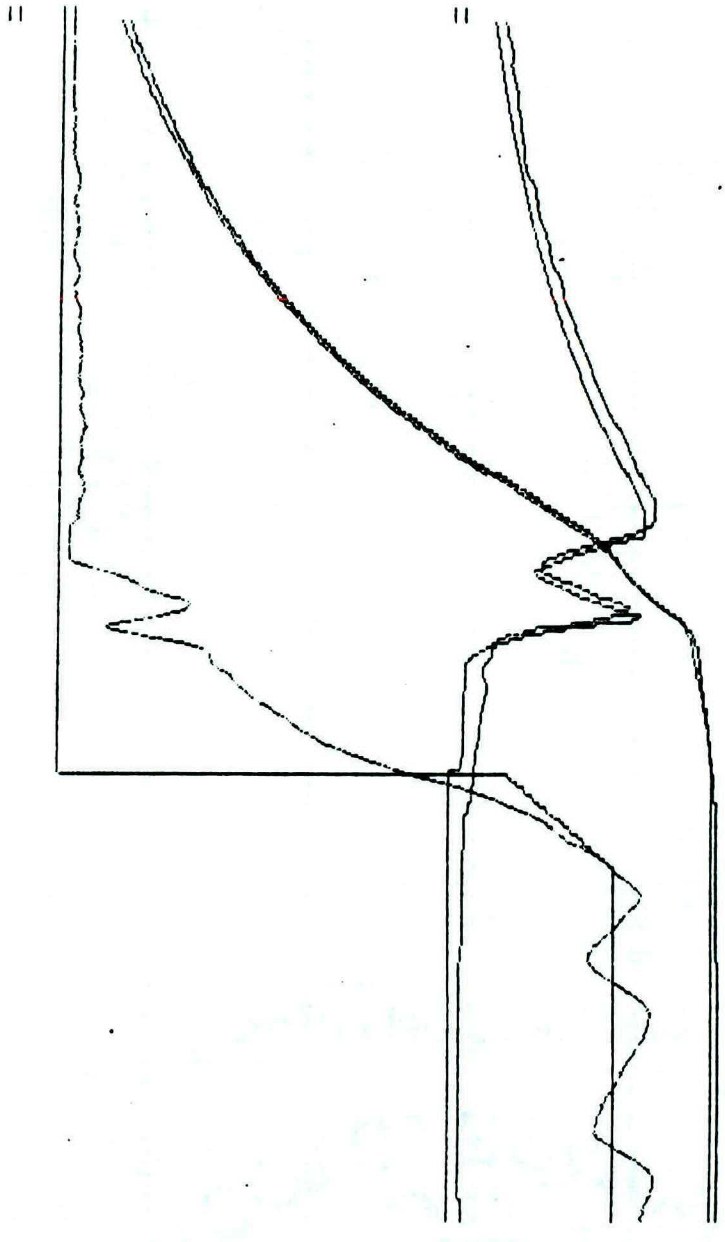

Figure A-10 Plot 948

Diagram to printer -after numb. cyc Cyc = 948 14.11.95 07:39:22

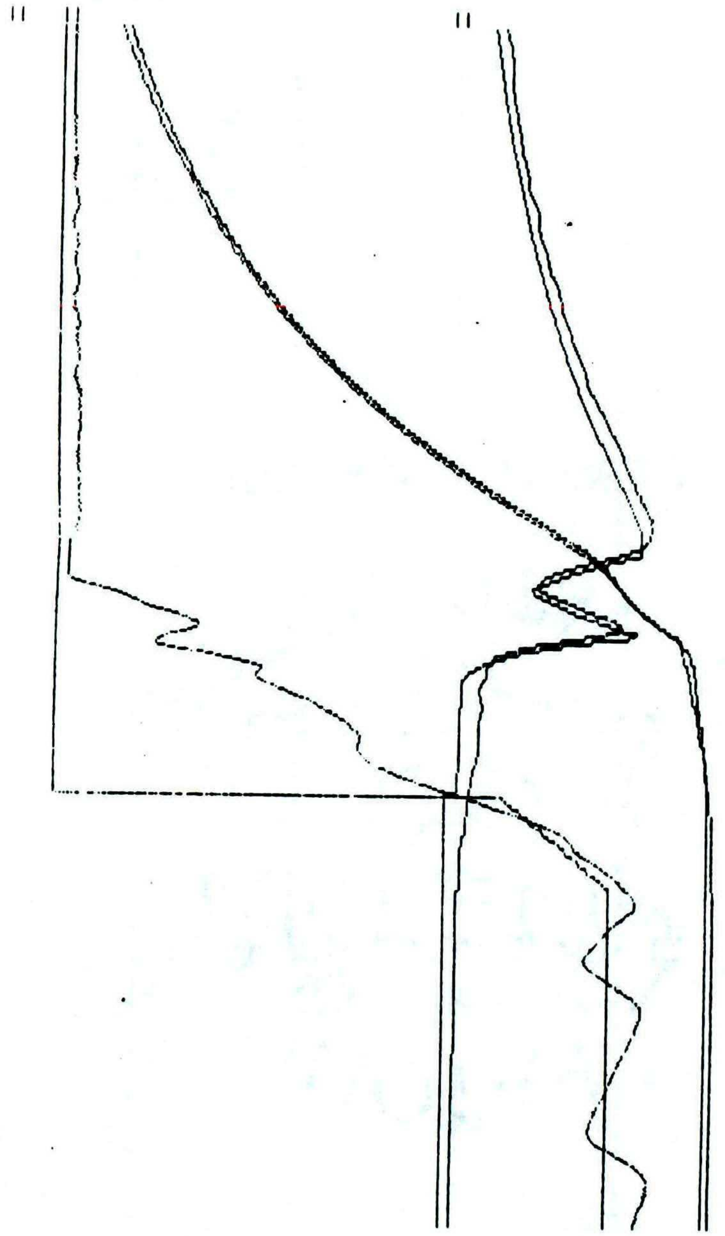

Figure A-11 Plot 949

agram to printer -after numb. cyc cyc 4 950

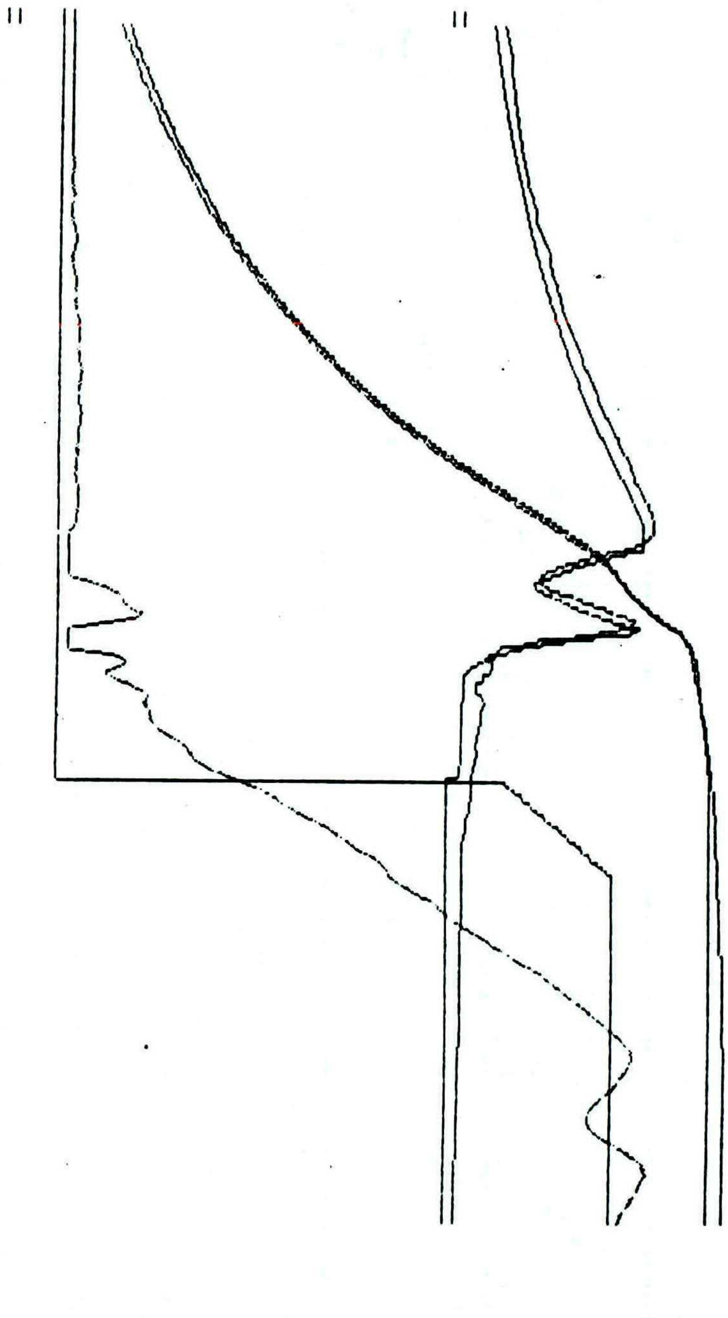

Figure A-12 Plot 950

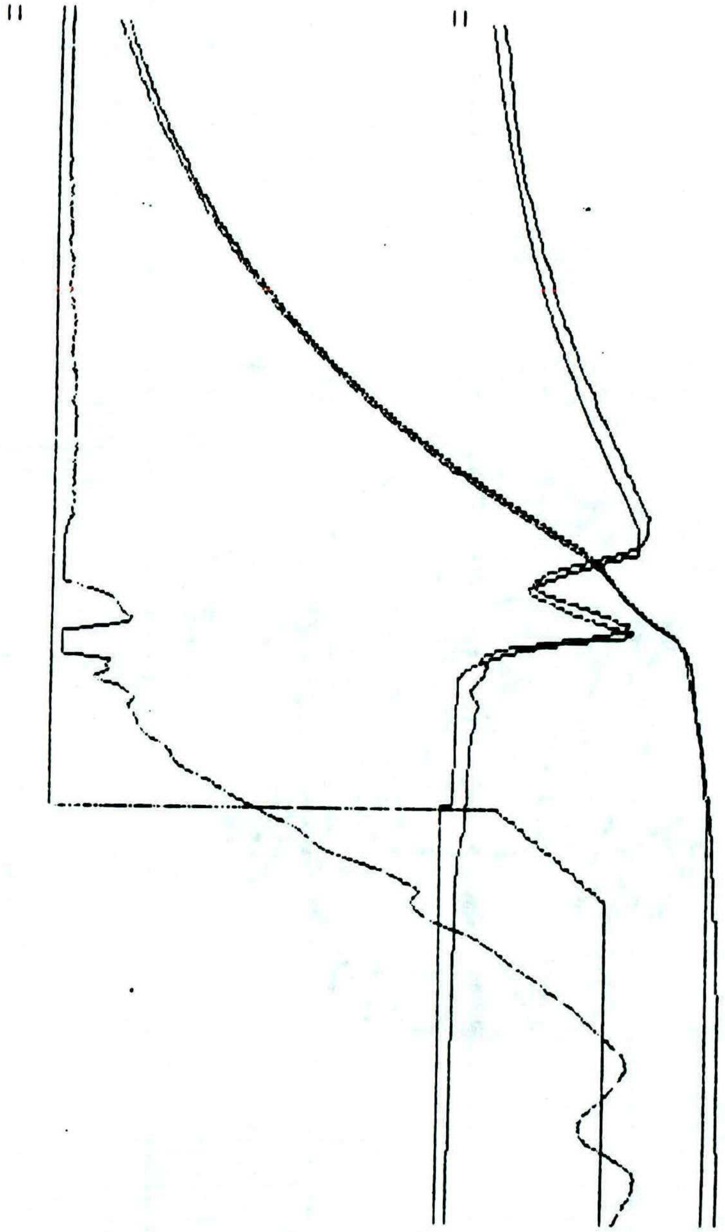

Figure A-13 Plot 951

Diagram to printer -after numb. cyc Cyc = 952 14.11.95 07:54:55

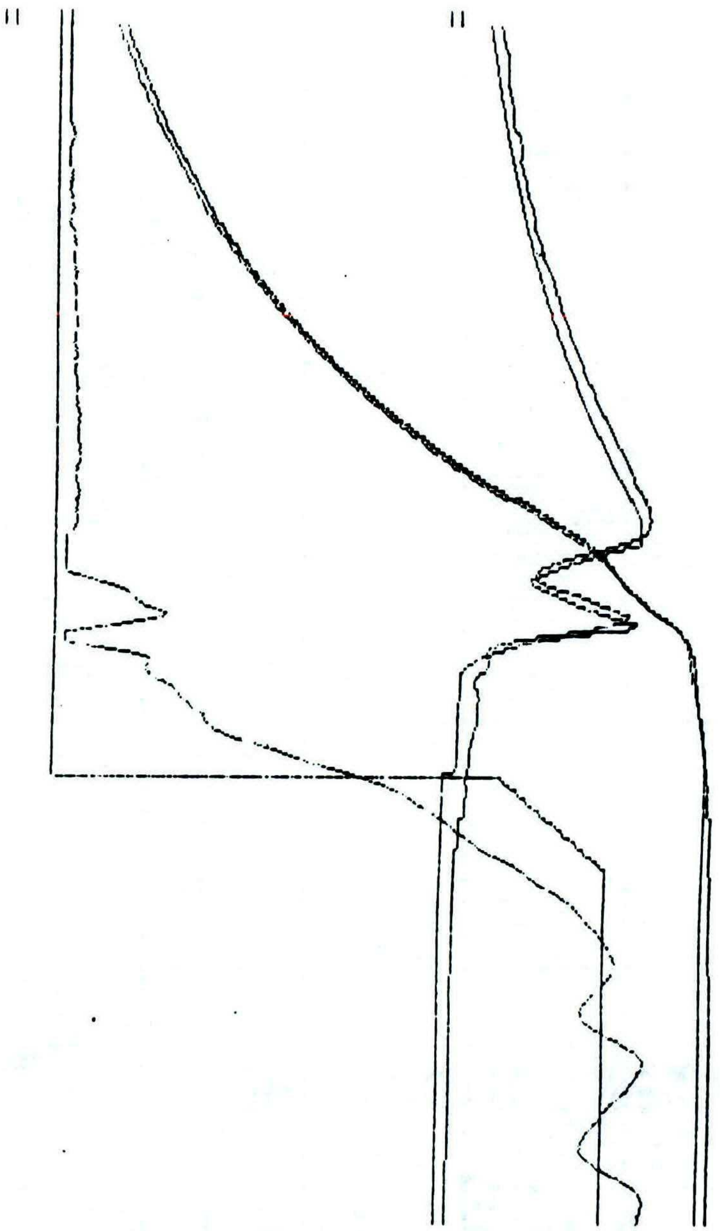

Figure A-14 Plot 952

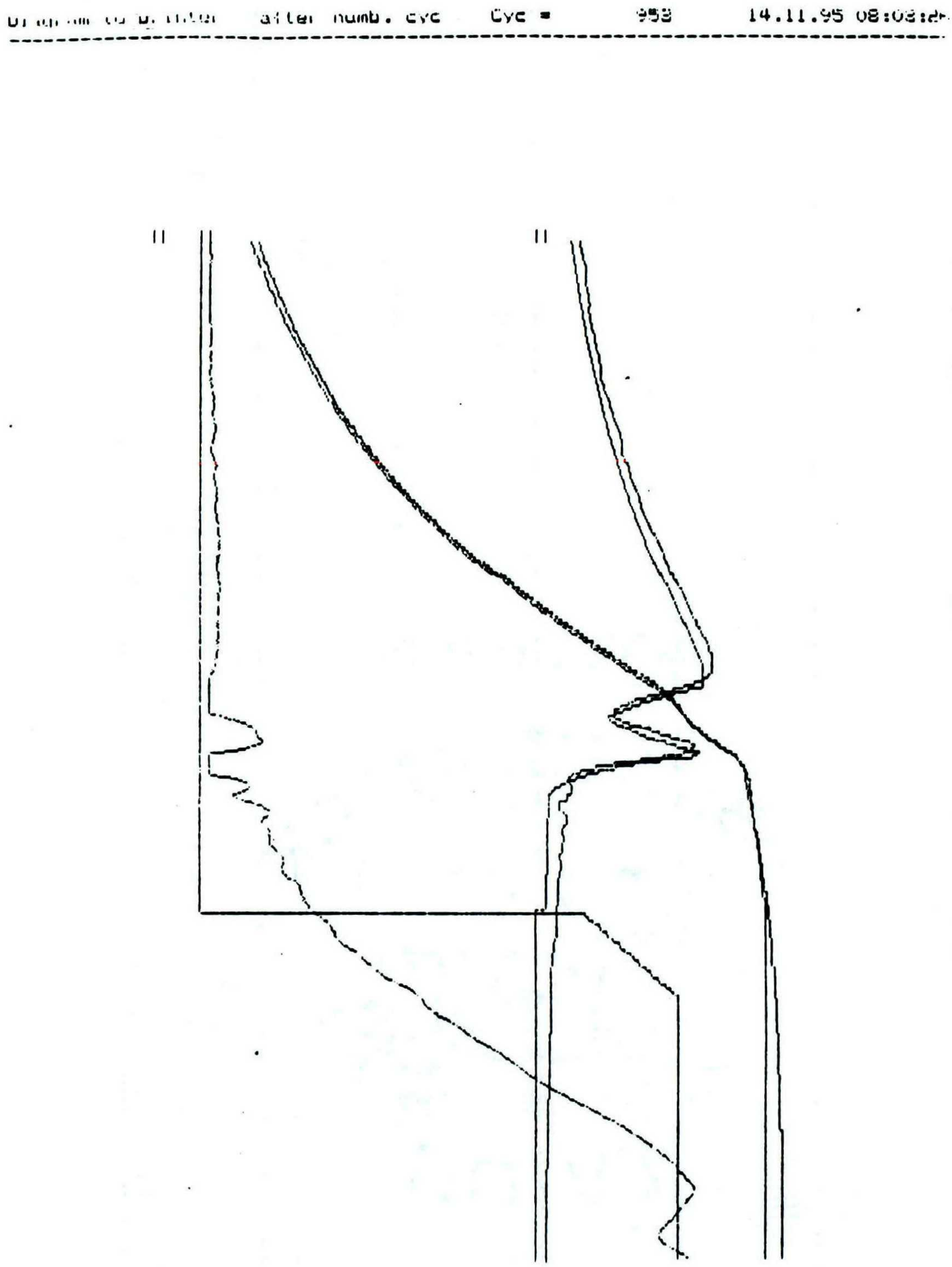

Figure A-15 Plot 953

Diagram to printer after numb. cyc   Cyc =   954   14.11.95 08:07:55

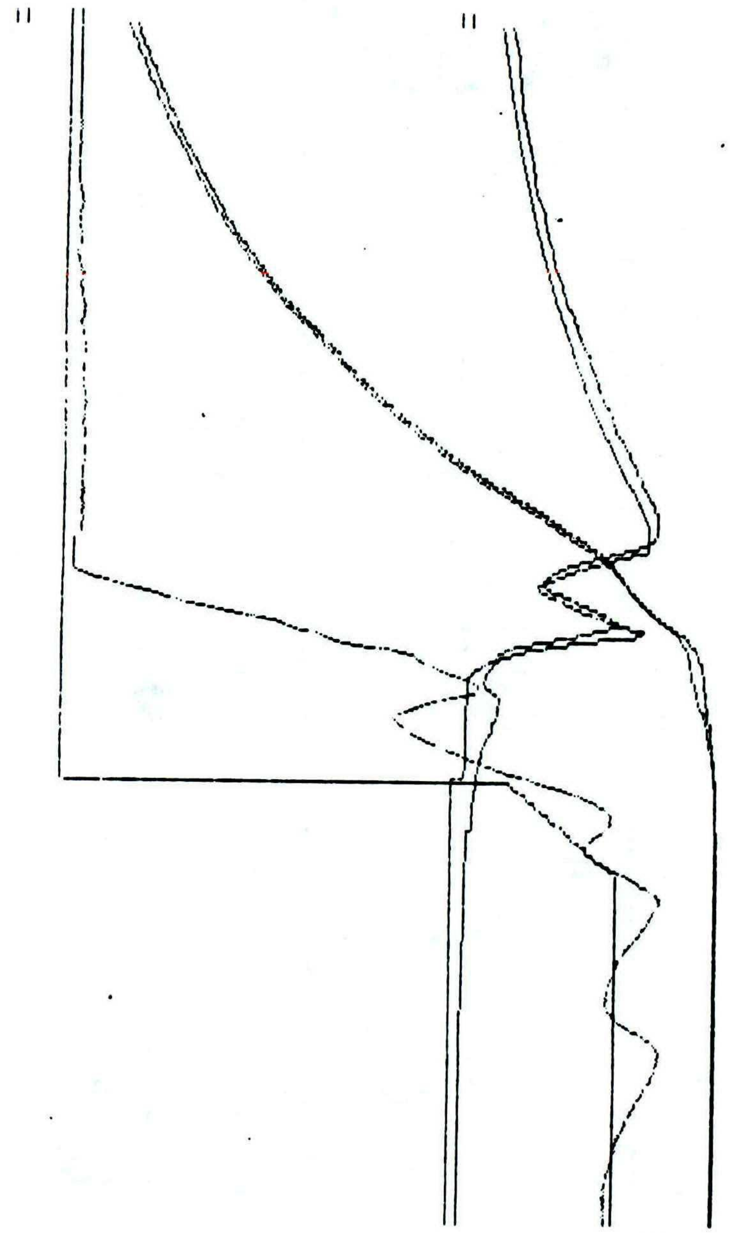

Figure A-16 Plot 954

APPENDIX B

SAMPLE CALCULATIONS FOR VISCOSITY

VISCOSITY VALUES FROM DINSDALE

FOR PLOT NO 937 (good)

v mm	p mm	flow rate Q m3/s	shear rate D /s	pressure Pa	s mm	stress Pa	viscosity Pa s
Viscosity computations for flow through the plate body							
22	0	0.0048532	14933.2964	0	20	0	0
15	11	0.003309	10181.793	11000000	16	-484425	-47.5776
30	18	0.006618	20363.586	18000000	12	-5652261	-277.567
41	0	0.0090446	27830.2342	0	8	0	0
18	0	0.0039708	12218.1516	0	5	0	0
5	20	0.001103	3393.931	20000000	3	490897.8	144.6399
4	30	0.0008824	2715.1448	30000000	2	657572.1	242.1867
2	57	0.0004412	1357.5724	57000000	1	1128644	831.3695
Viscosity computations for flow through the runner							
22	0	0.0048532	11007.0576	0	1	0	0
15	11	0.003309	7504.812	11000000	4	489775	65.26146
30	18	0.006618	15009.624	18000000	8	400725	26.69787
41	0	0.0090446	20513.1528	0	12	0	0
18	0	0.0039708	9005.7744	0	15	0	0
5	20	0.001103	2501.604	20000000	17	209529.4	83.75803
4	30	0.0008824	2001.2832	30000000	18	296833.3	148.3215
2	57	0.0004412	1000.6416	57000000	19	534300	533.9574

FOR PLOT NO 938 (not good, metal temperature too low)

v mm	p mm	flow rate Q m3/s	shear rate D /s	pressure Pa	s mm	stress Pa	viscosity Pa s
Viscosity computations for flow through the plate body							
33	0	0.0072798	22399.9446	0	26	0	0
27	0	0.0059562	18327.2274	0	20	0	0
17	2	0.0037502	11539.3654	2000000	18	-61597.7	-5.33805
14	11	0.0030884	9503.0068	11000000	17	-398724	-41.9576
17	25	0.0037502	11539.3654	25000000	15	-1402395	-121.531
29	37	0.0063974	19684.7998	37000000	12	-1.2E+07	-590.229
31	36	0.0068386	21042.3722	36000000	10	5473768	260.1308

22	40	0.0048532	14933.2964	40000000	8	2448249	163.9456
12	53	0.0026472	8145.4344	53000000	7	2497773	306.647
8	63	0.0017648	5430.2896	63000000	6	2413830	444.5122
6	60	0.0013236	4072.7172	60000000	5	1936715	475.5339
7	62	0.0015442	4751.5034	62000000	4	1728898	363.8634
6	61	0.0013236	4072.7172	61000000	3.2	1533991	376.6506
5	63	0.001103	3393.931	63000000	3	1546328	455.6156
4	70	0.0008824	2715.1448	70000000	2	1534335	565.1024
3	83	0.0006618	2036.3586	83000000	1	1643464	807.0604

Viscosity computations for flow through the runner

33	0	0.0072798	16510.5864	0	1	0	0
27	0	0.0059562	13508.6616	0	6	0	0
17	2	0.0037502	8505.4536	2000000	8	44525	5.234877
14	11	0.0030884	7004.4912	11000000	9	217677.8	31.07689
17	25	0.0037502	8505.4536	25000000	11	404772.7	47.58979
~~29~~	~~37~~	~~0.0063974~~	~~14509.3032~~	~~37000000~~	~~14~~	~~470692.9~~	~~32.44076~~
31	36	0.0068386	15509.9448	36000000	16	400725	25.83665
22	40	0.0048532	11007.0576	40000000	18	395777.8	35.95673
12	53	0.0026472	6003.8496	53000000	19	496805.3	82.74779
8	63	0.0017648	4002.5664	63000000	20	561015	140.1638
6	60	0.0013236	3001.9248	60000000	21	508857.1	169.5103
7	62	0.0015442	3502.2456	62000000	22	501918.2	143.3132
6	61	0.0013236	3001.9248	61000000	21.5	505307	168.3277
5	63	0.001103	2501.604	63000000	23	487839.1	195.0105
4	70	0.0008824	2001.2832	70000000	24	519458.3	259.5626
3	83	0.0006618	1500.9624	83000000	25	591292	393.9419

FOR PLOT NO 939 (very bad)

v	p	flow rate Q	shear rate D	pressure	s	stress	viscosity
mm	mm	m3/s	/s	Pa	mm	Pa	Pa s

Viscosity computations for flow through the plate body

21	1	0.0046326	14254.5102	1000000	18	-30798.9	-2.16064
16	18	0.0035296	10860.5792	18000000	16	-792695	-72.9883
31	36	0.0068386	21042.3722	36000000	12	-1.1E+07	-537.227
42	36	0.0092652	28509.0204	36000000	9	3142042	110.2122
18	43	0.0039708	12218.1516	43000000	7	2026495	165.8594
5	54	0.001103	3393.931	54000000	5	1743044	513.5766
5	57	0.001103	3393.931	57000000	3	1399059	412.2236
3	83	0.0006618	2036.3586	83000000	1	1643464	807.0604

Viscosity computations for flow through the runner

21	1	0.0046326	10506.7368	1000000	1	178100	16.95103
16	18	0.0035296	8005.1328	18000000	2	1602900	200.234
31	36	0.0068386	15509.9448	36000000	6	1068600	68.89773
42	36	0.0092652	21013.4736	36000000	9	712400	33.90206
18	43	0.0039708	9005.7744	43000000	11	696209.1	77.30697
5	54	0.001103	2501.604	54000000	14	686957.1	274.6067
5	57	0.001103	2501.604	57000000	16	634481.3	253.6298
3	83	0.0006618	1500.9624	83000000	17	869547.1	579.3263

FOR PLOT NO 940 (good, stuck in the mould)

v	p	flow rate Q	shear rate D	pressure	s	stress	viscosity
mm	mm	m3/s	/s	Pa	mm	Pa	Pa s

Viscosity computations for flow through the plate body

20	1	0.004412	13575.724	1000000	20	-23679.8	-1.74427
15	12	0.003309	10181.793	12000000	17	-434971	-42.7205
26	22	0.0057356	17648.4412	22000000	15	-1234107	-69.9273
33	29	0.0072798	22399.9446	29000000	12	-9106420	-406.538
22	22	0.0048532	14933.2964	22000000	8	1346537	90.17009
8	37	0.0017648	5430.2896	37000000	7	1743728	321.1114
7	44	0.0015442	4751.5034	44000000	6	1685850	354.8034
5	44	0.001103	3393.931	44000000	5.5	1541699	454.2517
5	48	0.001103	3393.931	48000000	5	1549372	456.5125
5	51	0.001103	3393.931	51000000	3	1251789	368.8317
4	58	0.0008824	2715.1448	58000000	2	1271306	468.2277
3	77	0.0006618	2036.3586	77000000	1	1524660	748.7187

Viscosity computations for flow through the runner

20	1	0.004412	10006.416	1000000	1	178100	17.79858
15	12	0.003309	7504.812	12000000	4	534300	71.19432
26	22	0.0057356	13008.3408	22000000	6	653033.3	50.20112
33	29	0.0072798	16510.5864	29000000	9	573877.8	34.75817
22	22	0.0048532	11007.0576	22000000	13	301400	27.38243
8	37	0.0017648	4002.5664	37000000	14	470692.9	117.5978
7	44	0.0015442	3502.2456	44000000	15	522426.7	149.1691
5	44	0.001103	2501.604	44000000	15.5	505574.2	202.1
5	48	0.001103	2501.604	48000000	16	534300	213.583
5	51	0.001103	2501.604	51000000	18	504616.7	201.7172

4	58	0.0008824	2001.2832	58000000	19	543673.7	271.6625
3	77	0.0006618	1500.9624	77000000	20	685685	456.8302

FOR PLOT NO 944 (high temperature)

v	p	flow rate Q	shear rate D	pressure	s	stress	viscosity
mm	mm	m3/s	/s	Pa	mm	Pa	Pa s

Viscosity computations for flow through the plate body

21	0	0.0046326	14254.5102	0	25	0	0
15	5	0.003309	10181.793	5000000	20	-118399	-11.6285
22	12	0.0048532	14933.2964	12000000	19	-321290	-21.515
27	14	0.0059562	18327.2274	14000000	17	-507466	-27.6892
~~34~~	~~7~~	~~0.0075004~~	~~23078.7308~~	~~7000000~~	12	-2198101	-95.2436
30	1	0.006618	20363.586	1000000	11	589578.2	28.95257
8	2	0.0017648	5430.2896	2000000	8	122412.4	22.54252
7	7	0.0015442	4751.5034	7000000	7	329894.5	69.4295
4	10	0.0008824	2715.1448	10000000	5	322785.8	118.8835
4	13	0.0008824	2715.1448	13000000	4	362510.9	133.5144
3	18	0.0006618	2036.3586	18000000	3	441808	216.9598
2	33	0.0004412	1357.5724	33000000	3	809981.3	596.6395

Viscosity computations for flow through the runner

21	0	0.0046326	10506.7368	0	1	0	0
15	5	0.003309	7504.812	5000000	6	148416.7	19.7762
22	12	0.0048532	11007.0576	12000000	7	305314.3	27.73805
27	14	0.0059562	13508.6616	14000000	9	277044.4	20.50865
34	7	0.0075004	17010.9072	7000000	14	89050	5.234877
30	1	0.006618	15009.624	1000000	15	11873.33	0.791048
8	2	0.0017648	4002.5664	2000000	18	19788.89	4.94405
7	7	0.0015442	3502.2456	7000000	19	65615.79	18.73535
4	10	0.0008824	2001.2832	10000000	21	84809.52	42.37757
4	13	0.0008824	2001.2832	13000000	22	105240.9	52.58671
3	18	0.0006618	1500.9624	18000000	25	128232	85.43319
2	33	0.0004412	1000.6416	33000000	25	235092	234.9413

FOR PLOT NO 956 (constant velocity test, very good)

v	p	flow rate Q	shear rate D	pressure	s	stress	viscosity

mm	mm	m3/s	/s	Pa	mm	Pa	Pa s

Viscosity computations for flow through the plate body

29	1	0.0063974	19684.7998	1000000	32	-9920.79	-0.50398
29	3	0.0063974	19684.7998	3000000	27	-39269.6	-1.99492
29	4	0.0063974	19684.7998	4000000	22	-76935.6	-3.90838
28.5	6	0.0062871	19345.4067	6000000	20	-142079	-7.34431
28	15	0.0061768	19006.0136	15000000	17	-543714	-28.6075
26	29	0.0057356	17648.4412	29000000	14	-2240082	-126.928
22	55	0.0048532	14933.2964	55000000	11	32426803	2171.443
17	80	0.0037502	11539.3654	80000000	9	6982316	605.0867
14	69	0.0030884	9503.0068	69000000	6	2643719	278.1981
10	60	0.002206	6787.862	60000000	6	2298886	338.676
7	62	0.0015442	4751.5034	62000000	5	2001272	421.1872
6	67	0.0013236	4072.7172	67000000	4.5	2004749	492.2387
5	69	0.001103	3393.931	69000000	4	1924097	566.9227
5	71	0.001103	3393.931	71000000	3	1742687	513.4716
4.5	75	0.0009927	3054.5379	75000000	2.5	1736834	568.6077
4	83	0.0008824	2715.1448	83000000	2	1819283	670.05
3	90	0.0006618	2036.3586	90000000	1.5	1872553	919.5596
2	95	0.0004412	1357.5724	95000000	1	1881074	1385.616

Viscosity computations for flow through the runner

29	1	0.0063974	14509.3032	1000000	1	178100	12.27488
29	3	0.0063974	14509.3032	3000000	6	89050	6.137442
29	4	0.0063974	14509.3032	4000000	11	64763.64	4.463594
28.5	6	0.0062871	14259.1428	6000000	13	82200	5.764722
28	15	0.0061768	14008.9824	15000000	16	166968.8	11.91869
26	29	0.0057356	13008.3408	29000000	19	271836.8	20.89712
22	55	0.0048532	11007.0576	55000000	22	445250	40.45132
17	80	0.0037502	8505.4536	80000000	24	593666.7	69.79835
14	69	0.0030884	7004.4912	69000000	27	455144.4	64.97894
10	60	0.002206	5003.208	60000000	27	395777.8	79.1048
7	62	0.0015442	3502.2456	62000000	28	394364.3	112.6033
6	67	0.0013236	3001.9248	67000000	28.5	418691.2	139.4743
5	69	0.001103	2501.604	69000000	29	423755.2	169.3934
5	71	0.001103	2501.604	71000000	30	421503.3	168.4932
4.5	75	0.0009927	2251.4436	75000000	30.5	437950.8	194.52
4	83	0.0008824	2001.2832	83000000	31	476848.4	238.2713
3	90	0.0006618	1500.9624	90000000	31.5	508857.1	339.0206
2	95	0.0004412	1000.6416	95000000	32	528734.4	528.3954

FOR PLOT NO 949 (very good -- compensated for acceleration)

v	p	flow rate Q	shear rate D	pressure	s	stress	viscosity
mm	mm	m3/s	/s	Pa	mm	Pa	Pa s

Viscosity computations for flow through the plate body

35	1	0.007721	23757.517	1000000	30	-10984.5	-0.46236
22	5	0.0048532	14933.2964	5000000	20	-118399	-7.92852
13	9	0.0028678	8824.2206	9000000	17	-326228	-36.9697
20	13	0.004412	13575.724	13000000	13	-1611851	-118.73
19	18	0.0041914	12896.9378	18000000	8	1101712	85.4243
12	21	0.0026472	8145.4344	21000000	5	677850.3	83.21843
5	25	0.001103	3393.931	25000000	4	697136.4	205.4068
4	33	0.0008824	2715.1448	33000000	3	809981.3	298.3197
4	43	0.0008824	2715.1448	43000000	2	942520	347.1343
2	60	0.0004412	1357.5724	60000000	1	1188047	875.1258

Viscosity computations for flow through the runner

35	1	0.007721	17511.228	1000000	1	178100	10.17062
22	5	0.0048532	11007.0576	5000000	11	80954.55	7.354785
13	9	0.0028678	6504.1704	9000000	14	114492.9	17.60299
20	13	0.004412	10006.416	13000000	18	128627.8	12.85453
19	18	0.0041914	9506.0952	18000000	23	139382.6	14.66245
12	21	0.0026472	6003.8496	21000000	26	143850	23.95963
5	25	0.001103	2501.604	25000000	27	164907.4	65.92067
4	33	0.0008824	2001.2832	33000000	28	209903.6	104.8845
4	43	0.0008824	2001.2832	43000000	29	264079.3	131.955
2	60	0.0004412	1000.6416	60000000	30	356200	355.9716

FOR PLOT NO 953 (very hot, quite nice)

v	p	flow rate Q	shear rate D	pressure	s	stress	viscosity
mm	mm	m3/s	/s	Pa	mm	Pa	Pa s

Viscosity computations for flow through the plate body

13	5	0.0028678	8824.2206	5000000	21	-106133	-12.0274
19	10	0.0041914	12896.9378	10000000	18	-307989	-23.8808
29	4	0.0063974	19684.7998	4000000	13	-495954	-25.1948
20	0	0.004412	13575.724	0	10	0	0
5	3	0.001103	3393.931	3000000	8	183618.6	54.10206
5	8	0.001103	3393.931	8000000	8	489649.7	144.2721

5	9	0.001103	3393.931	9000000	7	424150.1	124.9731
5	12	0.001103	3393.931	12000000	6	459777.2	135.4704
4	15	0.0008824	2715.1448	15000000	5	484178.8	178.3252
3	20	0.0006618	2036.3586	20000000	4	557709.1	273.8757

Viscosity computations for flow through the runner

13	5	0.0028678	6504.1704	5000000	1	890500	136.9122
19	10	0.0041914	9506.0952	10000000	4	445250	46.83837
29	4	0.0063974	14509.3032	4000000	9	79155.56	5.455504
20	0	0.004412	10006.416	0	12	0	0
5	3	0.001103	2501.604	3000000	14	38164.29	15.25593
5	8	0.001103	2501.604	8000000	14	101771.4	40.68247
5	9	0.001103	2501.604	9000000	15	106860	42.71659
5	12	0.001103	2501.604	12000000	16	133575	53.39574
4	15	0.0008824	2001.2832	15000000	17	157147.1	78.52315
3	20	0.0006618	1500.9624	20000000	21	169619	113.0069

FOR PLOT NO 945 (quite nice)

v	p	flow rate Q	shear rate D	pressure	s	stress	viscosity
mm	mm	m3/s	/s	Pa	mm	Pa	Pa s

Viscosity computations for flow through the plate body

15	2	0.003309	10181.793	2000000	18	-61597.7	-6.04979
23	13	0.0050738	15612.0826	13000000	17	-471219	-30.183
35	15	0.007721	23757.517	15000000	10	2280737	96.00064
7	4	0.0015442	4751.5034	4000000	6	153259.1	32.25486
7	10	0.0015442	4751.5034	10000000	6	383147.7	80.63714
5	15	0.001103	3393.931	15000000	4	418281.9	123.2441
3	12	0.0006618	2036.3586	12000000	3	294538.7	144.6399
3	36	0.0006618	2036.3586	36000000	2	789086.5	387.4988
2	50	0.0004412	1357.5724	50000000	1	990038.8	729.2715

Viscosity computations for flow through the runner

15	2	0.003309	7504.812	2000000	1	356200	47.46288
23	13	0.0050738	11507.3784	13000000	2	1157650	100.6007
35	15	0.007721	17511.228	15000000	9	296833.3	16.95103
7	4	0.0015442	3502.2456	4000000	13	54800	15.6471
7	10	0.0015442	3502.2456	10000000	13	137000	39.11776
5	15	0.001103	2501.604	15000000	15	178100	71.19432
3	12	0.0006618	1500.9624	12000000	16	133575	88.9929

3	36	0.0006618	1500.9624	36000000	17	377152.9	251.2741
2	50	0.0004412	1000.6416	50000000	18	494722.2	494.405

FOR PLOT NO 946 (new velocity)

v	p	flow rate Q	shear rate D	pressure	s	stress	viscosity
mm	mm	m3/s	/s	Pa	mm	Pa	Pa s

Viscosity computations for flow through the plate body

23	0	0.0050738	15612.0826	0	23	0	0
14	3	0.0030884	9503.0068	3000000	19	-80322.5	-8.45233
16	12	0.0035296	10860.5792	12000000	17	-434971	-40.0505
26	15	0.0057356	17648.4412	15000000	13	-1859828	-105.382
~~29~~	~~4~~	~~0.0063974~~	~~19684.7998~~	~~4000000~~	~~10~~	~~608196.5~~	~~30.89676~~
6	6	0.0013236	4072.7172	6000000	6	229888.6	56.446
4	11	0.0008824	2715.1448	11000000	5	355064.4	130.7718
3	12	0.0006618	2036.3586	12000000	5	387343	190.2136
3	17	0.0006618	2036.3586	17000000	4	474052.8	232.7943
2	30	0.0004412	1357.5724	30000000	2	657572.1	484.3735

Viscosity computations for flow through the runner

23	0	0.0050738	11507.3784	0	1	0	0
14	3	0.0030884	7004.4912	3000000	5	106860	15.25593
16	12	0.0035296	8005.1328	12000000	7	305314.3	38.13982
26	15	0.0057356	13008.3408	15000000	11	242863.6	18.66984
29	4	0.0063974	14509.3032	4000000	14	50885.71	3.507109
6	6	0.0013236	3001.9248	6000000	18	59366.67	19.7762
4	11	0.0008824	2001.2832	11000000	19	103110.5	51.52221
3	12	0.0006618	1500.9624	12000000	19	112484.2	74.94139
3	17	0.0006618	1500.9624	17000000	20	151385	100.8586
2	30	0.0004412	1000.6416	30000000	23	232304.3	232.1554

FOR PLOT NO 947 (very good)

v	p	flow rate Q	shear rate D	pressure	s	stress	viscosity
mm	mm	m3/s	/s	Pa	mm	Pa	Pa s

Viscosity computations for flow through the plate body

13	6	0.0028678	8824.2206	6000000	18	-184793	-20.9416
25	16	0.005515	16969.655	16000000	11	9433252	555.8894
27	4	0.0059562	18327.2274	4000000	38	-30749.7	-1.67781
5	6	0.001103	3393.931	6000000	5	193671.5	57.06407
5	15	0.001103	3393.931	15000000	4	418281.9	123.2441
3	24	0.0006618	2036.3586	24000000	2	526057.7	258.3325
2	44	0.0004412	1357.5724	44000000	1	871234.2	641.7589

Viscosity computations for flow through the runner

13	6	0.0028678	6504.1704	6000000	1	1068600	164.2946
25	16	0.005515	12508.02	16000000	8	356200	28.47773
27	4	0.0059562	13508.6616	4000000	11	64763.64	4.79423
5	6	0.001103	2501.604	6000000	14	76328.57	30.51185
5	15	0.001103	2501.604	15000000	15	178100	71.19432
3	24	0.0006618	1500.9624	24000000	17	251435.3	167.5161
2	44	0.0004412	1000.6416	44000000	18	435355.6	435.0764

FOR PLOT NO 948 (very big, large flash all around)

v	p	flow rate Q	shear rate D	pressure	s	stress	viscosity
mm	mm	m3/s	/s	Pa	mm	Pa	Pa s

Viscosity computations for flow through the plate body

20	0	0.004412	13575.724	0	20	0	0
13	7	0.0028678	8824.2206	7000000	17	-253733	-28.7542
27	23	0.0059562	18327.2274	23000000	10	3497130	190.8161
23	18	0.0050738	15612.0826	18000000	7	848300.2	54.33613
6	34	0.0013236	4072.7172	34000000	5	1097472	269.4692
4	37	0.0008824	2715.1448	37000000	4	1031762	380.0025
4	52	0.0008824	2715.1448	52000000	3	1276334	470.0796
3	55	0.0006618	2036.3586	55000000	2	1205549	592.012
2	69	0.0004412	1357.5724	69000000	1	1366254	1006.395

Viscosity computations for flow through the runner

20	0	0.004412	10006.416	0	1	0	0
13	7	0.0028678	6504.1704	7000000	4	311675	47.91926
27	23	0.0059562	13508.6616	23000000	11	372390.9	27.56682
23	18	0.0050738	11507.3784	18000000	14	228985.7	19.89903
6	34	0.0013236	3001.9248	34000000	16	378462.5	126.0733
4	37	0.0008824	2001.2832	37000000	17	387629.4	193.6904
4	52	0.0008824	2001.2832	52000000	18	514511.1	257.0906

3	55	0.0006618	1500.9624	55000000	19	515552.6	343.4814
2	69	0.0004412	1000.6416	69000000	20	614445	614.051

FOR PLOT NO 951 (high repeatability, steady state, hot)

v mm	p mm	flow rate Q m3/s	shear rate D /s	pressure Pa	s mm	stress Pa	viscosity Pa s

Viscosity computations for flow through the plate body

13	5	0.0028678	8824.2206	5000000	20	-118399	-13.4175
26	12	0.0057356	17648.4412	12000000	13	-1487863	-84.3056
26	30	0.0057356	17648.4412	30000000	9	2618369	148.3626
6	8	0.0013236	4072.7172	8000000	7	377022.3	92.57267
~~4~~	~~9~~	~~0.0008824~~	~~2715.1448~~	~~9000000~~	~~6~~	~~344832.9~~	~~127.0035~~
4	13	0.0008824	2715.1448	13000000	5	419621.6	154.5485
3	22	0.0006618	2036.3586	22000000	3	539987.5	265.1731
2	35	0.0004412	1357.5724	35000000	2	767167.4	565.1024

Viscosity computations for flow through the runner

13	5	0.0028678	6504.1704	5000000	1	890500	136.9122
26	12	0.0057356	13008.3408	12000000	8	267150	20.53682
26	30	0.0057356	13008.3408	30000000	12	445250	34.22804
6	8	0.0013236	3001.9248	8000000	14	101771.4	33.90206
4	9	0.0008824	2001.2832	9000000	15	106860	53.39574
4	13	0.0008824	2001.2832	13000000	16	144706.3	72.30673
3	22	0.0006618	1500.9624	22000000	18	217677.8	145.0255
2	35	0.0004412	1000.6416	35000000	19	328078.9	327.8686

FOR PLOT NO 952 (not bad)

v mm	p mm	flow rate Q m3/s	shear rate D /s	pressure Pa	s mm	stress Pa	viscosity Pa s

Viscosity computations for flow through the plate body

13	5	0.0028678	8824.2206	5000000	18	-153994	-17.4513
26	18	0.0057356	17648.4412	18000000	10	2736884	155.078
6	8	0.0013236	4072.7172	8000000	5	258228.7	63.40452
3	17	0.0006618	2036.3586	17000000	3	417263.1	204.9065

4	26	0.0008824	2715.1448	26000000	3	638167.1	235.0398
2	53	0.0004412	1357.5724	53000000	2	1161711	855.7265

Viscosity computations for flow through the runner

13	5	0.0028678	6504.1704	5000000	1	890500	136.9122
26	18	0.0057356	13008.3408	18000000	9	356200	27.38243
6	8	0.0013236	3001.9248	8000000	14	101771.4	33.90206
3	17	0.0006618	1500.9624	17000000	16	189231.3	126.0733
4	26	0.0008824	2001.2832	26000000	16	289412.5	144.6135
2	53	0.0004412	1000.6416	53000000	17	555252.9	554.8969

FOR PLOT NO 954 (failed, cold)

v	p	flow rate Q	shear rate D	pressure	s	stress	viscosity
mm	mm	m3/s	/s	Pa	mm	Pa	Pa s

Viscosity computations for flow through the plate body

16	2	0.0035296	10860.5792	2000000	18	-61597.7	-5.67168
14	13	0.0030884	9503.0068	13000000	15	-729245	-76.7384
30	40	0.006618	20363.586	40000000	8	2448249	120.2268
7	62	0.0015442	4751.5034	62000000	5	2001272	421.1872
5	73	0.001103	3393.931	73000000	4	2035638	599.7878
6	59	0.0013236	4072.7172	59000000	3	1448148	355.573
5	60	0.001103	3393.931	60000000	2	1315144	387.4988
2	82	0.0004412	1357.5724	82000000	1	1623664	1196.005

Viscosity computations for flow through the runner

16	2	0.0035296	8005.1328	2000000	1	356200	44.49645
14	13	0.0030884	7004.4912	13000000	4	578825	82.63627
30	40	0.006618	15009.624	40000000	11	647636.4	43.14807
7	62	0.0015442	3502.2456	62000000	14	788728.6	225.2065
5	73	0.001103	2501.604	73000000	15	866753.3	346.479
6	59	0.0013236	3001.9248	59000000	16	656743.8	218.7742
5	60	0.001103	2501.604	60000000	17	628588.2	251.2741
2	82	0.0004412	1000.6416	82000000	18	811344.4	810.8242

FOR PLOT NO 955 (very nice, CvS)

v	p	flow rate Q	shear rate D	pressure	s	stress	viscosity
mm	mm	m3/s	/s	Pa	mm	Pa	Pa s
Viscosity computations for flow through the plate body							
30	1	0.006618	20363.586	1000000	25	-15007.4	-0.73697
30	3	0.006618	20363.586	3000000	20	-71039.3	-3.48855
30	6	0.006618	20363.586	6000000	11	3537469	173.7154
30	3	0.006618	20363.586	3000000	8	183618.6	9.017009
5	9	0.001103	3393.931	9000000	6	344832.9	101.6028
5	12	0.001103	3393.931	12000000	5	387343	114.1281
5	20	0.001103	3393.931	20000000	3	490897.8	144.6399
3	38	0.0006618	2036.3586	38000000	2	832924.6	409.0265
Viscosity computations for flow through the runner							
30	1	0.006618	15009.624	1000000	1	178100	11.86572
~~30~~	~~3~~	~~0.006618~~	~~15009.624~~	~~3000000~~	~~6~~	~~89050~~	~~5.93286~~
30	6	0.006618	15009.624	6000000	15	71240	4.746288
30	3	0.006618	15009.624	3000000	18	29683.33	1.97762
5	9	0.001103	2501.604	9000000	20	80145	32.03744
5	12	0.001103	2501.604	12000000	21	101771.4	40.68247
5	20	0.001103	2501.604	20000000	23	154869.6	61.90811
3	38	0.0006618	1500.9624	38000000	25	270712	180.3589

APPENDIX C

FLOW 3D PREPIN FILE

```
edit
Flatplate
    $xput
        iedt=2, ifin=2, frcfin=1.0,
        pltfrc=0.1, prtfrc=0.1,
        itb=1, ifenrg=2, ihtc=2, ifrho=1, sprtdt=0.01, gz=-980.0,
        hpltdt=0.01, avrck=-10.0, iadiz=1, hflvl=21000.0e+01,
        imphtc=1, delt=1.0e-3, dtmin=1.0e-7, pvoid=1.013e+06,
        wi=150, autot=2.0, icolor=1,
    $end
    $limits
        itflmx=30, ncflmx=4,
    $end
    $props
        mui=3.66, muc0=1.0, muc1=1.34e-05, muc2=0.15, muc3=0.01,
        mutmp1=2.0, mutmp2=814.0, mutmp3=16.85,
        rhof=2.68e+03, rhofs=2.68e+03,
        clht1=389.0e+05, cvs1=963.0e+05,
        thc1=150.0e+05, thcs1=170.0e+05, tstar=886.0,
        tl1=886.0, ts1=815.0, tsdrg=1.0,
    $end
    $bcdata
        timbct(2)=0.1, timbct(3)=0.2,
        tbct(1,1)=523.0, tbct(1,2)=523.0, tbct(1,3)=523.0,
        tbct(1,4)=523.0, tbct(1,5)=853.0, tbct(1,6)=523.0,
        tbct(2,1)=523.0, tbct(2,2)=523.0, tbct(2,3)=523.0,
        tbct(2,4)=523.0, tbct(2,5)=853.0, tbct(2,6)=523.0,
        tbct(3,1)=523.0, tbct(3,2)=523.0, tbct(3,3)=523.0,
        tbct(3,4)=523.0, tbct(3,5)=853.0, tbct(3,6)=523.0,
        wl=2, wr=2, wf=2, wbk=2, wt=2,
        wb=6, wbct(1,5)=300.0, wbct(2,5)=300.0, wbct(3,5)=300.0,
        hwall1(1)=21000.0e+03, hwall1(2)=21000.0e+03, hwall1(3)=21000.0e+03,
        hwall1(4)=21000.0e+03, hwall1(5)=21000.0e+03, hwall1(6)=21000.0e+03,
    $end
    $mesh
        nxcelt=28, px(1)=-7.5, px(2)=0.0, px(3)=7.5,
        nycelt=10, py(1)=-2.0, py(2)=0.0, py(3)=0.5,
        nzcelt=50, pz(1)=-15.0, pz(2)=0.0, pz(3)=10.0,
    $end
    $obs
        nobs=1, tobs(2)=0.7, twobs(1,1)=523.0, twobs(2,1)=523.0,
        hobs1(1)=25000.0e+03,
        kobs(1)=44.4e+05,
        rcobs(1)=5.856e+07,
        iofo(1,1)=1, cc(1)=-1.0,
        igen(1)=0, ioh(1)=1,
        xl(1)=-7.5, xh(1)=7.5, yl(1)=-2.0, yh(1)=0.5,
        zl(1)=-15.0, zh(1)=10.0,
        iofo(2,1)=2, igen(2)=3, ioh(2)=0,
        iofo(3,1)=3, igen(3)=0, ioh(3)=0,
        xl(3)=-1.27, xh(3)=1.27, yl(3)=-0.5, yh(3)=0.0,
        zl(3)=-15.0, zh(3)=-14.0,
    $end
    $fl
    $end
    $bf
    $end
    $temp
        tempi=853.0, tvoid=523.0,
    $end
    $grafic
        ncplts=1, contyp(1)='tn', iperc(1)=3, yc1(1)=-0.05, yc2(1)=0.0,
        nvplts=1, contpv(1)='p', iperv(1)=3, yv1(1)=-0.05, yv2(1)=0.0,
    $end
    $parts
    $end
```

APPENDIX D

MATLAB CODE FOR MUCAL

```
v1=2.73e5;
co=1;
n=0.25;

vo=3.66;
c1=1.34e-5;

a=1.2;
b=814;
c=-0.4;
ts=886;


t=838;

x=exp(a*((ts/(t-b))-c));
vt=x*vo;
ct=x*c1;

 for e=1:3000;
  f1(e)=v1+(vt-v1)*(co+ct^2*e^2)^((n-1)/2);
 end


t=848;

x=exp(a*((ts/(t-b))-c));
vt=x*vo;
ct=x*c1;

 for e=1:3000;
  f2(e)=v1+(vt-v1)*(co+ct^2*e^2)^((n-1)/2);
 end


t=853;

x=exp(a*((ts/(t-b))-c));
vt=x*vo;
ct=x*c1;

 for e=1:3000;
  f3(e)=v1+(vt-v1)*(co+ct^2*e^2)^((n-1)/2);
 end


t=858;

x=exp(a*((ts/(t-b))-c));
vt=x*vo;
ct=x*c1;

 for e=1:3000;
  f4(e)=v1+(vt-v1)*(co+ct^2*e^2)^((n-1)/2);
 end


t=868;

x=exp(a*((ts/(t-b))-c));
vt=x*vo;
ct=x*c1;

 for e=1:3000;
  f5(e)=v1+(vt-v1)*(co+ct^2*e^2)^((n-1)/2);
 end
```

```
t=878;

x=exp(a*((ts/(t-b))-c));
vt=x*vo;
ct=x*c1;

 for e=1:3000;
  f6(e)=v1+(vt-v1)*(co+ct^2*e^2)^((n-1)/2);
 end



d=1:3000;
```